The Role of KCC3 in Neuronal Homeostasis

By

Bianca Flores

Dissertation

Submitted to the Faculty of the

Graduate School of Vanderbilt University

in partial fulfillment

of the requirements

for the degree of

DOCTOR OF PHILOSOPHY

In

Neuroscience

June 30th, 2020

Nashville, Tennessee

Approved:

David Jacobson, Ph.D.

Nellie Byun, Ph.D.

Amanda Peltier, M.D.

Eric Delpire, Ph.D.

ACKNOWLEDGEMENTS

I would like to thank all of the ancestors, past and present, who have made countless and unspoken sacrifices in order for me to be the first doctor in our family. I would like to honor and thank the Matriarch of our family, my grandmother, for helping to raise me and for always making me feel heard. I would like to thank both of my parents for always showing up for me when I needed them most and for showing me that with hard work, optimism, and gratitude, anything is possible. Thank you, dad for making the dangerous journey across the border when you did, so that your children could have a better life. Thank you, mom for being a grounding force in my life, for helping me to stay focused, and for always reminding me of the bigger picture. Thank you to my siblings, Jeremy, Cris, and Marissa, who contributed and self-sacrificed in different ways so that I could be where I am today. I am grateful to Max and Ruby for their unconditional love and for being a source of therapy for me. Thank you Peaches, Luna, and Koa for completing the energy circle, and with Max and Ruby, always protecting me. An endless thank you to Anisha, Pantelis, and Jonathan for helping me to stay grounded, and for always being there when I needed them. Thank you to the Vanderbilt IMSD program and Vanderbilt SACNAS who provided community, educational support, and created a safe space for me during my time here.

TABLE OF CONTENTS

LIST OF FIGURES

Page

LIST OF TABLES

CHAPTER 1

Cell Volume Regulation and the Cation Chloride Cotransporters

Introduction

Cell volume regulation is a fundamental aspect of cell homeostasis. Most mammalian cells live in an environment of constant osmotic pressure, and therefore have kept all basic mechanisms of cell volume maintenance and regulation. Important cell processes like cell division, migration, and even cellular metabolism force cells to change their shape and volume (Wehner et al., 2003). In order to rapidly and efficiently adapt to these changes, cells utilize specific transporters and channels to maintain their volume. In general, the cell membrane is typically regarded as a semi-permeable membrane, i.e. a membrane more permeable to water than to any osmolytes. Even in the absence of water channels (aquaporins), which increase the water permeability of membranes, the intrinsic water permeability of the lipid bilayer is several orders of magnitude more permeable to water than to ions. Thus, cells experience osmotic challenges when the extracellular environment becomes hypo- or hypertonic with respect to the intracellular environment. This is the case of cells in the kidney which experience large changes in extracellular osmolarity based on the hydration status of the body. Once the cells have equilibrated the osmotic pressure by gaining or losing water, they then attempt to recover their volume. This is achieved by moving ions and organic osmolytes through proteins embedded within the lipid bilayer to transport ions. Therefore, as ions move across the membrane, water follows, and the volume is restored. In

response to a hypotonic shock, a cell undergoes a swelling phase followed by a regulatory volume decrease (RVD) phase. In contrast, when a cell is exposed to a hypertonic condition, water leaves the cell and the cell shrinks. This is followed by an uptake of ions helping the cell undergo regulatory volume increase (RVI). The efflux and influx of ions relevant to cell volume regulation is mediated by channels and transporters, including electroneutral cation-chloride cotransporters.

Cation chloride cotransporters (CCCs) are among other physiological roles implicated in cell volume regulation following osmotic swelling or shrinkage (Delpire et al., 1991). Nine cation chloride cotransporters constitute the *SLC12A* family of solute carriers. They are a part of the amino acid-polyamine-organocation (APC) superfamily. Seven of the nine *SLC12A* cotransporters can be further subdivided between sodium-dependent and sodium-independent cotransporters. The remaining two proteins, CCC8 and CCC9, are considered orphan transporters as their function has yet to be determined. The Na^+ independent cotransporters (KCCs) carry 1 K^+ and 1 Cl^- ions across the membrane per transport cycle. Comparatively, the Na^+-dependent K^+ (NKCCs) transporters carry 1 Na^+, 1 K^+ and 2 Cl^- ions across the membrane, whereas the Na^+-Cl^- cotransporter, NCC, transports 1 Na^+ for every 1 Cl^-. Thus, the cation chloride cotransporters exhibit a 1:1 cation to anion stoichiometry and are therefore electroneutral. Their function does not affect nor is affected by the membrane potential.

Cation chloride cotransporters are secondary active transport mechanisms. This means that these transporters derive their energy from ion gradients established by primary transporters such as the Na^+/K^+ ATPase or pump. Because of the tight coupling between

substrates, these transporters can drive one ion against its own gradient. For instance, K-Cl cotransport can drive Cl^- outward against its gradient due to the large K^+ gradient generated by the Na^+-K^+ ATPase (Gamba, 2005). Thus, in neurons, an active K-Cl cotransporter helps to maintain a very low intracellular chloride concentration, thereby allowing hyperpolarizing GABA responses and inhibition. Moreover, because they are moving solutes across the plasma membrane, the cotransporter create a gradient for water to move in and out of the cell.

The CCCs: structure, function, and pharmacology

Almost all of the cotransporters share a similar 12 transmembrane domain with intracellular N and C-termini. The only exception is that one of the orphan cotransporters CCC9 has 11 transmembrane domains and a putative extra-cellular C-terminus. The other orphan co-transporter (CCC8 or CIP) is more closely related in structure to the K-Cl cotransporters. There are some differences between the Na^+ dependent (NKCC1, NKCC2, and NCC) and Na^+ independent (KCC1-4) transporters in structure and function, but overall, they appear highly homologous. For example, KCC1 shares about 25% sequence homology with NKCC/NCC whereas the four KCCs are approximately 65%-71% identical (Gillen et al., 1996; Mount et al., 1999). Na^+ dependent transporters have an extracellular loop between transmembrane domains 7 & 8. Comparatively K-Cl co-transporters have an extracellular loop between transmembrane domains 5 & 6 **(Figure 1-1)**.

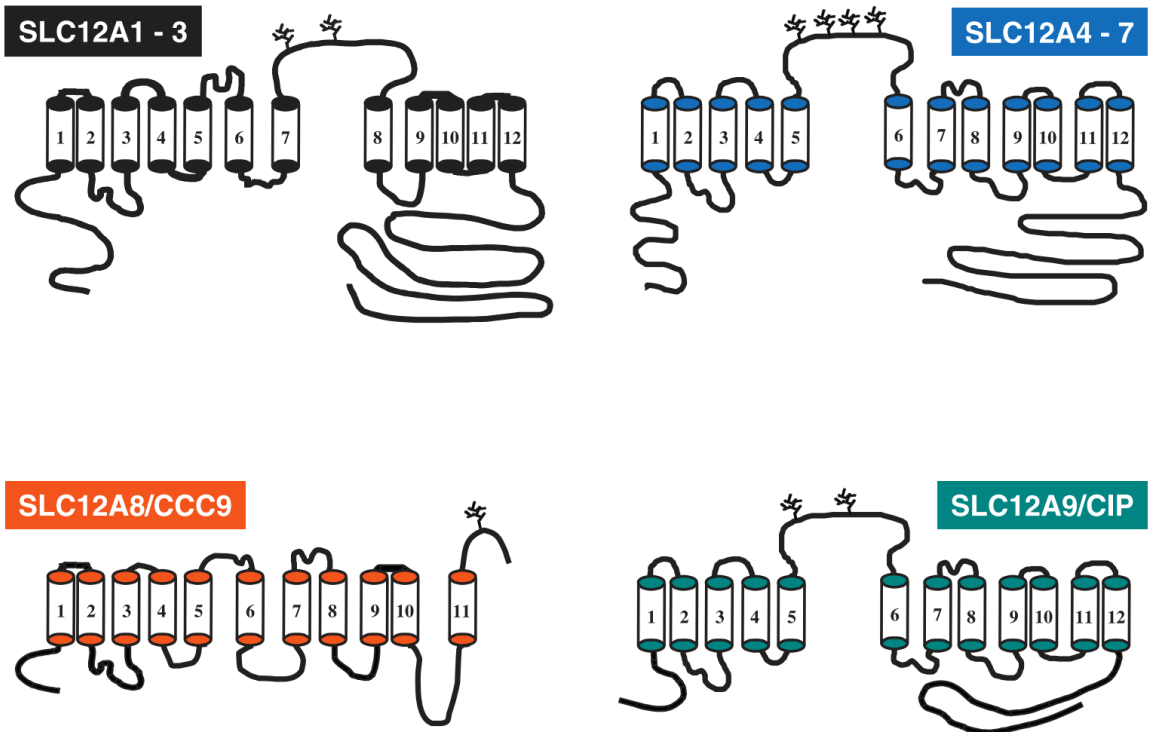

Figure 1-1 Topology structures of the cation chloride cotransporters. All structures are based on hydropathy plot analysis. SLC12A1-3A (Black) are the Na^+ dependent co-transporters. SLC12A4-7 (blue) are the Na^+ independent co-transporters. SLC12A8/CCC9 (orange) and SLC12A8/CIP (teal) are the two orphan co-transporters. Figure adapted from Gamba 2005.

The recent cryo-electron microscopy (EM) structures of KCC1 and NKCC1 (Liu et al. 2019; Chew et al. 2019) confirmed the basic structure of the cotransporters which was based on hydropathy, i.e. cytosolic termini and 12 transmembrane domains. The cryo-EM structures will allow a more detailed understanding on how the cotransporters bind and transport ions across the plasma membrane. As the hydropathy plots provided valuable information on the number of transmembrane domains, and the position of the termini and putative glycosylation sites, the cryo-EM structures provide insights to the ion binding sites, and the path of ions through the protein which is embedded in the membrane.

As for their function, the CCCs are phosphorylated by the WNK/SPAK-OSR1 kinases. WNK (With No Lysine-K)/SPAK (SPS1-related proline-arginine rich kinase)-OSR1(Oxidative Stress Response Kinase) exist in the same complex to reciprocally regulate the cation chloride cotransporters (Alessi et al., 2014; Gagnon et al., 2006; Piechotta et al., 2003; Piechotta et al., 2002). Specifically, the WNK/SPAK-OSR1 kinase cascade activates the Na^+-dependent cotransporters while inactivating Na^+-independent (K-Cl) cotransporters. WNK kinases act upstream of SPAK-OSR1, which are the terminal kinases as they bind and phosphorylate the cotransporters (Gagnon et al., 2006; Kahle et al., 2003) **(Figure 1-2)**.

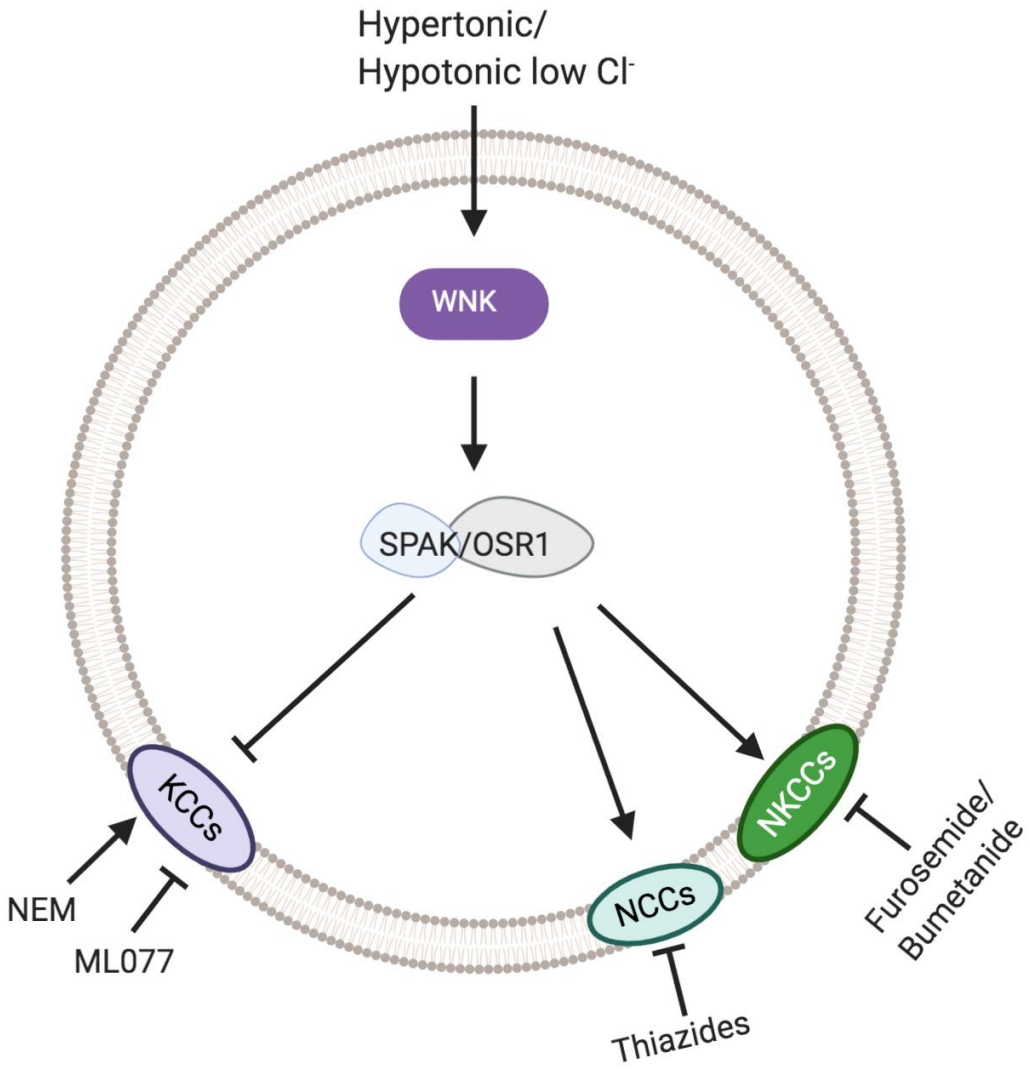

Figure 1-2. WNK/SPAK-OSR1 regulation of CCCs. WNK becomes activated in hypertonic or hypotonic low Cl^- which then phosphorylates SPAK/OSR1. SPAK or OSR1 phosphorylate all of the cation chloride cotransporters activating NKCC/NCC activity while inactivating KCC activity.

Na^+ dependent Transporters

The Na^+ dependent cotransporters, NKCC1 (SLC12A2), NKCC2 (SLC12A1), and NCC (SLC12A3) are critical in several cell types (epithelial cells, neurons, etc.) to help establish the chloride gradient and regulate cell volume through the import of Cl^- (Gamba, 2005). This set of transporters become active during cell shrinkage and helps the cells undergo regulatory volume increase (RVI). NKCC1 and NKCC2 transport 1 Na^+, 1 K^+, and 2 Cl^- ions into the cell, whereas NCC transports 1 Na^+ and 1 Cl^- into the cell. Interestingly, it has been found that hypertonic conditions and hypotonic low Cl^- conditions further stimulate WNK/SPAK-OSR1 activity (C. Richardson & Alessi, 2008). In these conditions, Na^+ dependent transporter activity is ramped up as WNK/SPAK-OSR1 works to phosphorylate conserved Threonine residues in the cytoplasmic N-terminus of NCC and NKCC1/2. In NKCC2 these residues have been identified as Thr^{95}, Thr^{100}, and Thr^{105} (C. Richardson et al., 2011).

In terms of their structure, initial hydropathy plots had suggested a 12 TM topology that form tight hairpin-like structures within the membrane (Gerelsaikhan & James, 2000). Further information about ion binding sites was elucidated from the recent cryo-Electron Microscopy (EM) structure of the zebrafish NKCC1 (Chew et al., 2019). The structure confirmed the presence of an extracellular loop between TM7 and TM8 and showed that it was stabilized by a disulfide bond. Furthermore, a structured element with TM5 and TM6 formed a cap domain that is important for cell surface expression (Chew et al., 2019). Most importantly, the structure revealed new information on ion coupling and showed that the Na^+ and K^+ binding

sites were in proximity and bind between the core and scaffold domains **(Figure 1-3)**. Comparatively, the Cl^- ion is transported adjacent to the cations with its movement assisted by backbone amides in TM1 (Chew et al., 2019).

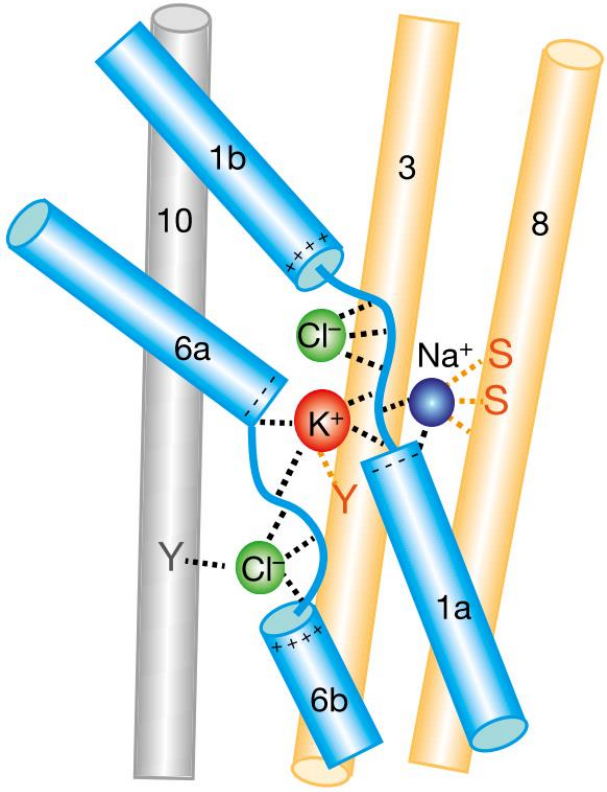

Figure 1-3. Ion binding sites elucidated from cryo-EM structure. Ion binding sites in the core domain (blue cylinders) of the cryo-EM structure of NKCC1. Figure from Chew et al., 2019.

An additional characterization of the cation chloride cotransporters has been based on which pharmacological treatments inhibit or stimulate them. Specifically, the sodium dependent transporter, NCC, is characterized by its thiazide sensitivity **(Figure 1-2)**. NCC was first purified from winter flounder urinary bladder (Gamba et al., 1993). Later Stokes and colleagues found Na^+ and Cl^- transport were inhibited in a dose dependent manner by hydrochlorothiazide and metolazone, two thiazide diuretics (Stokes et al., 1984). Structurally, it was found that transmembrane domain 11 in NCC defined the affinity for thiazides (Castañeda-Bueno et al., 2010). It should be noted that NCC is not inhibited by other diuretics like amiloride or bumetanide/furosemide. Currently, thiazide diuretics are used to treat high blood pressure and swelling (Gamba, 2009). In the clinic, they are sometimes also given in addition to loop diuretics, such as furosemide. Comparatively, the NKCCs (NKCC1 and NKCC2) have been shown to be inhibited by bumetanide or furosemide (**Figure 1-2**) (Payne et al., 1995). These two drugs are called loop diuretics because they inhibit NKCC2 in the loop of Henle, a major site of Na^+ reabsorption in the kidney. NKCC1 plays a critical role in establishing a chloride concentration gradient that promotes GABA-mediated excitation in immature neurons. Bumetanide has been considered for the treatment of neonatal epilepsy and autism (Ben-Ari, 2017; Kahle & Staley, 2008). Interestingly, a furosemide variant, azosemide, was found to be a more potent inhibitor of NKCC1 than bumetanide. It also more readily crosses the blood brain barrier (Hampel et al., 2018).

Na^+ independent cotransporters

Like the Na^+ dependent transporters, the K-Cl cotransporters are important transport mechanisms in several cell types (i.e. neurons, red blood cells, nephrons, etc.). They mediate the efflux of Cl^- to maintain the concentration gradient and help regulate cell volume. All K-Cl cotransporters increase their activity in hypotonic conditions and thus are important regulators in cell swelling conditions (Rinehart et al., 2009). It should be noted that KCC2 is already active in isotonic conditions, and increases its activity in hypotonic conditions. In this context, the WNK-SPAK/OSR1 kinases phosphorylate K-Cl cotransporters in conserved threonine residues in the C-terminus to inactivate its activity. Specifically, in KCC3, T1048 and T991 are phosphorylated. I focus most of my dissertation on a KCC3-T991A mutant transporter which renders the transporter constitutively active. The two threonine are highly conserved among the K-Cl cotransporters (Kahle et al., 2016).

Like the NKCCs and NCC, initial hydropathy plots of K-Cl cotransporters were examined following their molecular cloning. A hydropathy plot of KCC2 also predicted the 12 TMD and the position of putative N-linked glycosylation sites on the extracellular loop between TM 5 & 6 (Payne et al., 1996). Furthermore, it was also found that a transmembrane domain residue at position 289 in mouse KCC3 (E289) was necessary for expression of the protein at the membrane (Ding et al., 2013). This site was conserved in SLC12A1-SLC12A7. The recent cryo-EM structure of human KCC1 (Liu et al., 2019) confirmed the overall architecture of the transporter that was originally derived from hydropathy plots. What was surprising was how highly conserved the ion binding sites were between the KCC1 and

NKCC1 structures (Delpire & Guo, 2020; Liu et al., 2019). Specifically the K^+ binding site is formed by the same five identical residues in KCC as it is in NKCC1 (Delpire & Guo, 2020), yet functional data had previously revealed NKCC1's higher affinity for K^+ (reviewed in Delpire & Guo, 2020). The cryo-EM structure of KCC1 revealed the possible path of ion permeation and provided important clues on the size of the hydrophobic cavities. Molecular docking studies suggested that ML077, a specific K-Cl inhibitor (Delpire et al., 2009), was binding deep in the ion permeation pathway and possibly interacting with a tyrosine residue important for the coordination of K^+ (Delpire & Guo, 2020). This was consistent with previous kinetic studies which demonstrated that ML077 acted as a competitive inhibitor for K^+ (Delpire et al., 2009). The cryo-EM structures of NKCC1 and KCC1 did not provide any insights into whether or not water molecules are co-transported alongside K^+ and Cl^- ions during a transport cycle, as suggested by functional studies (Hamann et al., 2010; Zeuthen, 1994). Additionally to ML077 and structural variants which are the most potent inhibitors of K-Cl cotransport, KCCs are also inhibited by furosemide, although at a much lower affinity (Mount et al., 1999) (**Figure 1-2**).

Localization of cation chloride cotransporters and their role in health and disease

Overall, because the CCCs are basic ion symporters that participate in ion homeostasis and cell volume maintenance and regulation, they are widely expressed in the body. Often, many of these cotransporters will overlap in expression in cells and tissues, as they have

reciprocal functions, such as transporting inward or outward and participating to regulatory volume increase or decrease. Because of their critical role in basic cellular physiology, the *SLC12A* family members have been implicated in various genetic disorders.

NCC (SLC12A3)

Initial characterization of NCC found that it was solely expressed in the kidney and the gene mapped to human chromosome 16q13 (Mastroianni et al., 1996). The cotransporter was localized to the distal convoluted tube where it mediates sodium and chloride reabsorption (Plotkin et al. 1996, Schmitt et al., 1999). Loss of NCC function results in a loss of NaCl reabsorption and Gitelman Syndrome (Gitelman et al., 1966). This syndrome is also characterized by an imbalance of K^+ (hypokalemia), $Ca2^+$ (hypocalciuria), and Mg^{2+} (hypomagnesemia). The disease manifests itself as extreme thirst, excessive urination, and metabolic deficits. Mice with NCC LOF displayed most of the phenotypes in patients with Gitelman (Schultheis et al., 1998). One major difference between the knockout mouse and Gitelman patients is the absence of clear hypokalemic alkalosis in the mouse (Schultheis et al., 1998). Currently, there is no cure for Gitelman syndrome, however, many patients manage their syndrome through increased intake of Na^+-, K^+-, and Mg^{2+}-rich foods and supplements.

Comparatively, mutations in upstream kinases can result in increased NCC function. Specifically, patients with mutations in WNK1 or WNK4 (Wilson et al., 2001) result in the increased NCC that develops into a disorder called pseudohypoaldosteronism type II or Gordon syndrome (Gordon, 1986). In these patients, the increased NaCl reabsorption results

in hyperkalemia and hypertension. This phenotype has also been reproduced in several mouse models: WNK4 knock-in mice (Chowdhury et al., 2013; Yang et al., 2010) and a constitutively active SPAK mouse (Grimm et al., 2017; Harris et al., 2018).

NKCC1 (SLC12A2)

Human *SLC121A2* has been mapped to chromosome 5 (5q23.3). Unlike the Na-Cl cotransporter which is almost exclusively expressed in kidney, NKCC1 is expressed in almost all tissues throughout the body. This includes lung, heart, skeletal muscle, liver, stomach, pancreas, intestine, bladder, testis, uterus, endocrine glands, brain, spinal cord, etc. The transporter has been studied in many systems, mostly Cl^- secreting epithelia (such as lung, gastrointestinal tract, and exocrine glands), but also the inner ear, and the nervous system (For comprehensive review, see (Delpire & Gagnon, 2018). As this dissertation is primarily focused in Neuroscience, cotransporters that are expressed in the central and peripheral nervous systems will be discussed in more detail. It should be noted that in neurons, NKCC1 and KCC2 functions are reciprocal, helping the neurons maintain or regulate their intracellular chloride concentration (Watanabe & Fukuda, 2015).

Several LOF mouse models of NKCC1 were generated and published in 1999 (Delpire et al., 1999; Dixon et al., 1999; Flagella et al., 1999). They displayed vestibular dysfunction and exhibited a shaker/waltzer behavior (Delpire et al., 1999). Despite being highly expressed in the central nervous system, there were no overt neurological phenotypes. However, the mice exhibited a sensory perception phenotype, due to the collapse of the high Cl^-

concentration existing in dorsal root ganglion neurons (Laird et al., 2004; Sung et al., 2000). Additional phenotypes include smaller size, intestinal obstruction (Flagella et al., 1999), alteration in airway ion transport (Grubb et al., 2001), male infertility (Pace et al., 2000), and deficit in saliva production (Evans et al., 2000).

Our laboratory documented the first human patient with a mutation in NKCC1 (Delpire et al., 2016). The patient carries a *de novo* 11-base pair deletion in exon 22 of the SLC12A2 gene, leading to premature termination and truncation of a large portion of the carboxyl-terminus of the protein. The patient suffers from multi-system dysfunction, including lung, gastrointestinal tract, bladder, exocrine glands, etc. (Delpire et al., 2016). Because NKCC1 regulates Cl^- in sensory neurons and in smooth muscle cells, it was hypothesized that perhaps what the multiple organ involvement was due to defects in sensory feedback and/or smooth muscle cell function (Delpire et al., 2016). Further work by our laboratory demonstrated that while there was no dominant-negative effect of the mutant transporter on the wild-type in fibroblasts, there was a significant dominant-negative effect in epithelial cells. Using epithelial cells in culture, the lab showed that truncation of the carboxyl-terminus resulted in mis-trafficking of the mutant transporter to the apical membrane of epithelial cells (Koumangoye et al., 2018). Because of dimerization, the mutant transporter was also able to mistraffic wild-type cotransporter to the apical membrane. This phenotype was also observed in salivary gland and intestine of mice engineered to carry the patient mutation (Koumangoye et al., 2018). Expression of the mutant transporter in mice results in decreased intestinal water secretion, abnormal mucus release, and invasion of endemic bacteria in the epithelial layer of

the intestine. This phenotype is consistent with the intestinal dysfunction observed in the patient (Koumangoye et al., 2018).

Last year, the case of a 5-year old boy with a complete loss of NKCC1 expression was reported (Macnamara et al., 2019). Consistent with the knockout mouse model, the patient suffers from sensorineural deafness, gastrointestinal obstruction. He also presented with developmental delay and accumulation of mucus in the lung.

NKCC2 (SLC12A1)

Similarly to NCC, NKCC2 is a renal specific cation chloride cotransporter. NKCC2 was initially mapped to mouse chromosome 2 by Quaggin and colleagues (Quaggin, et al., 1995). Soon after, it was mapped to human chromosome 15q; consistent with mouse to human homology mapping (Simon et al., 1996). In the kidney, the cotransporter is found in the thick ascending limb in the Loop of Henle and in macula densa (Kaplan et al., 1996; Payne & Forbush, 1994). Disruption of NKCC2 in human results is Bartter's syndrome, another salt wasting disorder. Bartter's syndrome is an autosomal recessive disorder that affects salt reabsorption in kidney. Patients present renal salt wasting, hypotension, and in extreme cases, young children can have stunted growth and seizures (Simon et al., 1996). In a knockout mouse model of NKCC2, mouse pups were born normally, but within the first week, they showed severe signs of dehydration, renal failure, and high plasma potassium **(Table 1-1)** (Takahashi et al., 2000). Despite NKCC1 also being expressed in the kidney, its expression is not sufficient to compensate for a loss of NKCC2. This is because the function

of the basolateral NKCC1 in alpha intercalated cells and inner medullary collecting duct is completely different than that of the apical NKCC2 in the tick ascending limb. Interestingly, Takahashi and colleagues were able to pharmacologically mimic the knockout NKCC2 phenotype in wild-type animals by administering furosemide. Wild-type mice treated with furosemide developed mild hydronephrosis and had comparable urine outputs than NKCC2 knockout mice (Takahashi et al., 2000). Importantly, this knockout mouse model recapitulated many of the phenotypes observed in patients with Bartter's syndrome (hydronephrosis, renal insufficiency, hypokalemia), but to differing degrees.

Gene (protein)	Expression *indicates ubiquitous	Mouse model phenotype	Human disease
SLC12A1 (NKCC2)	Kidney (thick ascending limb in the loop of Henle (Quaggin et al., 1995)	Hypotension, dehydration, renal salt wasting	Bartter's Syndrome (Simon et al., 1996)
SLC12A2 (NKCC1)	Kidney, PNS, CNS, Epithelial Cells, Salivary glands basolateral membrane, epithelial cells* (Delpire et al, 1999; Nejsum et al., 2005)	Deafness & Shaker/Waltzer behavior	One documented human case (Delpire et al., 2016) Killquist patient (Killquist et al., 2019)
SLC12A3 (NCC)	Kidney (Distal convoluted tubule of nephron) (Schmitt et al., 1999)	Hypokalemic alkalosis, hypomagnesemia, hypercalciuria	Gitelman syndrome (Simon et al., 1996)
SLC12A4 (KCC1)	*Brain, Colon, Heart, Kidney (Gillen et al., 1996), red blood cells	No phenotype when disrupted by itself	N/A
SLC12A5 (KCC2)	Neuronal specific *Ubiquitous in the CNS (Williams et al., 1999)	Motor deficits/abolished respiration	Linked to Idiopathic epilepsy (Kahle et al., 2014)
SLC12A6 (KCC3)	Broadly expressed throughout PNS/CNS (Mount et al., 1999; Byun and Delpire 2007)	HSMN phenotype and tissue vacuolization	HSMN/ACC (Howard et al., 2002); Gain of function (Kahle et al., 2016)
SLC12A7(KCC4)	Lung, heart, and kidney (Mount et al., 1999), abundant throughout CNS and PNS	Deafness and renal tubular acidosis	N/A
SLC12A8(CCC9)	Small intestine, stomach, testis, thyroid and colon (Hewett et al., 2002)	N/A	Researched as a psoriasis susceptibility candidate gene (Hewett et al., 2002)
SLC12A9 (CCC6/CIP1)	Muscle, brain, and kidney (Caron, et al., 2000)	N/A	N/A

Table 1-1. SLC12A family tissue expression and mouse model phenotypes. A range of phenotypes results from the disruption of each co-transporter with the physiological significance of some co-transporters yet to be determined.

KCC1 (SLC12A4)

Similar to NKCC1, KCC1 is ubiquitously expressed. KCC1 has been detected in the brain, colon, heart and kidney (Gillen et al., 1996). Importantly, KCC1 has also been implicated in regulating cell volume in red blood cells (Quarmyne et al., 2011; Rust et al., 2007). However, because of its ubiquitous distribution, it is hypothesized to be a "house-keeping" cation chloride cotransporter (Garneau et al., 2019; Marco B. Rust et al., 2007). Based on its expression pattern, it would seem KCC1 would play an integral role in cell volume maintenance/overall cell homeostasis. However, no human disease has been directly linked with a mutation in KCC1 (**Table 1-1**). In knockout mouse models of KCC1 observing specifically red blood cells, there was no phenotype in mice lacking KCC1 (Marco B. Rust et al., 2007). However, when this mutation was compounded with a LOF of KCC3, only then did red blood cells exhibit a defect in cell volume regulation, suggesting that RBC cell volume is mainly regulated by KCC3 or regulated by both KCC3 and KCC1. Interestingly, KCC1 has been implicated in the growth of cervical and endometrial cancers (Shang et al., 2011; Zhang et al., 2009). When KCC1 was knocked down via RNA interference, cancer cell invasion decreased (Shang et al., 2011). Though LOF of KCC1 has not been directly linked to diseased mouse models or human genetic disorders, a gain of function of KCC1 resulted in sickle cell disease pathology in a humanized mouse model (Brown et al., 2015). Constitutively active KCC1 resulted in sickling, tissue damage, and ultimately premature death. Thus far, there has been no direct link with human sickle cell disease other than indication of increased K-Cl cotransport activity (Brown et al., 2015). It is clear that the

increased KCC activity in sickle cell disease accelerates the dehydration of red blood cells and the sickling process. Thus, KCCs could become potential therapeutic targets in the future.

KCC2 (SLC12A5)

KCC2 was first cloned in 1996 and labeled as a "neuronal-specific" isoform of the K-Cl cotransporters (Payne et al., 1996). It is found in most brain structures (Lu et al., 1999) including cerebellum (Notartomaso et al., 2017), hippocampus (Kelley et al., 2018), and even the retina (Vu et al., 2000). Interestingly, KCC2 is not expressed in the peripheral nervous system (Sedmak et al., 2015). Recent work has showed that KCC2 might be expressed in pancreatic beta cells (Kursan et al., 2017). Because of its importance in the CNS, the knockout of KCC2 in mice results in severe motor deficits that lead to the premature death of mouse pups due to respiratory failure **(Table 1-1)** (Hübner et al., 2001). Note that expression of KCC2 is driven by two separate promoters: KCC2a accounts for 5-10% of total KCC2 levels while KCC2b accounts for 90-95% of total KCC2 expression. Knockout of the KCC2b isoform results in pups surviving the perinatal period and exhibiting severe tonic/clonic seizures (Woo et al., 2002). KCC2 expression increases during development (Lu et al., 1999) leading to a shift in GABA responses from depolarizing to hyperpolarizing. Mutations in KCC2 have been also been associated with idiopathic epilepsy (Kahle, et al., 2014) and febrile seizures (Puskarjov et al, 2014). Additionally, deficient KCC2 expression has also been implicated in Rett syndrome, a neurodevelopmental disorder characterized by breathing abnormalities and severe seizures (Hinz et al., 2019). KCC2's role in establishing the chloride

gradient in the CNS in conjunction with NKCC1 will be discussed further below.

KCC3 (SLC12A6)

KCC3 is expressed throughout the PNS, CNS (Byun & Delpire, 2007; Pearson et al., 2001), and had a broad range of expression in the lung, heart, esophagus and several other tissue systems (Mount et al., 1999; Shiozaki et al., 2014). It should be noted that KCC3 also exists in two different isoforms: KCC3a and KCC3b. The KCC3a isoform encodes 99 amino acids and contains several sites for phosphorylation for inactivation. Comparatively, KCC3b encodes 39 amino acids and has a unique amino-terminus (Hebert et al., 2004). Moreover, KCC3a is expressed in the nervous system as well as the heart and skeletal muscle, while KCC3b expression is restricted to the kidney (Pearson et al, 2001; Arroyo et al., 2013) Several studies have confirmed KCC3a as the only expressed isoform of KCC3 in the nervous system (Le Rouzic et al., 2006; Pearson et al., 2001; Shekarabi et al., 2011). The focus of this dissertation will remain on KCC3a and will simply be referred to as KCC3.

KCC3 is the first K-Cl cotransporter that was directly linked with human disease. LOF of KCC3 results in hereditary sensorimotor neuropathy with agenesis of the corpus callosum (HSMN/ACC). HSMN/ACC is also referred to as Agenesis of the corpus callous with Peripheral Neuropathy (or ACCPN) as well as Andermann syndrome, following the first description of the disease in the medical literature (Andermann et al., 1972). HSMN/ACC is a genetic disorder that affects a mainly French-Canadian population in the Charlevoix/Lac St Jean region. Interestingly, researchers had first mapped HSMN/ACC to human chromosome

15q before they knew the gene that was disrupted (Casaubon et al., 1996). Later, Mount and colleagues mapped KCC3 to chromosome to human chromosome 15 (Mount et al., 1999). It was until individuals were actually screened for mutations in KCC3 that it was confirmed that mutations in KCC3 caused HSMN/ACC (Howard, Mount, et al., 2002). Furthermore, the LOF mouse model recapitulates the peripheral neuropathy phenotype (Howard, Mount, et al., 2002).

Since KCC3 is expressed in the PNS and CNS, a disruption in this cotransporter is more commonly associated with peripheral neuropathy as opposed to epilepsy or defects in red blood cells like the other isoforms (Howard et al., 2002; Kahle et al., 2016; Shekarabi et al., 2011). Interestingly, a GOF of KCC3 results in nearly the same phenotype in mice and humans as a LOF (severe peripheral neuropathy). As my dissertation work focuses on this aspect, gain-of-function mutations will be discussed more extensively in chapters 2-4.

Currently, there appear to be no compensatory mechanisms involved when KCC3 is disrupted. KCC3 can be co-expressed with other K-Cl cotransporters in multiple cell types, yet a KCC3 LOF appears to be not compensated by other mechanisms involved in cell volume regulation. For example, KCC3 happens to be co-expressed with KCC2 in many central neurons, yet tissue vacuolization still occurs in mouse models and patients with a LOF of KCC3 in the CNS (Auer et al., 2016; Boettger et al., 2003).

KCC4 (SLC12A7)

KCC4 also has ubiquitous expression, but is more abundantly expressed in the nervous system, lung, heart, and kidney (Mount et al., 1999). Importantly, like several other cotransporters, KCC4 is localized to the kidney, with the distal convoluted tubule and connecting tubule exhibiting the most abundant expression of KCC3 (Velázquez & Silva, 2003). However, within the nervous system, KCC4 has been localized to the forebrain and in sensory neurons and cranial nerves (Karadsheh et al., 2004; Le Rouzic et al., 2006). Interestingly, a LOF mouse model of KCC4 demonstrated both deafness and renal tubular acidosis (Boettger et al., 2002). The mice exhibited no motor or vestibular deficits, but severe hearing loss, suggesting an important and unanticipated role for KCC4 in maintaining K^+ in the inner ear. In contrast to NKCC1 which is expressed on the basolateral membrane of stria vascularis epithelium, where it participates in the secretion of the K^+-rich endolymph, KCC4 is expressed in hair cells. In addition to the hearing loss, LOF mice demonstrate urinary acidification resulting in renal tubular acidosis (Boettger et al., 2002). Currently, there are no documented human cases of a disruption in KCC4.

Orphan Cotransporters: CCC9 (SLC12A8) and CCC8 (SLC12A9)

CCC9 and CCC8 (sometimes referred to as CIP1) are orphan members of the *SLC12A* family. Their function as ion transporters has yet to be determined. While CCC9 expression seems broad, the highest levels of expression were observed in the small intestine, stomach, testis, thyroid and colon (Hewett et al., 2002). The gene was first identified as a potential gene

for psoriasis susceptibility (Hewett et al., 2002). Hewett an colleagues detected ubiquitous expression, but A splice variant of CCC9 was found to promote polyamine amino acid transport in HEK293 cells (Daigle et al., 2009). Interestingly CCC9 is the only member of the family that lacks the key residues coordinating the first Cl^- binding site (Delpire & Guo, 2020). Comparatively, CCC8 has been detected in the muscle, brain, and kidney (Caron, et al., 2000). However, its physiological relevance is still unclear.

Roles for KCC2 and NKCC1 in neurodevelopment

In addition to volume regulation, cation-chloride cotransporters play a role in establishing the chloride concentration gradient (Delpire, 2000; Kahle et al., 2008). As mentioned above, the electroneutral cation-chloride cotransporters transport Cl^- with Na^+ and/or of K^+ in a 1 cation:1 anion stoichiometry (Gamba, 2005). In the nervous system, the level of Cl^- defines the direction and strength of GABAergic and glycinergic neurotransmission. Neurotransmitter signals are necessary for patterning synaptic connections in the brain's intricate network of electrical synapses (Ben-Ari, 2002). These connections are part of a dynamic and delicate balance of excitation and inhibition necessary for the development of synapses and overall brain homeostasis. Unsurprisingly, disruption in the maintenance of intracellular chloride in the developing or in the adult nervous system can lead to an array of nervous system disorders.

The primary regulation of chloride in the nervous system is dependent on CCCs. Immature neurons have a relatively high $[Cl^-]_i$ with a depolarized GABA reversal potential

(E_{GABA-A}), while mature neurons have low levels of $[Cl^-]_i$ and hyperpolarized E_{GABA-A}. The developmental change in that occurs in E_{GABA-A} is correlated with expression changes in NKCC1 and KCC2 (Plotkin et al., 1997; Lu et al., 1999; Glykys et al., 2009). KCC3 expression is also low during development and increases in the late prenatal period in humans and postnatal period in rodents (Pearson et al., 1991; Lucas et al., 2012) thus it seems that KCC3 could also participate in the GABA developmental shift. This shift, in which GABA switches from depolarizing to hyperpolarizing, seems to mainly occur in central neurons where KCC2 expression is predominant.

NKCC1 and KCC2 are reciprocally regulated during development. Expression and function of NKCC1 is highest when the neurons are born in the subventricular zone and migrate to their final destination (Owens et al., 1996; Owens & Kriegstein, 2002). Then, during neuronal maturation, expression of NKCC1 decreases (Plotkin et al., 1997; Sedmak et al., 2015). In contrast, expression of KCC2 in rodent is low at birth and increases during postnatal development (Clayton et al., 1998; Lu et al., 1999). As NKCC1 is a Cl^- loader and KCC2 a Cl^- exporter, the differential expression of these two transporter accounts for the developmental decrease in the neuronal Cl^- concentration and the well-established "chloride-switch" leading to the change in GABA effect from depolarizing in immature neurons to hyperpolarizing in mature neurons (Kahle et al., 2015, 2008; Lucas et al., 2012).

It should be noted that each brain region can have differing levels of NKCC1 and KCC2 expression during the developmental period; the developmental switch occurs during the first two weeks in rodents, and late in pregnancy (prior to birth) in humans (Kahle et al., 2016).

The change also seems to occur progressively from hindbrain to forebrain. While NKCC1 and KCC2 have major roles, other transport mechanisms might be part of the developmental switch (Kaila et al., 1999; Lucas et al., 2012; Ludwig et al., 2003).

In sensory neurons, KCC2 is not expressed and the GABA shift does not occur. While expression of NKCC1 in sensory neurons somewhat decreases during development, it remains high during adulthood (Lucas et al., 2012). A separate K-Cl cotransporter, KCC3, is expressed in sensory neurons. It is interesting that this transporter does not fulfill the same role as KCC2 in central neurons, that is, affect intracellular Cl^- levels. Indeed, changes in $[Cl]_i$ in sensory neurons appears to be solely under the influence of NKCC1, but not KCC3. This might be due to absence of KCC3 function under normal isotonic conditions.

Despite having the exact basic function, i.e. transporting K^+ and Cl^- out of the cell, KCC2 and KCC3, seems to have somewhat different physiological roles and lead to different types of diseases. Due to its basal activity under isosmotic conditions, KCC2's main function is the regulation of intracellular Cl^-, and consequently strengthening of GABA hyper-polarizing response and GABA inhibition. Thus, disruption in that process leads to brain hyperexcitability and development of epileptic seizures (Kahle et al, 2014; Puskarjov et al, 2014; Saitsu et al, 2016). In contrast, KCC3, which is also expressed in central neurons but is inactive under isosmotic conditions, plays only a minor role in the GABA switch (Boettger et al., 2003). Instead, as a transporter activated by hypotonicity, KCC3 seem to play a critical role in cell volume regulation and its disruption leads to cellular swelling, vacuolization, and nerve pathology.

In addition to KCC2 and KCC3, there are two other K-Cl cotransporters, KCC1 and KCC4 (Mount et al., 1999; Su et al., 1999). These transporters are also expressed in the nervous system and as KCC3 they are also silent under isotonic conditions and activated by hypotonicity. While KCC1 mRNA is detected in all cells, KCC4 expression is highest in cranial nerves (Karadsheh et al., 2004). The role of KCC4 in cranial nerve has still yet to be examined. A global knockout mouse model of KCC4 was generated. The mice displayed hearing loss, disruption with their vestibular system, and renal tubular acidosis (Boettger et al., 2002). There were no phenotypes indicative of disruption of KCC4 in cranial nerves.

Peripheral nerves and Peripheral neuropathy

Peripheral neuropathy is defined by the damage of nerves *outside* of the brain and spinal cord. It interrupts communication signals between the PNS and CNS. Peripheral nerves consist of sensory nerves (nerves that control nociception, thermoception, proprioception, etc.), motor nerves (movement of muscles), and autonomic nerves (nerves that regulate unconscious activity, i.e. breathing, digestion, gland function). The focus of this dissertation will remain on sensory and motor nerve fibers as that is what is primarily affected in by disruption of KCC3.

Peripheral nerves can be distinguished between two different roots: the dorsal root (sensory), and the ventral root (motor). The bundle of dorsal root sensory neurons is known as the dorsal root ganglion because the somas exist as a cluster (ganglion) of neurons that have

nerve endings that synapse onto the spinal cord. In contrast, the ventral root simply comprises of motor nerves in which the motor neuron soma exists on the spinal cord with nerve endings that synapse onto the neuromuscular junctions. When either of these nerve endings or bundles is damaged, it results is peripheral neuropathy. Peripheral neuropathy can be classified as either sensory neuropathy, motor neuropathy, or both (sensorimotor neuropathy).

Causes of peripheral neuropathy can range from blunt force trauma, alcoholism, mismanagement of diabetes, autoimmune disorders, or as a result of inherited mutations. Overall, there are multiple causes of peripheral neuropathy, but the effect is the same: disruption of sensory signals to and from the brain with significant sensory and motor symptoms. Although nerve pathologies may be similar from the aforementioned causes (i.e. axonal degeneration/demyelination) (Ammendola, 2001; Katona & Weis, 2018), the focus of this dissertation will remain on inherited neuropathies as a LOF of KCC3 results in inherited neuropathy.

Hereditary peripheral neuropathies

Hereditary peripheral neuropathies occur at a prevalence of 1:2500 (Eggermann et al., 2018). There are four major types of inherited neuropathies: (1) Hereditary sensorimotor neuropathy (HSMN), (2) hereditary sensory neuropathy (HSN), (3) hereditary motor neuropathy (HMN), and (4) hereditary sensory and autonomic neuropathy (HSAN). Both loss and gain of function of KCC3 result in HSMN. It should be noted that a KCC3 LOF can also

results in Agenesis of the Corpus Callosum (Filteau et al., 1991; Howard, Mount, et al., 2002; Uyanik et al., 2006), although this phenotype does not have 100% penetrance. Furthermore a GOF results in only HSMN and no ACC (Kahle et al., 2016)

Patients with HSMN can experience a variety of painful sensory and motor symptoms from sharp stabbing, numbness, tingling, and overall motor weakness and muscle atrophy. In general, symptoms of sensory neuropathy will precede motor (Watson & Dyck, 2015). One of the most well characterized inherited neuropathies is Charcot-Marie-Tooth Disease (CMT) which is categorized as a HSMN. Unlike HSMN associated with KCC3 (HSMN/ACC) which a one gene to one disease direct connection, CMT is actually associated with mutations in several genes that contribute to the sub-categories of HSMN (Dyck, 1975).

Stratification of CMT and comparisons to HSMN/ACC

Because there are a variety of different genetic causes of CMT, there is heterogeneity in representation of phenotypes. Moreover, CMT can be considered as an all-encompassing name for a range of peripheral neuropathies, and thus has been categorized into 5+ different sub-types **(Table 1-2).** It should be noted the Type V/VI/VII are mainly categorized by their associated phenotypes and categorization has evolved; therefore, the focus will remain on types I-IV (NINDS, 2019). CMT I-IV/X presents extreme heterogeneity in causes as well in phenotypes. Though in some types of CMT, symptoms can appear as early as infancy, whereas other types may not have symptoms until adulthood (Reilly, 2009). This somewhat in

contrast to HSMN/ACC as individuals affected show delay in motor milestones immediately in infancy, with the neuropathy aggressively progressing (Andermann & Andermann, 1994).

Type	Inheritance Pattern	Phenotypes	Cause
Ia and Ib	Autosomal dominant	Myelin Sheath absnormalities	(Ia) duplication of PMP22 (Ib) Disruption in Myelin protein zero
II	Autosomal dominant	Axonal degeneration	Mutations in Mitofusin 2 (most common)
III (Dejerine Sottas Syndrome)	No specific inheritance pattern	Demyelinating neuropathy and muscle atrophy that begins in infancy	Demyelinating neuropathy that begins in infancy
IV	Autosomal recessive	Demyelinating motor and sensory neuropathy	5+ genes (CMT4, GDAP1, EGR2) etc.
CMTX	X-linked inheritance	Demyelinating neuropathy	Point mutation in Connexin-32 gene on X chromosome

Table 1-2. List of sub-categories of HSMN (CMT). Although somewhat related in phenotypes, CMTI-IV and CMTX result from a variety of different genetic mutations.

Several of the proteins (nearly 90% of cases) with CMT have some direct relation with myelin and axonal maintenance (Ramchandren, 2017), whereas HSMN associated with KCC3 is strictly associated with its ability to transport ions and regulate cell volume (Flores et al., 2019; Kahle et al., 2016, 2008); in fact HSMN/ACC was the first documented HSMN to be associated with a disruption of an ion transporter (Howard, Mount, et al., 2002). An additional important distinction between these two types of inherited neuropathies is that HSMN with KCC3 is inherited as an autosomal recessive neuropathy, whereas CMT can be inherited as autosomal dominant or recessive **(Table 1-2).**

HSMN associated with KCC3 and CMT-associated HSMN display similarities in that both neuropathies affect proteins that have been implicated in maintaining the integrity of peripheral node (Morelli et al., 2017; Sun et al., 2016). Furthermore, both types of inherited neuropathies have neuropathology displaying axonal and myelin disintegration (Hantke et al., 2014; Howard et al., 2002b; Kahle et al., 2016; Li, 2014). Currently, there are no pharmacological treatments for either inherited neuropathies other than medication for pain management.

Diagnoses and physical presentations: CMT vs HSMN/ACC

In order to diagnose inherited neuropathies, most medical examinations include detailing family and personal history. As for physical symptoms, medical doctors will look for muscle atrophy, signs of “hammer toes”, deformity that causes the foot to bend downwards,

other general foot/hand deformities, and changes in sensory perception (thermo- and nociception). As an additional confirmation of CMT specifically, patients will undergo nerve conduction studies and sometimes electromyogram tests (EMG). When possible, whole exome sequencing can be done for patients on a panel of genes associated with CMT. However, because sequencing can be expensive and individuals may have not access or resources to this, many medical doctors can diagnose HSMN (CMT) with a high degree of certainty from family history and nerve conduction studies.

Sporadic HSMN associated with KCC3 is typically detected by whole exome sequencing. For individuals that live in the Quebec region of Charlevoix/Saguenay Lac-St Jean region (Deleu et al., 1997; Mathieu et al., 1990), the prevalence (1 carrier in 20) of a specific mutation (Howard, Mount, et al., 2002) makes it easier to diagnose, and a targeted genetic test in now available. As a result, many individuals receive genetic counseling as they plan their family.

Many individuals that have a LOF of KCC3 Charlevoix/Saguenay Lac-St Jean region also display dysmorphic features, such as square faces, large angled mandibles, and high arched palates (Andermann & Andermann, 1994). It is unclear if these features are directly related to the loss of KCC3 function or to a side effect of improper development of the corpus callosum. There has been only one documented human case of gain of function mutation in KCC3. This case is the main focus of my dissertation.

Summary and dissertation goals

Ultimately, KCC3 has been shown to play an important role in the development of peripheral neuropathy. Being a part of a family of secondary active transport mechanisms involved in the transport of cations, Cl^-, and water KCC3 plays a significant role in cell volume regulation. The past two decades, has seen the development of mouse models that lack KCC3 expression, either globally, or in specific cell types (Ding and Delpire, 2014; Shekarabi et al., 2012; Howard et al., 2002). This dissertation work focuses on the physiological impacts of a gain of function of KCC3 found in a patient with a unique mutation in the cotransporter. We assess the consequences of expressing this mutant transporter using a mouse model we created to reproduce the patient mutation and assess the effect of the mutation on cell volume regulation in sensory neurons. In addition, through the use of inducible systems, we seek to determine the importance of KCC3 expression in the adult mouse. The goal of this work is to contribute foundational knowledge to the physiology of KCC3 and determine if the SLC12A6 gene could be considered as a candidate for gene therapy.

Specific aims

Specific aim I: Characterize a gain-of-function mutation in KCC3 in mice.

Hypothesis: A mouse model recapitulating a gain-of-function of KCC3 found in a human patient will exhibit locomotor deficits.

Specific aim II: Assess sciatic nerve fibers of homozygous T991A mice

Hypothesis: Nerve fibers from T991A mice will appear shrunken compared to nerve fibers isolated from wild-type mice.

Specific aim III: Assess cell volume regulation in gain-of-function, loss-of-function, and wild-type sensory neurons.

Hypothesis: KCC3 is involved in the mechanism of regulatory volume decrease in sensory neurons.

Specific aim IV: Assess the importance of temporal expression of KCC3 in adult mice.

Hypothesis: Tamoxifen-induced disruption of KCC3 in adult mice will result in severe locomotor deficits. Re-introducing a functional KCC3 in adult diseased mice will result in a rescue of locomotor phenotypes.

CHAPTER 2

Peripheral Motor Neuropathy is Associated with Defective Kinase Regulation of the KCC3 Cotransporter

Introduction

Inherited peripheral neuropathies are heterogenous, involving at least 75 different loci (Klein et al., 2013; Rossor et al., 2015; Tazir et al., 2014), and are classified in part by whether the affected gene product involves the myelin sheath, axon, or both in sensory or motor neurons or both. Consideration of both the gene mutation and the resulting pathological and clinical phenotype is required to develop an appropriate diagnosis. This classification scheme is complicated, however, because different mutations in the same gene can yield distinct disease phenotypes. For example, dominant gain-of-function (GOF) duplications in *PMP22*, encoding peripheral myelin protein 22, cause Charcot-Marie-Tooth disease 1A (CMT1A; OMIM# 601097); in contrast, recessive loss-of-function (LOF) deletion in *PMP22* cause Hereditary Neuropathy with liability of Pressure Palsies (HNPP; OMIM# 162500) (van Paassen et al., 2014). CMT1A is characterized by distal muscle weakness with atrophy, sensory loss, slowed nerve conduction velocity, and foot deformities. HNPP is a slowly progressing pressure-induced demyelinating neuropathy causing mild symptoms, such as numbness and pain, to more severe symptoms involving muscle atrophy and paralysis of affected areas.

The *SLC12A* gene family encodes K^+-Cl^- cotransporters (KCCs), which are electroneutral transporters that use outwardly-directed K^+ gradients generated by the Na^+/K^+ ATPase to mediate the regulated extrusion of K^+ and Cl^- ions from cells (Adragna et al., 2004; Lauf et al., 1992). As such, KCCs play important roles in cell volume homeostasis, epithelial transport, and neuronal excitability (K. B. Gagnon & Delpire, 2013). KCC3 is encoded by *SLC12A6*, which is expressed in neurons and glial cells of the central nervous system (CNS) (Boettger et al., 2003; Pearson et al., 2001; Shekarabi et al., 2011) and in the primary sensory (that is, the dorsal root ganglion [DRG]) and motor nerves of the peripheral nervous system (PNS) (Byun & Delpire, 2007; Pearson et al., 2001). The function and regulation of KCC3 in both the CNS and PNS are not well understood.

Autosomal recessive homozygous or compound heterozygous LOF mutations in *SLC12A6* cause the Mendelian disease Agenesis of the Corpus Callosum with Peripheral Neuropathy (ACCPN; OMIM #218000) (Boettger et al., 2003; Howard, Mount, et al., 2002; Uyanik et al., 2006). ACCPN patients and KCC3-knockout (KO) mice exhibit severe peripheral nerve degeneration (Byun & Delpire, 2007; Deleu et al., 1997; Ding & Delpire, 2014; Larbrisseau et al., 1984; Shekarabi et al., 2012); however, ACCPN patients also exhibit severe brain phenotypes, including maldevelopment of the corpus callosum, hydrocephalus, developmental delay, mental retardation, and seizures (Deleu et al., 1997; Albert Larbrisseau et al., 1984). GOF mutations in KCC3 have not been identified in any organism, and the clinical consequences of overactive KCC3 *in vivo* are unknown.

Here, we describe a child with a severe and progressive peripheral neuropathy that affects primarily motor, rather than sensory, neurons and with normal brain structure and function. The patient harbored a *de novo* heterozygous mutation in KCC3 (T991A), an important regulatory site of KCC3 activity required for normal cell volume homeostasis, as demonstrated in HEK293 cells (Adragna et al., 2015; De Los Heros et al., 2014; Rinehart et al., 2009). We show in patient-derived cells and *in vivo* with a mouse engineered with the same mutation that the T991A in KCC3 abolished WNK (with no lysine) kinase-dependent inhibitory phosphorylation of this site, thereby constitutively enhancing the activity of the transporter even under basal conditions. Dephosphorylation at this site normally occurs in response to cell swelling. These observations advance our understanding of KCC3 in human physiology, reveal a critical dependence of PNS neurons on kinase-regulated KCC3 activity, and implicate abnormal cell volume homeostasis as a previously unreported contributing mechanism to the pathogenesis of peripheral neuropathy.

Materials and Methods

Patient recruitment

This study was approved by the Institutional Review Board of the National Institute of Neurological Disorders and Stroke (NINDS) and National Institutes of Health (NIH). Written informed consent was obtained by a qualified investigator. DNA from blood and skin fibroblasts was obtained based on standard procedures. Medical history was obtained and clinical evaluations were performed as part of the standard neurologic evaluation.

Cell culture, Transfections and Cell Treatments

HEK293 (human embryonic kidney 293) and human fibroblast cells were cultured on 10-cm-diameter dishes in DMEM supplemented with 10% (v/v) fetal bovine serum, 2 mM L-glutamine, 100 U/ml penicillin and 0.1 mg/ml streptomycin. For transfection experiments, each dish of adherent HEK293 cells was transfected with 20 μL of 1 mg/ml polyethylenimine (Polysciences) (Durocher, 2002). 36 hours post-transfection cells were stimulated with either control isotonic or hypotonic medium for a period of 30 minutes. Cells were lysed in 0.3 ml of ice-cold lysis buffer/dish, lysates were clarified by centrifugation at 4°C for 15 minutes at 26,000 g, and the supernatants were frozen in aliquots in liquid nitrogen and stored at –20°C. Protein concentrations were determined using the Bradford method. Where indicated cells were treated with the indicated concentrations of the SPAK/OSR1 CCT domain inhibitor STOCK1S-50699 (Mori et al., 2013), which was purchased from InterBioScreen Ltd.

Antibodies

We used antibodies recognizing the following proteins or phosphorylated sequences: KCC3 phospho-Thr^{991} [residues 975-989 of human KCC3 phosphorylated at Thr^{991}, SAYTYER(T)LMMEQRSRR]; KCC3 phospho-Thr$^{1039/1048}$ [residues 1032-1046 or 1041-1055 of human KCC3 phosphorylated at Thr$^{1039/1048}$, CYQEKVHM(T)WTKDKYM]. NKCC1 total antibody [residues 1-288 of human NKCC1]; NKCC1 phospho-Thr^{203}/Thr^{207}/Thr^{212} antibody [residues 198-217 of human NKCC1 phosphorylated at Thr^{203}, Thr^{207} and Thr^{212}, HYYYD(T)HTN(T)YYLR(T)FGHNT]; SPAK-total antibody [full-length GST-tagged human SPAK protein]; SPAK/OSR1 (S-motif) phospho-Ser^{373}/Ser^{325} antibody [367-379 of human SPAK, RRVPGS(S)HLHKT, which is highly similar to residues 319-331 of human OSR1 in which the sequence is RRVPGS(S)GRLHKT]; OSR1 total antibody [residues 389-408 of human OSR1]; ERK1 total antibody [full-length human ERK1 protein]. All antibodies were raised in sheep and affinity-purified on the appropriate antigen by the Division of Signal Transduction Therapy Unit at the University of Dundee, and previously characterized (De Los Heros et al., 2014). Secondary antibodies coupled to horseradish peroxidase used for immunoblotting were obtained from Pierce. IgG used in control immunoprecipitation experiments was affinity-purified from pre-immune serum using Protein G-Sepharose.

Buffers and solutions

Buffer A contained 50 mM Tris/HCl, pH7.5 and 0.1 mM EGTA. Lysis buffer was 50 mM Tris/HCl, pH 7.5, 1 mM EGTA, 1 mM EDTA, 50 mM sodium fluoride, 5 mM sodium

pyrophosphate, 1 mM sodium orthovanadate, 1% (w/v) NP-40, 0.27 M sucrose, 0.1% (v/v) 2-mercaptoethanol and protease inhibitors (1 tablet per 50 ml). TBS-Tween buffer (TTBS) was Tris/HCl, pH 7.5, 0.15 M NaCl and 0.2% (v/v) Tween-20. SDS sample buffer was 1X-NuPAGE LDS sample buffer (Invitrogen), containing 1% (v/v) 2-mercaptoethanol. Isotonic high potassium buffer was 95 mM NaCl, 50 mM KCl, 1 mM $CaCl_2$, 1 mM $MgCl_2$, 1 mM Na_2HPO_4, 1 mM Na_2SO_4 and 20 mM HEPES (pH 7.4). Hypotonic high potassium buffer was 80 mM KCl, 1 mM $CaCl_2$, 1 mM $MgCl_2$, 1mM Na_2HPO_4, 1 mM Na_2SO_4 and 20 mM HEPES (pH 7.4). Isotonic buffer was 135 mM NaCl, 5 mM KCl, 0.5 mM $CaCl_2$, 0.5 mM $MgCl_2$, 0.5 mM Na_2HPO_4, 0.5mM $Na_2SO_4$and 15 mM HEPES (pH 7.5). Hypotonic low chloride buffer was 67.5 mM sodium-gluconate, 2.5 mM potassium-gluconate, 0.25 mM $CaCl_2$, 0.25 mM $MgCl_2$, 0.5 mM Na_2HPO_4, 0.5 mM Na_2SO_4 and 7.5 mM HEPES (pH 7.5).

Immunoprecipitation with phosphorylation specific-antibodies

KCC3 phosphorylated at the Thr^{991} and Thr^{1048} residues were immunoprecipitated from human fibroblast cell lysates. The phosphorylation-specific antibody was coupled with protein-G–Sepharose at a ratio of 1 mg of antibody per 1 mL of beads. A total of 2 mg of clarified cellular lysates was incubated with 15 µg of antibody conjugated to 15 µL of protein-G–Sepharose in the presence of 20 µg/mL of lysate of the corresponding non-phosphorylated peptide. Incubation was for 2 hours at 4°C with gentle agitation, and the immunoprecipitates were washed three times with 1 mL of lysis buffer containing 0.15 M NaCl and twice with 1 mL of buffer A. Bound proteins were eluted with 1X LDS sample buffer.

Immunoblotting

Cell lysates (15 µg) in SDS sample buffer were subjected to electrophoresis on polyacrylamide gels and transferred to nitrocellulose membranes. The membranes were incubated for 30 min with TTBS containing 5% (w/v) skimmed milk. The membranes were then immunoblotted in 5% (w/v) skim milk in TTBS with the indicated primary antibodies overnight at 4°C. Sheep antibodies were used at a concentration of 1-2 µg/ml. The incubation with phosphorylation-specific sheep antibodies was performed with the addition of 10 µg/mL of the non-phosphorylated peptide antigen used to raise the antibody. The blots were then washed six times with TTBS and incubated for 1 hour at room temperature with secondary HRP-conjugated antibodies diluted 5000-fold in 5% (w/v) skimmed milk in TTBS. After repeating the washing steps, the signal was detected with the enhanced chemiluminescence reagent. Immunoblots were developed using a film automatic processor (SRX-101; Konica Minolta Medical) and films were scanned with a 600-dpi resolution on a scanner (PowerLook 1000; UMAX). Figures were generated using Photoshop/Illustrator (Adobe). The relative intensities of immunoblot bands were determined by densitometry with ImageJ software.

K^+ influx assay in human fibroblast cells and HEK293 Cells

Human fibroblast cells were plated in 12-well plates (2.4 cm diameter/well) and the $^{86}Rb^+$ uptake assay was performed on cells that were 80% confluent. HEK-293 cells were plated at a confluence of 50–60% in 12-well plates (2.4-cm-diameter per/well) and transfected with wild-type full-length KCC3 or a human disease mutant form of full-length flag-tagged

KCC3 (T991A). Each well of HEK-293 cells was transfected with 2.5 µl of 1 mg/ml polyethylenimine and 1 µg of plasmid DNA. K^+ influx measurement, through $^{86}Rb^+$-uptake assay, was performed on the cells at 36 hours post-transfection. In both cases, culture medium was removed from the wells and replaced with either isotonic or hypotonic medium for 15 min at 37°C. Cell medium was removed by means of aspiration with a vacuum pump and replaced with stimulating medium plus inhibitors including 1 mM ouabain and 0.1 mM bumetanide, to prevent $^{86}Rb^+$ uptake by the Na^+/K^+ ATPase and NKCC1, for a further 15 min. After this period, the medium was removed and replaced with isotonic medium plus inhibitors containing 2 µCi/ml $^{86}Rb^+$, for 10 min, at 37°C. After this incubation period, cells were rapidly washed three times with the respective ice-cold nonradioactive medium. The cells were lysed in 300 µl of ice-cold lysis buffer and $^{86}Rb^+$ uptake tracer activity was quantified with a PerkinElmer liquid scintillation analyser. K^+ influx was calculated from $^{86}Rb^+$ uptake and expressed in pmoles K^+/mg protein/min.

CRISPR/cas9 generation of KCC3-T991A mice

A 20 bp sequence (ATATGAGCGCACCCTGATGA, boxed in **Fig. 2-5A**) located in exon 22 of mouse *Slc12a6* and followed by TGG as proto-spacer adjacent motif was selected for guide RNA targeting sequence. This sequence flanked by *Bbs*I sites was added to a guide RNA sequence in pX330, a vector expressing the guide RNA under a strong U6 promoter and cas9 under a hybrid chicken beta-actin (Cbh) promoter. The vector was injected alongside a 179 bp repair oligonucleotide into 498 mouse embryos. The repair oligo contained 83 bp

homology arms, a codon substituting Thr991 to Ala, a unique *Sac*I restriction site and a few additional third base mutations to prevent targeting of cas9 to the repair DNA. Out of 498 embryos injected, 283 were transferred to 13 pseudo-pregnant females thereby generating 54 pups. At weaning, genotyping was done by amplifying a 479 bp fragment followed by *Sac*I digest. Eight *Sac*I-sensitive (positive) animals out of 54 (15%) were identified. We sequenced the *Sac*I containing mutant alleles and identified 4 mice carrying the proper mutation, whereas the other 4 mice carried additional insertions or deletions (**Fig. 2-5D**). We selected two lines (#31 and #51) and crossed them to C57BL/6J mice to demonstrate germline transmission. The lines were then further bred to C57BL/6J to dilute any possible off-target effects.

Mouse fibroblasts

The tip of a mouse tail (5 mm) was minced using sterile fine forceps and sterile razor blades in a 35-mm culture dish containing 2 ml DMEM/F12 containing 350 U/ml penicillin, 350 ug/ml streptomycin, and 2 mg/ml collagenase D (from *Clostridium histolyticum*, Roche Diagnostics, Indianapolis, IN). The 2 ml medium containing small tail chunks was then added to 3 ml identical medium in a 15-ml conical tube and rotated overnight at room temperature. The next day, 5 ml complete DMEM/F12 medium (10% fetal bovine serum, 150 U/ml penicillin, and 150 ug/ml streptomycin) was added to each tube and the remaining large pieces of tails were allowed to sediment by gravity to the bottom of the tube (1-2 min). The supernatant (10 ml) was recovered, placed in new tubes, and spun at 150 x g for 4 min. The supernatants were aspirated, the pellet were resuspended in 0.5 ml complete DMEM/F12

medium, and placed in 24-well plate for growth. Upon confluence, the cells were detached and successively moved to 35-mm and 100-mm plates.

$^{86}Rb^{+}$ uptake in mouse fibroblasts

35-mm dishes were coated with 1 ml water containing 0.1 mg/ml poly-D-lysine, overnight in 37°C incubator. The dishes were then rinsed twice with 1 ml water and covered with 2 ml fibroblasts (1 x 10 cm dish resuspended in 16 ml medium or 1:8 splitting ratio) for 2 hour incubation at 37°C to allow the cells to stick. All dishes were plated from the same cell resuspension, thereby guarantying equal seeding. After 2 hours, the dishes were moved to room temperature and preincubated for 15-20 min in a isosmotic solution containing 140 mM NaCl, 5 mM KCl, 2 mM $CaCl_2$, 1 mM $MgSO_4$, 5 mM HEPES, pH 7.4, 1 mM glucose. At the end of the pre-incubation period, the medium was aspirated and replaced with identical solution containing 100 mM ouabain, 20 mM bumetanide, 1 mCi/ml $^{86}Rb^{+}$ in the presence or absence of 2 mM furosemide. After 15 min $^{86}Rb^{+}$ uptake, the dishes were washed 3 times with ice-cold buffer, exposed to 500 µl 0.25N NaOH for 1 hour, and neutralize with 250 µl acetic acid glacial. Samples of 300 µl were added to 5 ml scintillation fluid in glass vials for $^{86}Rb^{+}$ counts and of 30 µl were used for protein assay (Biorad). Each condition was done in triplicates and K^{+} flux was calculated from $^{86}Rb^{+}$ counts (cpm) and expressed in nmoles K^{+} per mg protein per min. Calculation is based on measuring and averaging the counts (cpm) of 5 ul aliquots of radioactice extracellular solution and relating these counts to the amount of K^{+} contained in these aliquots (e.g. 1 cpm = 2.5 pmoles K^{+}).

Cell volume experiments

Cell volume changes in patient and parental cells were determined using calcein as a marker of intracellular water volume as described previously (Adragna et al., 2015). Briefly, cells on coverslips were incubated with 0.5 μM calcein-AM for 30 min at 37°C. The cells were placed in a heated (37°C) imaging chamber (Warner Instruments, Hamden, CT) on a Nikon Ti Eclipse inverted epifluorescence microscope equipped with perfect focus, a 40X Super Fluor oil immersion objective lens, and a Princeton Instruments MicroMax CCD camera. Calcein fluorescence was monitored using a FITC filter set (excitation 480 nm, emission 535 nm, Chroma Technology, Rockingham, VT). Images were collected every 60 sec with MetaFluor image-acquisition software (Molecular Devices, Sunnyvale, CA) and regions of interest (~10-15 cells) were selected. Baseline drift resulting from photobleaching and dye leakage was corrected as described previously (Lenart, Kintner, Shull, & Sun, 2004). The fluorescence change was plotted as a function of the reciprocal of the relative osmotic pressure and the resulting calibration curve applied to all subsequent experiments as previously described (Lenart et al., 2004). The HEPES-buffered isotonic solution contained (in mM, pH 7.4): 100 NaCl, 5.4 KCl, 1.3 $CaCl_2$, 0.8 $MgSO_4$, 20 HEPES, 5.5 glucose, 0.4 $NaHC0_3$, and 70 sucrose with 310 mOsm determined using an osmometer (Advanced Instruments, Norwood, MA). Anisosmotic solutions (150, 280 mOsm) were prepared by removal or addition of sucrose to the above solution.

Accelerated rotarod assay

A neuromotor coordination task was performed using an accelerating rotating cylinder (model 47600: Ugo Basile, S.R. Biological Research Apparatus, Comerio, Italy) in two cohorts of mice: 12 wild-type mice and 12 heterozygous T991A mice, and 8 wild-type, 7 heterozygotes, and 7 homozygote mice. The cylinder was 3 cm in diameter and was covered with scored plastic. Mice were confined to a 4 cm long section of the cylinder by gray Plexiglas dividers. Two to five mice were placed on the cylinder at once. The rotation rate of the cylinder increased over a 4 min period from 4 to 40 rpm. The latency of each mouse to fall off the rotating cylinder was automatically recorded by the device. Mice that remained on the rotarod during the 300 sec trial period were removed and given a score of 300 sec. The test was performed three trials daily for 3 consecutive days with an intertrial interval of at least 30 min.

Wire hang grip test

To assess forelimb strength and coordination, we utilized the wire hang grip test. The wire was 50 cm long and 2 mm in diameter. The string was approximately 33.5 cm above the table surface with bedding placed underneath to prevent injury to any mice that fell. We trained the mice for 2 trials followed by 3 test trials in one day. The mice were allowed to hang on the wire for a maximum of 60 seconds, but timing ceased when the mouse fell. The mice were scored on latency to fall. Those that did not fall were given a score of 60 seconds.

Force grip test

We utilized the Chatillon digital force meter (San Diego Instruments, San Diego, CA) to assess force grip strength in all limbs of the mice. Training and testing were done on the same day: We trained the mice for three practice trials with ten-minute relief periods between each trial, followed by three test trials. The mice were allowed to initially grip the wire with all four paws and were then pulled horizontally with consistent force to determine grip strength. We normalized grip strength values to account for any variances due to body weight versus grip strength through the formula: $Force_{mouse}$/$body\ weight_{mouse}$.

Balance beam

To assess motor coordination and balance, we utilized a 1-meter long, steel balance beam. We utilized two beams of varying thickness: a standard-sized beam (12 mm), and a thinner beam (6mm), both of which had square cross sections to assess finer motor movements. The beam was placed approximately 50 cm from the ground and positioned between two pillars. At the start of the balance beam, mice began on an open, square platform and ended in an enclosed, black box with bedding as motivation for the mice to cross. We trained the mice for two days (three trials per day for each beam) beginning with the thicker beam (12 mm) and progressing to the thinner beam (6 mm). The mice were tested consecutively on each beam with ten-minute relief periods between each trial. The third day was used as a test day with three trials for each beam. The mice had approximately 60 seconds to traverse the beam and were scored on the neurological scoring system for beam

walking adapted from Feeny and Colleagues(Feeney, Gonzalez, & Law, 1982). This scoring system is based on the ability of the mouse to cross the beam and accounts for the number of paw slips. The mice received a score ranging from 1-7 based on their ability to complete the task, to place affected limbs on beam, and on the number of paw slips. This neurological scoring system considers a high score of 7 to be indicative of a wild-type mouse phenotype with no coordination deficits and a low score of 1 indicative motor defects [score of 7: mouse crosses beam with no more than two paw slips; 6: is able to cross beam but uses affected limbs more than halfway along beam; 5: is able to cross beam but uses affected limbs less than halfway along beam; 4: crosses beam and is able to place affected limbs at least once on horizontal beam; 3: crosses beam but drags (affected) hind limbs; 2: is unable to cross beam, but is able to hold horizontal balance for at least 5 seconds; 1: is unable to cross beam].

Nerve conduction studies

We measured the nerve conduction amplitude and latency in both sensory and motor neurons of the mouse tail and the sciatic nerve. Mice were anesthetized with isoflurane vaporizer (Vaporizer Sales & Service Inc., Rockmart, GA) with a continual flow of oxygen. Body temperature was maintained with a warming pad. For tail nerve conduction studies, we determined tail motor latency through proximal stimulation using single Nicolet 0.4 mm steel needle electrodes (Rythmlink International LLC, Columbia, SC) with an additional grounding electrode. For sensory and motor sciatic nerve measurements, we stimulated proximally at the sciatic nerve. For all nerve conduction measurements, we stimulated with stimulus duration of

20 ms and a stimulation range of 10-25 mA, with 25 mA being the supramaximal stimulus. We assessed latencies and traces using the Viking Software where latency is measured from initial onset to maximum negative peak.

Transmission electron microscopy

Sciatic nerves were dissected from adult mice, then nerves were fixed with 2.5% glutaraldehyde in 0.1 M sodium cacodylate for one hour at room temperature (RT) and then at 4°C overnight. The Vanderbilt EM core further processed the sciatic nerves samples by washing them and fixing in 1% osmium tetroxide solution for 1h at RT, and then with 0.5% osmium for 24 hours. The tissue samples underwent a series of ethanol dehydration steps (50% 5 min, 75% 15 min, 95% 2×15 min, 100% 3×20 min) before they were embedded in Spurr resin at 60°C for 24-48 h. Semi-thin sections (500 nm) were stained with toluidine blue and examined for positioning. Ultra-thin sections (80 nm) were then stained with uranyl acetate and lead citrate and placed on copper grids. Images were observed using a Phillips/FEI T-12 Transmission Electron Microscope.

Statistical analysis

Two-way ANOVA followed by Tukey's multiple comparisons test was used to assess statistical significance among wild-type, heterozygous, and homozygous groups of mice for the accelerated rotarod, wire hang grip, force grip, and balance beam behavioral assays, followed by Tukey's multiple comparisons test. For the force grip assay, we divided each

force value obtained by the weight of the mouse (Force/$mass_{mouse}$) to account for any variation due to mass differences. For nerve conduction studies we used one-way ANOVA followed by Tukey's multiple comparisons test to analyze statistical significance among all three genotypes. For all statistical analysis we considered $P < 0.05$ to be statistically significant. GraphPad Prism (version 7.0, GraphPad Software, Inc., La Jolla, CA) was used for all statistical tests.

Three-dimensional structure modeling

The three dimensional structure of human KCC3 C-terminal domain (CTD) was modeled by the I-TASSER server (J. Yang et al., 2014). Structure templates against the primary sequence KCC3 733-1150 identified from PDB database were used for comparative modeling. The top ranking template is the cytoplasmic domain of a prokaryotic cation chloride cotransporter (PDB accession code 3G40), which shows 21.1% sequence identity with KCC3 CTD. Among the top five models predicted by I-TASSER, the one with good topology and secondary structure assignment and a high C-score was chosen. The secondary structure elements of KCC3 were predicted by PredictProtein. PyMOL was used for molecular visualization.

Results

Clinical presentation of predominantly peripheral motor neuropathy

A 10-year-old boy presented to the Neuromuscular and Neurogenetic Disorders of Childhood Section at the National Institutes of Health (NIH) for diagnostic evaluation of an early-onset and progressive motor-predominant axonal neuropathy. At 9 months of age, the patient first exhibited foot-dragging while cruising. At 15 months, he developed bilateral foot drop and experienced frequent falls when walking. He had no early delays in fine motor skill acquisition; but, at 3 years of age, he had further progression, from distal to proximal, of leg weakness followed by hand weakness. At 8 years, he required an assistive device to ambulate. At 9 years, he lost the ability to independently ambulate. The patient reported no numbness, tingling, hearing problems, learning difficulty, or seizures. Cognitive development was normal as assessed by neuropsychological testing. Family history was noncontributory.

On examination at age 10 at the NIH, there were no dysmorphic features (such as high arched palate, abnormal distance between eyes, or syndactyly), and he had normal cognition, hearing, and language. There were no clinical signs of spasticity. He had pronounced muscle atrophy in his gastrocnemius, quadriceps, and hamstrings, as well as in his intrinsic hand muscles, biceps, and triceps. He had severe weakness in a distal to proximal distribution, with near lack of anti-gravity strength (scoring 2 out of a possible 5) with attempted wrist extension and finger extension and spread, and scoring 1 to 2 out of a possible 5 in strength in all lower extremity muscle groups. Deep tendon reflexes were absent. Vibration sense, joint position sense, and pinprick testing were normal.

At 6 years of age, nerve and muscle biopsies were performed at the Virginia Commonwealth University Children's Hospital. The nerve biopsy showed two nerve fascicles with mild loss of myelinated axons. A neurofilament stain also indicated mild axonal loss, whereas Luxol Fast Blue and Periodic Acid Schiff stains indicated intact myelination. No onion bulbs were detected, indicating absence of demyelination followed by re-myelination. Hematoxylin & eosin stained sections of muscle showed scattered hypertrophic and numerous atrophic fibers, indicative of denervation. Adipose tissue and endomysial connective tissue were both increased in focal areas. Of note, there was no evidence of muscle regeneration or degeneration, inflammation (infiltration of immune cells), vasculitis (inflammation and narrowing of the blood vessels), or perifascicular atrophy (reduction in diameter of fibers in the periphery of the fascicle).

Brain magnetic resonance imaging (MRI) was unremarkable and revealed an intact corpus callosum, brain stem, cerebellum, and cortical folding pattern (**Fig. 2-1A and 2-1B**). Comparison of muscle by ultrasound analysis between the patient and a healthy age- and gender-matched child revealed increased echogenicity (an indication of adipose or fibrous tissue), reduced bulk, and prominent atrophy (**Fig. 2-1C and D**).

Data from nerve conduction studies performed at ages 7 and 9 years were compatible with the diagnosis of a progressive predominantly motor axonal neuropathy with secondary demyelinating features (**Table 2-1**). At 7 years, the tibial, median, and ulnar motor nerve studies all showed a marked reduction in amplitude with moderate slowing; the facial motor nerve was also reduced in amplitude. Median and ulnar sensory responses showed mildly

reduced amplitudes with mild slowing; the sural sensory response was normal. At 9 years, the peroneal motor response was absent, and median and ulnar motor studies showed a further reduction in amplitude. The sural sensory response showed mild slowing, and the median and ulnar sensory responses showed a further mild reduction in amplitude and mild slowing of conduction velocity, indicating the presence of milder sensory nerve involvement in addition to the predominant motor neuropathy. Blood counts were normal. The mean corpuscular volume and osmotic fragility of red blood cells (RBCs) was normal. Blood pressure and serum and urine electrolytes were normal (**Table 2-2**).

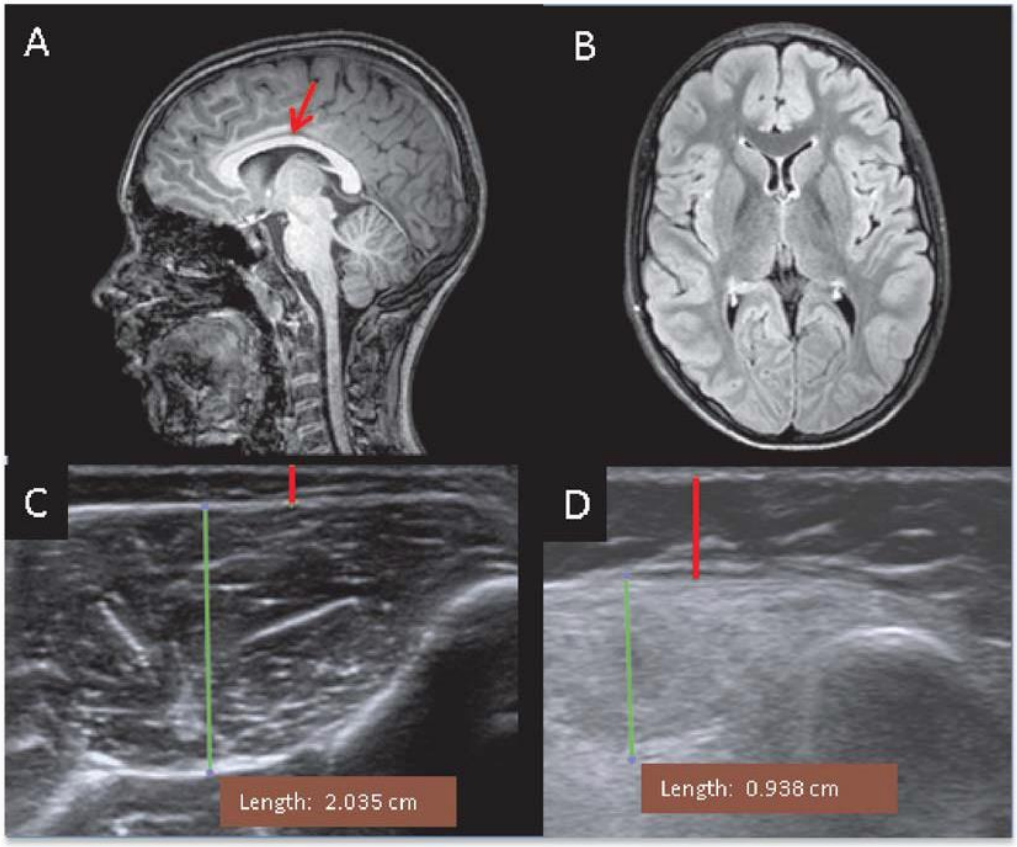

Figure 2-4 Brain and muscle imaging of a patient with a KCC3 T991A mutation. (**A**) T1 sequence brain MRI, mid-sagittal view. Corpus callosum is indicated by red arrow. (**B**) FLAIR sequence brain MRI, axial view, demonstrating normal brain volume. (**C**) Muscle ultrasound (performed on Siemens AcusonS2000) of the tibialis anterior (TA) muscle from a healthy 10-year-old-boy to represent normal echogenicity and bulk. (**D**) Abnormal muscle ultrasound of the TA muscle from our patient at 7-years-old. In C and D, the green line indicates depth of muscle, and the red line indicates the subcutaneous fat layer.

Nerve	Age 7 years			Age 9 years		
Motor Nerve (& muscle)	**Amp (mV); [LLN]**	**CV (m/s); [LLN]**	**DL (ms); [ULN]**	**Amp (mV); [LLN]**	**CV (m/s); [LLN]**	**DL (ms); [ULN]**
Peroneal –EDB	Not done	Not done	Not done	**NR**	**NR**	**NR**
Peroneal -TA	Not done	Not done	Not done	**NR**	**NR**	**NR**
Tibial -AHL	**0.4** [> 2.5]	**NR** [A] [> 40]	**6.1** [< 6]	Not done	Not done	Not done
Median - APB	**1.1** [> 4.5]	**31** [> 50]	**4.8** [< 4.5]	**0.2** [> 4.5]	**14** [> 50]	**5.5** [< 4.5]
Ulnar - ADM	**0.5** [> 4.5]	**14** [> 50]	**4.3** [< 3.5]	**0.1** [> 4.5]	**NR**	**6.3** [< 3.5]
Facial – nasalis	**0.3** [> 1.0]	N/A	**5.8** [<4.2]	Not done	Not done	Not done
Sensory Nerve	**Amp (uV); [LLN]**	**CV (m/s); [LLN]**	**--**	**Amp (mV); [LLN]**	**CV (m/s); [LLN]**	**--**
Sural	17 [> 6]	42 [> 40]	--	8 [> 6]	**27** [> 40]	--
Median	**13** [>15]	**44** [> 50]	--	**9** [>15]	**44** [> 50]	--
Ulnar	**7** [> 15]	**33** [> 50]	--	**6** [>15]	**41** [> 50]	--

Table 2-1. Nerve conduction studies with patient. Abnormal results are highlighted in **bold**.

Abbreviations:
Amp = amplitude
DL = Distal latency
CV = conduction velocity
LLN = lower limit of normal
ULN = upper limit of normal
N/A = not applicable
EDB = Extensor digitorum brevis muscle (peroneal motor innervated muscle in foot)
TA = Tibialis anterior muscle (peroneal motor innervated muscle in leg)
AHL = Abductor hallucis longus muscle (tibial motor innervated muscle in foot)
ADM = Abductor digitorum minimi (ulnar motor innervated muscle in hand)
APB = Abductor pollicis brevis (median motor innervated muscle in hand)
NR = no response
NR^A = no response – no conduction velocity was calculated because the proximal site recording could not be elicited and a velocity could therefore not be calculated

Test	Result
EMG [1]	Abnormal: Motor > Sensory Axonal Neuropathy
MRI brain [2]	Normal
MR spectroscopy brain	Normal
Serum electrolytes [3]	Normal (except low creatinine)
Urine electrolytes [4]	Normal
Hearing	Normal to speech and pure tones; normal tympanometry and auditory brainstem response
Osmotic fragility	Normal erythrocyte osmotic fragility
Peripheral blood smear	No acanthocytes; normal smear
Creatine kinase	Normal [136]

Table 2-2. Summary of clinical studies of a patient with a KCC3 T991A mutation.

[1]**EMG** – see Table 1 for specific nerve conduction study data and interpretation.
[2]**MRI brain**– see Figure 1 for picture of normal MRI brain including normal brain volume and corpus callosum.
[3]**Serum electrolytes** - Specific values are as follows: [Na = 138; K = 3.9; Cl 100; HCO_3^- = 23, BUN = 9; Creatinine = **0.12 L** (normal 0.3-0.7)];
[4]**Urine electrolytes** - Specific values are as follows: [Urine Na = 93; Urine K 86.5; Urine Cl = 124]

Identification of the mutation in the clinical case

Genetic testing before referral to our center included a negative complete Charcot-Marie-Tooth (CMT) panel (including *PMP22* deletion and duplication testing and sequencing, and *CX32*, *MPZ*, *PMP22*, *EGR2*, *NFL*, *PRX*, *GDAP1*, *LITAF*, *MFN2*, *SH3TC2* sequencing), and negative targeted sequencing for other relevant disease-causing genes, including *SETX*, *HSBP8*, *HSPB1*, *GARS*, *BSCL2*, *ATP7A*, *TRPV4* and *IGHMBP2*. Clinical whole exome sequencing on DNA derived from the blood of the patient and both of his parents was performed at Emory Genetics using the Agilent V5Plus targeted sequence capture method and IlluminaHiSeq 2000 sequencing instruments. Variants were analyzed using bioinformatics analysis through the Emory Genetics Laboratory, with a "Neuropathy Boost option" to ensure complete coverage of genes known to cause neuropathy-related disease.

A heterozygous c.2971A>G (T991A) mutation in exon 22 of *SLC12A6*, the gene encoding the KCC3 cotransporter, was identified (reference NM_133647.1), and confirmed by Sanger sequencing (**Fig. 2-2A**). Parental segregation testing was negative, demonstrating that the mutation was *de novo*. This mutation has not been previously reported in the literature and was not represented in any of the major databases of genetic mutations, including dbSNP, NHLBI EVS, ExAC Browser, or GEM (Gonzalez et al., 2013). Thr^{991} is conserved among the four different human KCC family members (KCC1-4) and in KCCs across evolution (**Fig. 2-2B, C**).

Thr^{991} resides in the KCC3 cytoplasmic C-terminus and is a critical regulatory residue of transporter activity in response to cell swelling (Kahle et al., 2008). To predict the effect of

this mutation, we generated a structural model of the human KCC3 C-terminal domain (**Fig. 2-2D**), using the cytoplasmic domain of a prokaryotic cation chloride cotransporter (PDB ID: 3G40) as a template. Ala substitution at this site is predicted to have significant functional impact by MutationTaster (Schwarz et al., 2010), SIFT (Ng & Henikoff, 2003), and PolyPhen-2 (Adzhubei et al., 2010).

Effect of KCC3 T991A mutation on KCC3 function

Given the importance of Thr^{991} phosphorylation for swelling-induced stimulation of KCC3 activity (De Los Heros et al., 2014; Rinehart et al., 2009), we assessed the phosphorylation and swelling-regulated function of KCC3 in patient and parental (control) fibroblasts. As positive controls, we expressed wild-type KCC3 (KCC3-WT) or KCC3-T991A in HEK293 cells, which have low endogenous levels of this protein (**Fig. 2-3A**). In all conditions tested, the T991A mutation reduced significantly KCC3 Thr^{991} phosphorylation, as assessed with an phosphorylation-specific antibody that recognizes KCC3 when phosphorylated at this residue (De Los Heros et al., 2014). The residual signal may represent incomplete absorption and removal of antibodies directed against the non-phosphorylated epitope.

The activity of KCCs and the Na^+-K^+-$2Cl^-$ cotransporters (NKCC) are regulated by a kinase cascade involving the WNK kinase family, which phosphorylates and activates the kinases SPAK and OSR1. Activated SPAK and OSR1 (collectively referred to as SPAK/OSR1) redundantly function to phosphorylate KCC and N(K)CC proteins. WNK-

dependent phosphorylation of KCCs inhibits their transporter function; whereas WNK-dependent phosphorylation of NKCCs stimulates their transporter function (Alessi et al., 2014; Gagnon et al., 2012; Kahle et al., 2010). Total abundance of KCC3, NKCC1, SPAK, OSR1, and extracellular signal-regulated kinase 1 (ERK1) signals appeared unchanged, whereas phosphorylated SPAK and NKCC1 signals increased upon exposure of the cells to the hypotonic low Cl^- solution (**Fig. 2-3A**, bottom), confirming that the cells responded positively to this treatment, as described (De Los Heros et al., 2014). Relative to parental fibroblasts, patient fibroblasts had ~50% less phosphorylation at Thr^{991} (**Fig. 2-3B, 2-3C**), consistent with the heterozygous nature of the KCC3 T991A mutation. Phosphorylation at Thr^{1048} was unchanged (**Fig. 2-3B, 2-3C**).

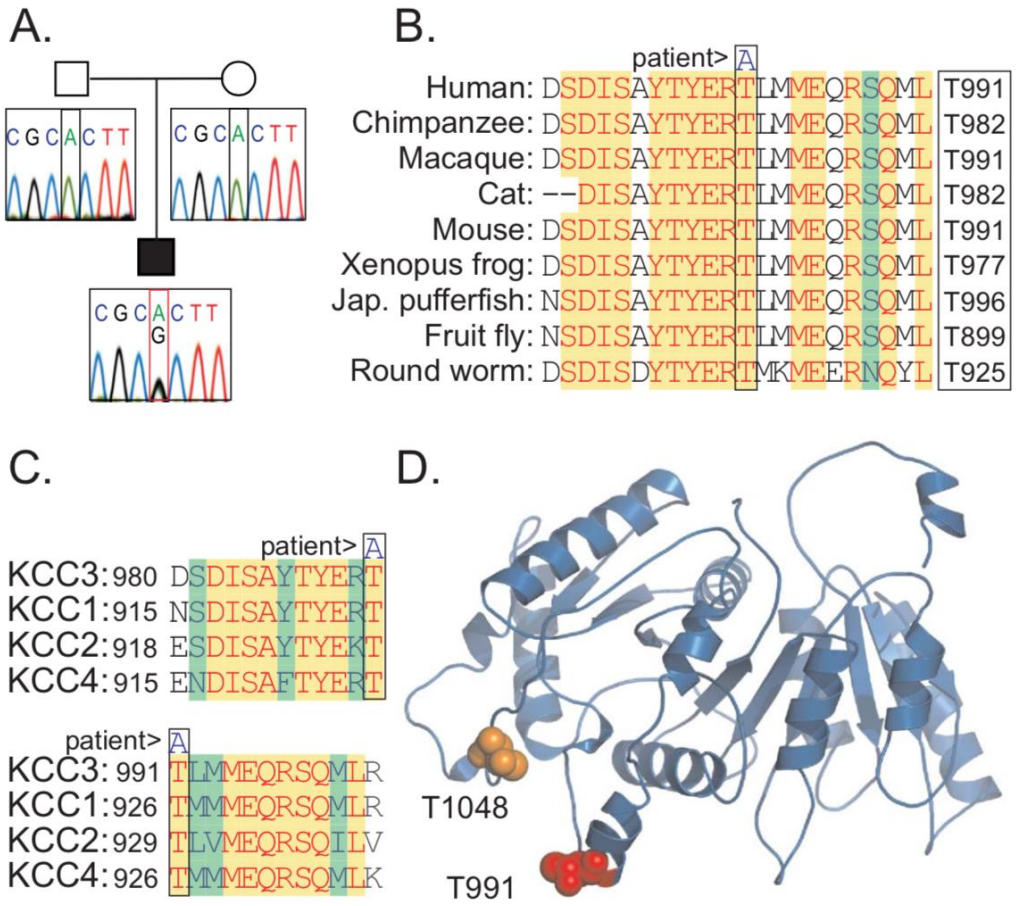

Figure 2-2. Identification of a *de novo* KCC3 T991A mutation in a patient with an early-onset, progressive, and severe axonal motor neuron neuropathy. (A) DNA chromatograms illustrating the detection of a heterozygous c.2971A>G mutation in exon 22 of *SLC12A6*, encoding a T991A substitution in KCC3. (**B**) Evolutionary conservation of amino acid Thr^{991} in KCC3 across the indicated species. Jap, Japanese. (**C**) Conservation of the homologous residues of amino acid Thr^{991} in KCC3 in other human KCC family members. (**D**) Cartoon of the modeled structure of the human KCC3 C-terminal domain (residues 733-1150), based on homology modeling by I-TASSER using the prokaryotic cation-Cl^- cotransporter (PDB ID: 3G40) as the template. Residues Thr^{991} and Thr^{1048} are presented in space fill and colored.

To confirm that the mutation altered KCC3 function, we assessed K-Cl cotransport activity by measuring $^{86}Rb^+$ uptake under various conditions in HEK293 cells transfected either with wild-type or KCC3-T991A cDNA **(Fig. 2-4A**), or in human fibroblasts isolated from parental controls or the KCC3-T991A patient (**Fig. 2-4B**). Transporters and channels that can conduct K^+ can also conduct $^{86}Rb^+$, which is a radioactive ion that can be conveniently measured. To isolate the KCC-mediated flux, we exposed the cells to ouabain and bumetanide which are inhibitors of the Na^+/K^+ pump and NKCC1, the transporters that mediate the bulk (85%) of total K^+ uptake in these cells (V. Mathieu et al., 2015) and then monitored $^{86}Rb^+$ uptake in the presence of hypotonic low Cl^-, conditions that cause an increase in cell volume and activation of the WNK-SPAK/OSR1 signaling pathway and increased KCC3 activity, and hypotonic low K^+, conditions that also promotes the cell swelling-induced dephosphorylation of T991 and T1048 via activation of PP1/PP2A phosphatases. We inhibited WNK-dependent SPAK and OSR1 activation with STOCK1S-50699, a drug that blocks the interaction between WNK and these downstream kinases and results in the activation of KCC3 by decreasing transporter phosphorylation in part at Thr991 (Gonzalez et al., 2013; Kahle et al., 2015). Both untransfected and wild-type KCC3 transfected HEK293 cells showed a significant increase in K^+ influx upon WNK-SPAK/OSR1 inhibition, consistent with increased KCC3 activity. In the absence of STOCK1S-50699, cells expressing KCC3-T991A exhibited significantly higher activity than cells expressing the wild-type KCC3. Furthermore, in all but the normal tonicity low Cl^- control condition, WNK-SPAK/OSR1 inhibition produced no significant increase in K^+ influx, indicating no additional activation of the KCC3 (**Fig. 2-4A).**

To isolate KCC3 activity in the patient and parental fibroblasts, we measured K^+ influx in the presence and absence of furosemide, a KCC inhibitor (**Fig. 2-4B**). Both the parental and patient fibroblasts exhibited furosemide reduction in K^+ influx under all conditions tested (**Fig. 2-4B**). However, compared with the parental cells, fibroblasts isolated from the patient had a greater furosemide-sensitive K^+ flux (difference between flux measured in the absence and presence of furosemide) under hypotonic low Cl^- conditions, indicating higher cotransporter activity in the patient cells compared with that in the parental cells (**Fig 2-4B**). The KCC3-T991A fibroblasts have significantly higher K^+ flux compared with the parental control fibroblasts; furosemide treated KCC3 control fibroblasts exhibit significantly decreased K^+ flux, and KCC3-T991A fibroblasts are also sensitive to furosemide treatment with significantly decreased K^+ flux. We also assessed cell volume regulation in KCC3-T991A patient fibroblasts and parental control fibroblasts, using methods described previously (Lenart et al., 2004). Parental cells exposed to hypotonic HEPES-MEM (150 mOsm/kg H_2O) exhibited a ~2.3 ± 0.6 fold increase in cell volume (at a rate of 1.03 ± 0.1 % cell volume/min) (**Fig. 2-4C-D**), which recovered to the original volume after returning cells to isotonic conditions. In contrast, the patient fibroblasts with KCC3-T991A had a compromised acute swelling response to hypotonic stress (1.4 ± 0.1 fold). These results are consistent with the hypothesis that the greater furosemide-sensitive flux in KCC3-T991A patient cells compromises cell volume regulation.

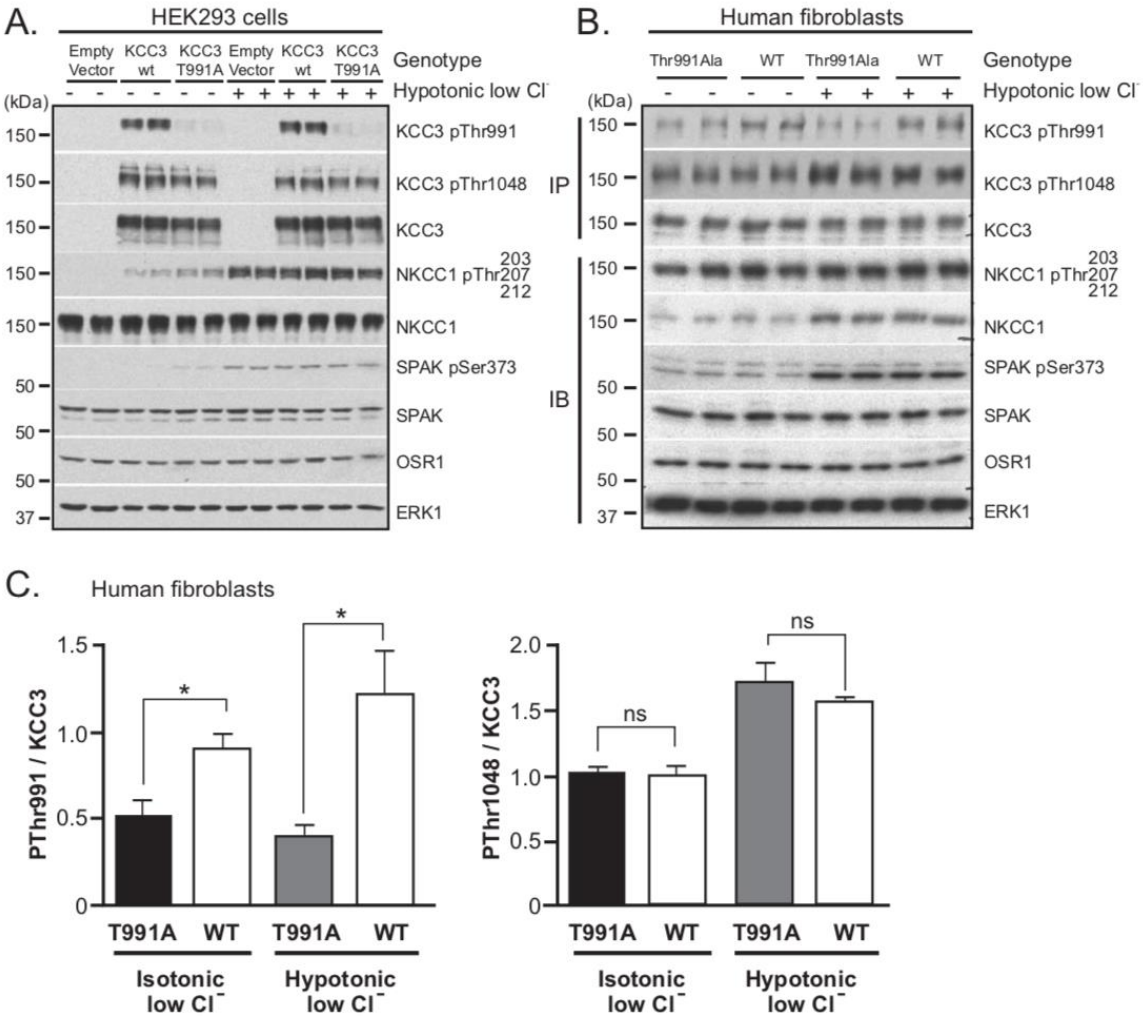

Figure 2-3. T991A decreases KCC3 phosphorylation by the WNK1-SPAK pathway in HEK293 cells and patient fibroblasts. (**A**) Phosphorylation of wild-type KCC3 (WT) or KCC3 T991A expressed in HEK293 cells. HEK293 cells were transfected with the indicated constructs and exposed to hypotonic low Cl^- conditions for 30 min. Lysates were subjected to immunoblot with antibodies recognizing the indicated proteins or phosphorylated proteins. ERK1 served as a loading control. (**B**) Phosphorylation of endogenous KCC3 and KCC3 T991A in human fibroblasts. Human fibroblast cells derived from the affected patient (heterozygous for KCC3 T991A) or his unaffected parental controls (WT) were exposed to hypotonic low Cl^- conditions for 30 min. Lysates were subjected to immunoprecipitation (IP) with antibodies recognizing either KCC3 pThr991 or KCC3 pThr1048, and immunoprecipitates were immunoblotted with KCC3 total antibody. Lysates (IB) were also analyzed for the presence of the indicated proteins and phosphorylated proteins. (**C**) Quantification of the results of the Western blots shown in B, statistically significant differences are indicated (repeated measures one-way ANOVA: $F(3, 4) = 14.54$, $P = 0.0129$). Data are shown as mean ± SEM. The quantification (ratio calculation) is based on phosphorylated species of KCC3/total KCC3.

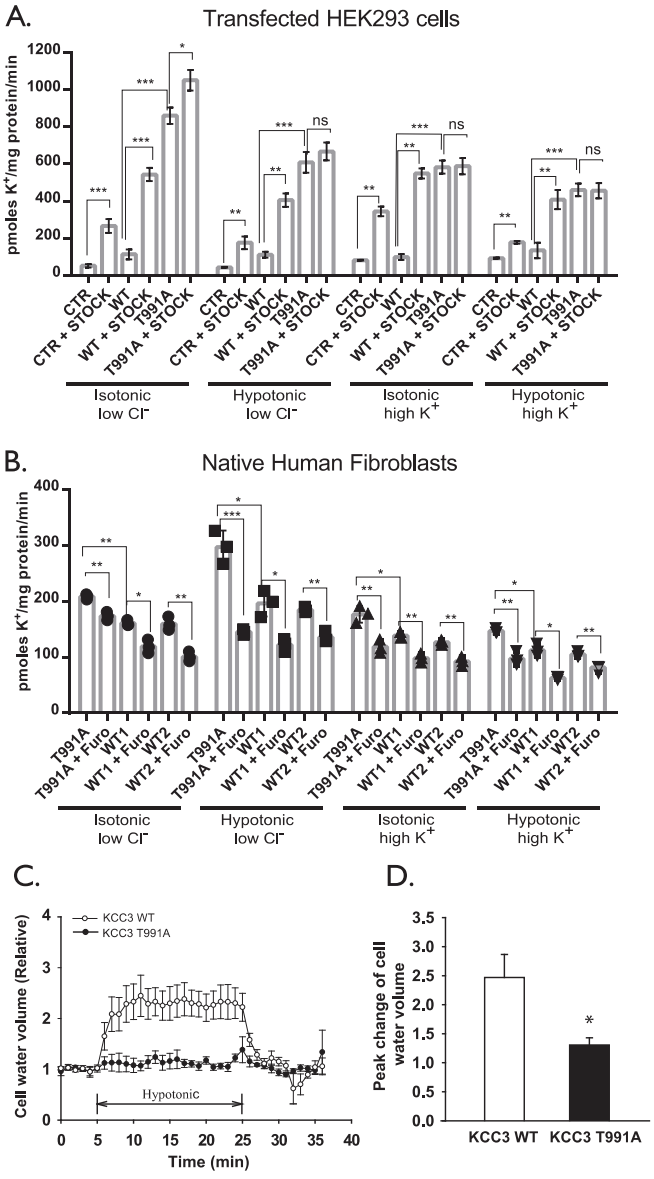
A.
Transfected HEK293 cells
pmoles K+/mg protein/min
CTR
CTR + STOCK
WT
WT + STOCK
T991A
T991A + STOCK
Isotonic low Cl-
Hypotonic low Cl-
Isotonic high K+
Hypotonic high K+
B.
Native Human Fibroblasts
pmoles K+/mg protein/min
T991A
T991A + Furo
WT1
WT1 + Furo
WT2
WT2 + Furo
Isotonic low Cl-
Hypotonic low Cl-
Isotonic high K+
Hypotonic high K+
C.
KCC3 WT
KCC3 T991A
Cell water volume (Relative)
Hypotonic
Time (min)
D.
Peak change of cell water volume
KCC3 WT
KCC3 T991A

Figure 2-4. T991A increases KCC3 activity and affects cell volume regulation in HEK293 cells and patient fibroblasts. (**A**) Transport activity of wild-type KCC3 (WT) and KCC3 T991A expressed in HEK293 cells. HEK293 cells were transfected, exposed to low Cl^- in isotonic conditions (isotonic low Cl^-), hypotonic low Cl^- conditions, high K^+ in isotonic conditions (isotonic high K^+), or hypotonic high K^+ conditions in the presence or absence of STOCK1S-50699 (STOCK, WNK-SPAK/OSR1 inhibitor), for an additional 30 min in the presence of 1 mM ouabain (Na^+/K^+-ATPase inhibitor) and 0.1 mM bumetanide (NKCC1 inhibitor), to functionally isolate KCC activity. K^+ influx is presented in pmoles K^+ per mg protein per min and plotted for both isotonic and hypotonic conditions. K^+ uptake was significantly increased upon WNK/SPAK inhibition in untransfected and transfected cells [repeated measures two-way ANOVA: $F(15, 40) = 38.43$, $P < 0.0001$]. KCC3-Thr991Ala transfected cells exhibited significantly higher activity than wild-type KCC3 in all condition [$F(5, 40) = 813.9$, $P < 0.0001$] (**B**) Activity of endogenous wild-type KCC3 (WT1 and WT2) and KCC3 T991A in human fibroblasts. Cells were exposed to the indicated conditions and then treated in the same conditions with 1 mM of furosemide (furo, a KCC inhibitor) for an additional 30 min in the presence of 1 mM ouabain and 0.1 mM bumetanide. K^+ influx was measured and analyzed as in A. Data from a single representative experiment is shown as mean ± SD. Statistical significance was determined by two-way ANOVA followed by Bonferroni post hoc tests (*, $P < 0.05$; **, $P < 0.01$; *** $P < 0.001$; ns, not significant or $P > 0.05$). Similar results were obtained in three separate experiments. (**C**) Relative change in cell water volume during acute hypotonic stress in KCC3 WT parental control fibroblasts and KCC3 T991A patient fibroblasts. Both cell types were exposed to isotonic HEPES-MEM (310 mOsm/kg H_2O), followed by hypotonic HEPES-MEM (150 mOsm/kg H_2O) for 20 min, and then isotonic HEPES-MEM for 5 min. (D) Summary data of cell volume increase. KCC3 T991A patient cells exhibited abnormal regulatory volume decrease compared to KCC3 WT cells. Data are mean ± SEM, n = 3 coverslips or experiments. *, $p = 0.02$ vs. WT.

Generation and characterization of KCC3$^{T991A/+}$ and KCC3$^{T991A/T1991A}$ mice

Using CRISPR/cas9 gene editing, we created a mouse that reproduces the T991A mutation found in the human patient (**Fig. 2-5A-D**). To demonstrate functional activation of K^+-Cl^- cotransport in this mouse, we isolated fibroblasts from mouse tails and measured K^+ influx through $^{86}Rb^+$ tracer uptake in the presence and absence of furosemide in an isotonic solution. As expected, under these conditions, the wild-type cells had very little K^+ flux, indicating very low KCC transporter activity (**Fig. 2-5E**). In contrast, we observed a high furosemide-sensitive K^+ influx in fibroblasts from KCC3-T991A heterozygous (KCC3$^{T991A/+}$) mice under these isotonic conditions, consistent with the mutation resulting in a constitutively active transporter (**Fig. 2-5E**).

We assessed motor function by accelerated rotarod test (von Horsten et al., 2003) in two cohorts of young [~ postnatal day 40 (P40) - mixed gender] mice with cohort 1 consisting of 12 wild-type and 12 KCC3-T991A heterozygote siblings KCC3$^{T991A/+}$; and cohort 2 consisting of 8 wild-type, 7 heterozygotes KCC3$^{T991A/+}$, and 7 homozygotes KCC3$^{T991A/T991A}$ siblings. In neither cohort of mice did the heterozygous mice exhibit impaired motor performance, however homozygous mice (KCC3$^{T991A/T991A}$) exhibited a significant locomotor deficit (**Fig. 5F).**

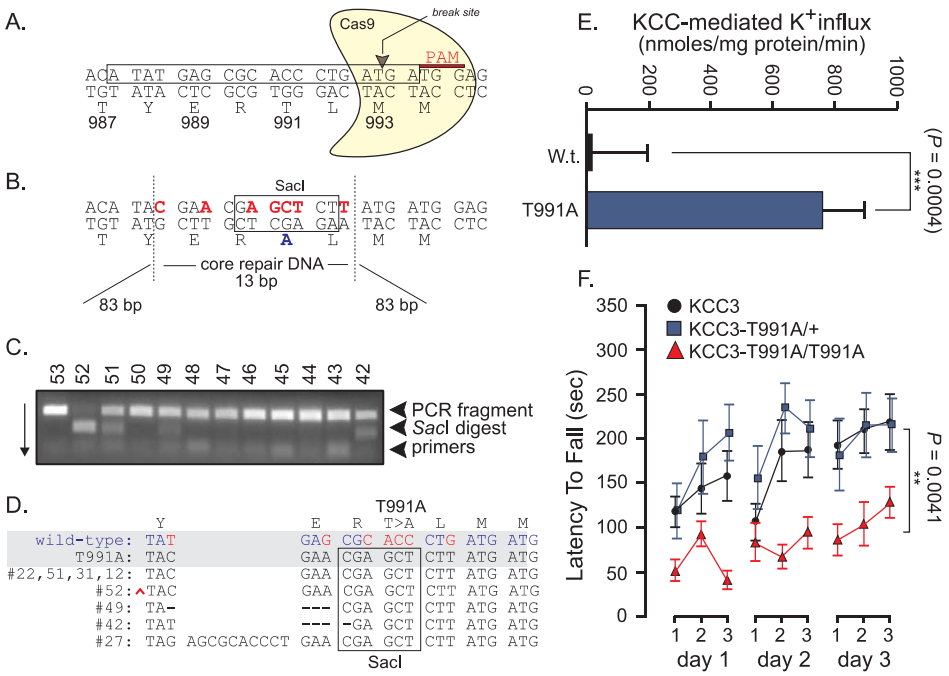

Figure 2-5. Genetically-modified KCC3-T991A mice exhibit locomotor deficits. (**A**) Portion of exon 22 of *Slc12a6* targeted for cas9 cleavage. A 20 bp (boxed) target sequence, upstream of TGG as Protospacer Adjacent Motif (PAM), was inserted into the guide RNA. (**B**) Schematic representation of a 179 bp repair fragment containing two 83 bp arms of recombination flanking a mutated 13 bp fragment. The codon change results in substitution of Thr991 into alanine and the introduction of a *Sac*I restriction site. (**C**) Sample genotyping gel showing a strong band (top) corresponding to full-length PCR fragment. Arrow shows direction of band migration. Arrowheads indicate the presence of *Sac*I-digested bands. The PCR fragment in sample #52 is completely digested, indicating that the mouse is homozygous for the *Sac*I site. (**D**) Sequence of mutant alleles from eight *Sac*I-positive mice compared to the wild-type and intended mutant allele (shaded in gray). Four mice (52, 49, 42, 27) have additional bp insertions or deletions. The ^ sign represents a 12 bp (TATGAGCGCACA) insertion upstream of the tyrosine codon. Only mice #22, 51, 31, and 12 had the desired mutation without other mutations. (**E**) K-Cl cotransport-mediated K^+ flux was measured under isosmotic conditions in fibroblasts isolated from wild-type and KCC3-T991A heterozygous mice (progeny of line #31). Flux was measured in triplicate under 0.1 mM ouabain, 20 μM bumetanide, and in the presence or absence of 2 mM furosemide. K-Cl cotransport is defined as the flux detected in the absence of furosemide minus the flux detected in the presence of furosemide. Experiment was reproduced once with similar data. (**F**) Accelerated rotarod data (7-8 mice per group, age P40, 3 trials a day for 3 days) report the time until the animal falls from the rod. KCC3-T991A wild-type, heterozygous, and homozygous mice were obtained from heterozygous breeding (line #31). Difference between genotypes was significant (two-way ANOVA: $F(2, 18) = 7.584$ $P = 0.0041$). No difference was measured between WT and T991A/+ mice in the first cohort of 24 mice (two-way ANOVA: $F(1, 22) = 3.681$, $P = 0.0681$ or ns).

We assessed motor function by accelerated rotarod test (von Horsten et al., 2003) in two cohorts of young [~ postnatal day 40 (P40) - mixed gender] mice with cohort 1 consisting of 12 wild-type and 12 KCC3-T991A heterozygote siblings $KCC3^{T991A/+}$; and cohort 2 consisting of 8 wild-type, 7 heterozygotes $KCC3^{T991A/+}$, and 7 homozygotes $KCC3^{T991A/T991A}$ siblings. In neither cohort of mice did the heterozygous mice exhibit impaired motor performance, however homozygous mice ($KCC3^{T991A/T991A}$) exhibited a significant locomotor deficit (**Fig. 5F).**

To assess overall motor coordination and fine motor movements, we utilized the balance beam task (von Horsten et al., 2003). The mice first began their trials on the standard-sized square beam (12 mm). We found a significant difference in performance between wild-type mice and homozygous mice, but no difference between heterozygous mice and wild-type mice (**Table 2-3**). During the task, wild-type and heterozygous mice quickly traversed the beam with little to no hind limb paw slips; whereas the $KCC3^{T991A/T991A}$ mice displayed a tendency to stall, indicated by the delayed time to reach the platform, and experienced multiple hind limb paw slips during their crossing (**Table 2-3**). To determine the robustness of this phenotype, we assessed the performance of the mice on a narrower 6 mm cross-sectional square beam. This size beam is considered a more difficult task for the mice, in particular for those that exhibit any limb deficits. On this beam, the wild-type and heterozygous mice continued to swiftly traverse with little to no paw slips (**Table 2-3**). However, the $KCC3^{T991A/T991A}$ mice experienced greater difficulty in crossing, with intense dragging of the hind limbs, and with multiple homozygous mice unable to complete the task.

Three out of six of the homozygous mice began traversing the beam, displaying appropriate forelimb coordination, but would immediately fall due to the dragging of their hind limbs and inability to properly place their hind limbs onto the beam in coordination with the fore limbs. We scored the mice on beam walking by adapting the scoring method of Feeny *et al*. (Feeney et al., 1982) to assign a neurological score to the mice: Score of 7 indicates that the mouse crossed the beam with no more than two paw and a score of 2 means that the mouse was unable to cross beam, but maintained horizontal balance for at least 5 seconds (see Materials and Methods for details). Overall, we observed a significant main effect of genotype on the beam walk score (**Table 2-3**). While no significant differences were observed per trial within a genotype, there was a statistically significant difference between the beam walk performance of wild-type and T991A/T991A mice (**Fig. 2-6A, Table 2-3**).

We also tested for forelimb motor deficits with the wire hang grip test (von Horsten et al., 2003). We observed no significant difference between genotypes (**Table 2-3**). While the mice were allowed to hang on the wire for 60 seconds, we observed the $KCC3^{T991A/T991A}$ mice clasping to the wire and thrashing to remain on the wire. They commonly used their hindlimbs and tail to secure themselves on the wire. Comparatively, both wild-type and $KCC3^{T991A/+}$ mice would often shift their grip to either side, but mainly used their forelimbs. Thus, although the $KCC3^{T991A/T991A}$ mice demonstrated no statistical differences in their latency to hang on the wire, we observed a unique behavior that might indicate forelimb weakness. To further assess forelimb and hind limb strength, we used the force grip assay, a

Measure	(N) per genotype	WT	T991A/+	T991A/T991A	WT vs. T991A/+	WT vs. T991A/T991A	T991A/+ vs T991A/T991A
Mass (g)	6; 7; 6	27.1 ± 1.9	31.3 ± 1.6	22.7 ± .48	P = 0.15	P = 0.14	P = 0.002
Rotarod	7; 7; 7	169 ± 11	191 ± 11	83 ± 6	P = 0.73	P = 0.02	P = 0.0045
12 mm beam (time to cross beam-sec)	6; 7; 6	6.3 ± 0.95	5 ± 0.3	16.38 ± 1.6	P = 0.73	P = 0.004	P = 0.0005
12 mm beam (paw slips)	6; 7; 6	.05 ± 0.06	.08 ± 0.06	9.9 ± 1.04	P = 0.74	P < 0.0001	P < 0.0001
6 mm beam (Failure to cross)	6; 7; 6	1 out of 6 mice in 1 of 3 trials	0	2 out of 6 mice in 2 out of 3 trials	n/a	n/a	n/a
6 mm beam (neurological score)	6; 7; 6	6.4 ± 0.33	6.6 ± 0.21	2.1 ± 0.26	P = 0.84	P < 0.0001	P < 0.0001
Grip test by wire hang (time)	6; 7; 6	27 ± 4.8	17.3 ± 3.2	38.8 ± 5.6	P = 0.55	P = 0.46	P = 0.07
Force grip test (N/g)	6; 7; 6	-0.045 ± 0.002	-0.041 ± 0.002	-0.051 ± 0.001	P = 0.85	P = 0.10	P = 0.03

Table 2-3. Size and strength properties of the engineered mice (2nd cohort).

au, arbitrary units; n/a, not applicable.

non-invasive method that uses a bar attached to a force transducer. All of the mice were first weighed to account for variability in mass versus force (**Table 2-3**). We did not detect any significant differences in weight or grip strength among the three mouse genotypes (**Fig. 2-6B, Table 2-3**).

We next assessed nerve function on the basis of the amplitude of the compound muscle action potentials (CMAPs) and the length of latencies using nerve conduction studies on the dorsal caudal tail nerve and the sciatic nerve (**Fig. 2-6C, D**). The sciatic nerve and dorsal caudal tail nerve branch provide sensory and motor innervation to the upper and lower leg and tail, respectively. A decrease in amplitude is representative of axonal loss, an increase in latency is representative of demyelination. We observed a trend toward a decreased amplitude for the sciatic nerve in heterozygous and homozygous mice compared with that of the wild-type mice, but the decrease did not reach statistical significance (**Fig. 2-6D, Table 2-4**). In contrast, we observed a significant reduction in the amplitude for motor function in the tail (**Fig. 2-6C, Table 2-4**). We also observed a statistically significant difference between wild-type and homozygous mice for the latencies in motor nerve tail conduction (**Table 2-4**).

We also assessed sensory nerve function by increasing the gain to record smaller sensory signals. Amplitude and conduction latencies measurements were made in all three genotypes. Sensory amplitudes were not statistically significantly different for either the tail or sciatic nerve for sensory measurements (**Fig. 2-6C, D, Table 2-4**), but the sensory nerve latencies tended to be higher in the $KCC3^{T991A/T1991A}$ mice compared with the wild-type and $KCC3^{T991A/+}$ mice (**Table 2-4**). **Figure 2-6E & 2-6F** show traces recorded from the

Measure	Nerve / Signal	WT	T991A/+	T991A/T991A	Mice per genotype	WT vs. T991A/+ (P value)	WT vs. T991A/T991A (P value)	T991A/+ vs T991A/T991A (P value)
Amplitude	Caudal / Sensory	265 ± 30	218 ±61	213 ± 34	6; 6; 6	P = 0.73	P = 0.68	P = 0.99
	Sciatic / Sensory	235 ± 78	192 ± 16	272 ± 77	5; 5; 6	P = 0.89	P = 0.92	P = 0.67
	Caudal / Motor	2657 ± 634	2578 ± 770	943 ± 215	5; 6; 6	P = 0.99	P = 0.14	P = 0.14
	Sciatic / Motor	6521 ± 1420	4223 ± 1118	5393 ± 1661	6; 6; 6	P = 0.50	P = 0.84	P = 0.83
Latency	Caudal / Sensory	1.58 ± 0.06	1.61 ± 0.04	1.70 ± 0.09	5; 6; 6	P = 0.95	P = 0.38	P = 0.51
	Sciatic / Sensory	1.88 ± 0.33	1.71 ± 0.36	2.11 ± 0.15	5; 5; 6	P = 0.91	P = 0.83	P = 0.58
	Caudal / Motor	3.20 ± 0.27	3.20 ± 0.53	4.80 ± 0.40	6; 6; 6	P > 0.99	P = 0.03	P = 0.03
	Sciatic / Motor	2.74 ± 0.37	2.34 ± 0.11	3.50 ± 0.48	6; 6; 6	P = 0.72	P = 0.32	P = 0.09

Table 2-4. Nerve conduction measurements in engineered mice. Sensory and motor signals were measured in dorsal caudal nerve (tail) and sciatic nerve (nerve) in wild-type (WT), heterozygous (T991A/+), and homozygous (T991A/T991A) mice. Significance was tested by one-way ANOVA followed by Tukey's Multiple Comparison Tests.

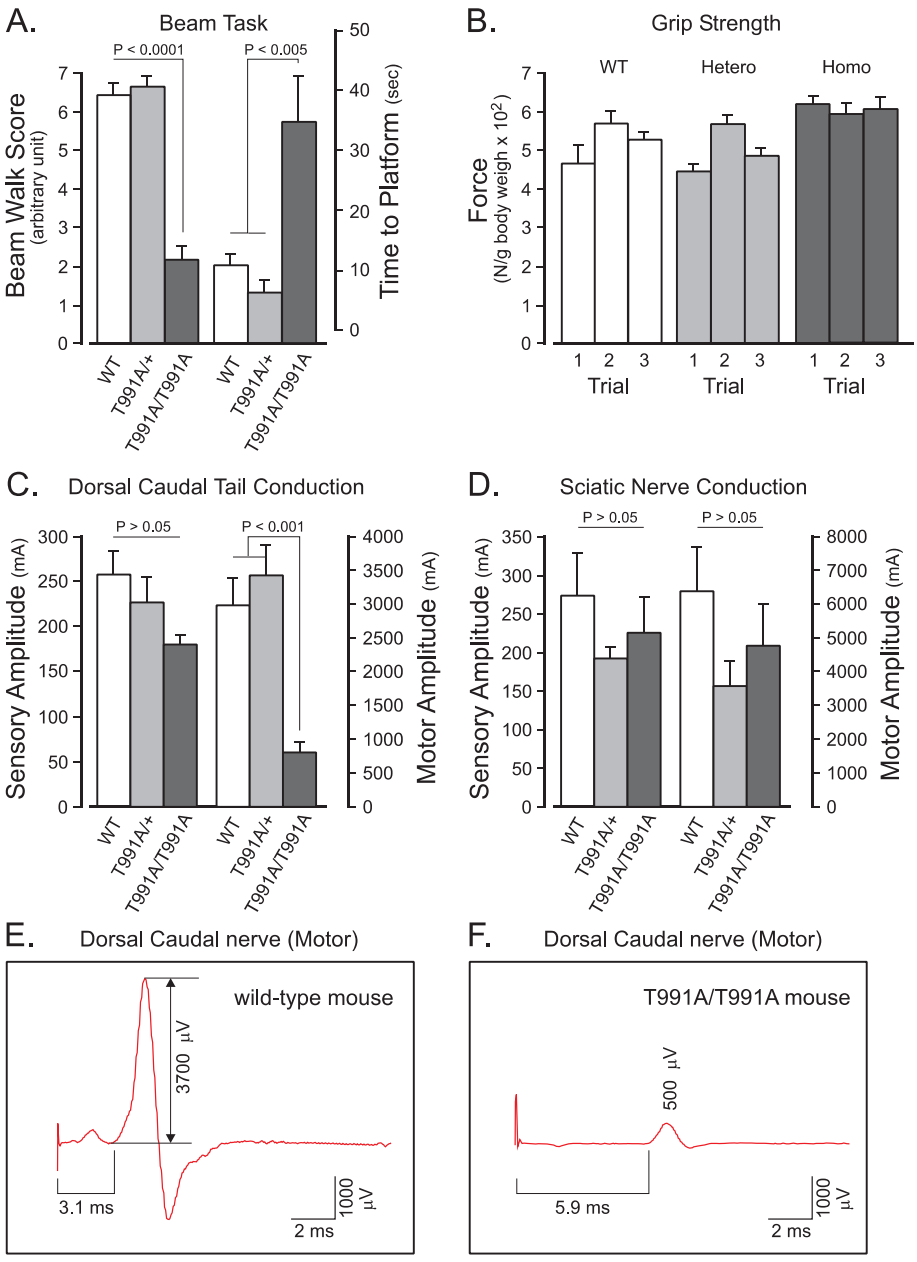
A.
Beam Task
P < 0.0001
P < 0.005
Beam Walk Score
(arbitrary unit)
Time to Platform (sec)
WT
T991A/+
T991A/T991A
B.
Grip Strength
WT
Hetero
Homo
Force
(N/g body weigh x 10²)
Trial
C.
Dorsal Caudal Tail Conduction
P > 0.05
P < 0.001
Sensory Amplitude (mA)
Motor Amplitude (mA)
D.
Sciatic Nerve Conduction
P > 0.05
P > 0.05
E.
Dorsal Caudal nerve (Motor)
wild-type mouse
3700 µV
3.1 ms
1000 µV
2 ms
F.
Dorsal Caudal nerve (Motor)
T991A/T991A mouse
500 µV
5.9 ms
1000 µV
2 ms

Figure 2-6. Genetically-modified KCC3-T991A mice exhibit hindlimb movement and nerve conduction deficits. (**A**) Response of wild-type (WT), heterozygous (T991A/+) and homozygous (T991A/T991A) mice to the 6-mm wide beam walk task. Mice were placed on the beam and allowed to cross to a safe platform. A performance score (1-7, see text) was given to each mouse (left axis). The time was also recorded (right axis). (**B**) Grip strength force was measured in all three genotypes using a bar attached to a force transducer. Data were corrected for body weight. The values (Y axis) are in Newtons (N) divided by gram of body weight. (**C**) Sensory (left axis) and motor (right axis) amplitudes of dorsal-caudal tail nerve responses to 20 or 25 mA stimuli in wild-type, heterozygous, and homozygous KCC3-T991A mice. (**D**) Sensory (left axis) and motor (right axis) amplitudes for sciatic nerves. Data were analyzed using one way ANOVA followed by Tukey's post-hoc tests, statistics are provided in **Table 2-4**. (**E-F**) Selected traces of motor conduction in dorsal caudal (tail) nerves from of wild-type and homozygous mice. The amplitude (in mV) is measured from the onset of the response peak to the top of the response peak. The latency to response is determined from the onset of the stimulus to the onset of the response peak. Tail nerves in this experiment were stimulated at 25 mA.

dorsal/caudal nerve of wild-type and KCC3$^{T991A/T1991A}$ mice with clear differences in amplitude and response latency between genotypes.

We assessed the integrity of sciatic nerves using ultrastructural analyses. Nerve fibers from wild-type and KCC3$^{T991A/T1991A}$ mice were cut transversally to observe the integrity of the myelin sheaths surrounding the axons (**Fig. 2-7A**). At high magnification (**Fig. 2-7B-2-7C** for wild-type and **2-7D-2-7E** for homozygotes), there was no abnormal pathology. At lower magnification, both genotypes exhibited fibers with double rings of myelination (**Fig. 2-7F-2-7G**). These events are indicative of improper initial contact between axons and Schwann cells (Heath, 1991), which can occur under non-pathological conditions or may indicate a neuropathology. Upon closer examination, sections of the nerves from the KCC3$^{T991A/T1991A}$ mice also showed breakage of the myelin sheaths enwrapping the axon (**Fig. 2-7H-2-7I**). This degeneration seemed to be specific to the fibers showing double myelinating Schwann cells, in that individual Schwann cells attempted re-myelination but did not appear to successfully re-myelinate. This pathology was not observed in fibers that had a single, successful Schwan cell myelination. We quantified the occurrence of this double myelination breakage by counting the number of degenerating Schwann cells that were present in relation to normal single or double myelinating Schwann cells. In 3 homozygous sections, we observed 8 fibers with double-myelin breakages and 67 adjacent normal fibers, thus representing 10% of the total number. Comparatively, this was observed only once in over 50 sections of wild-type sciatic nerve.

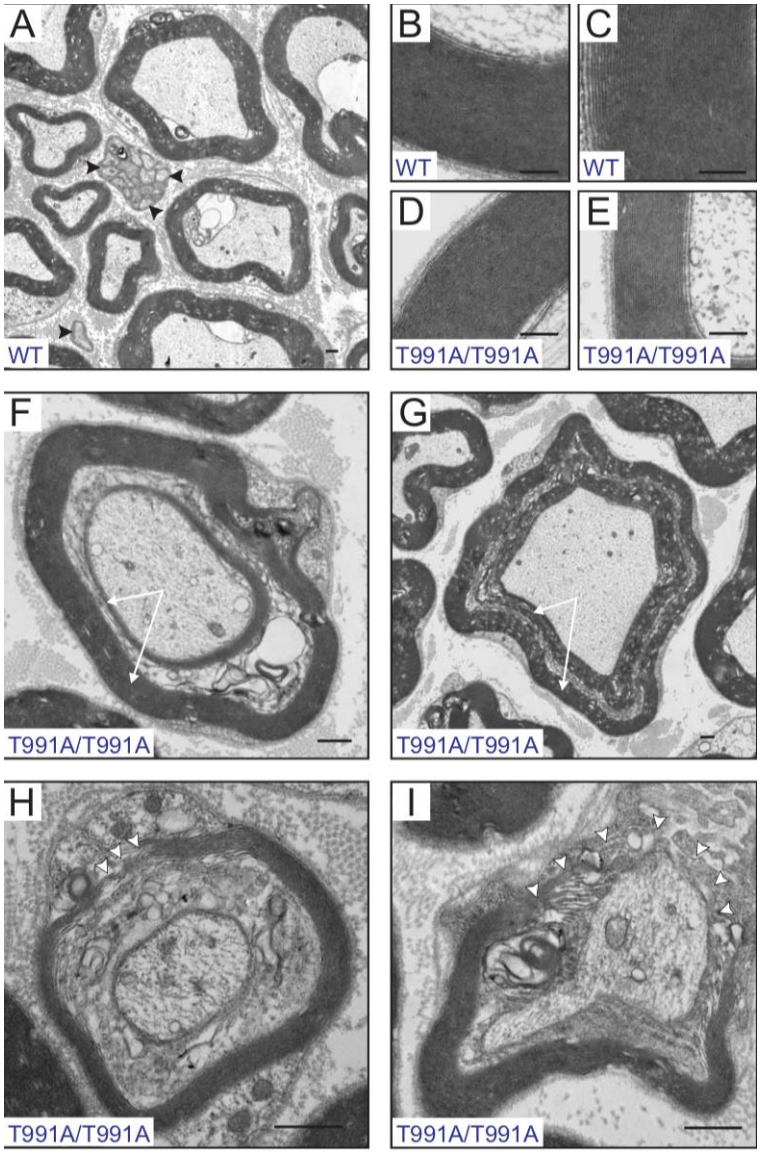

Figure 2-7. Electron micrographs of sciatic nerve fibers isolated from KCC3 wild-type and T991A mice. Dissected fragments of sciatic nerves were fixed and processed for electron microscopy. (**A**) Typical view of a transversally cut nerve fascicle (from wild-type mouse) showing a majority of myelinated fibers and a few unmyelinated fibers (arrowheads). (**B-C**) Higher magnification of wild-type fibers showing packed myelin sheaths. (**D-E**) Similar views from homozygous T991A/T991A nerves. (**F-G**) Double myelination pathology observed in nerves from T991A/T991A mice. (**H-I**) Breakage in myelin observed in nerves fromT991A/T991A mice. All bars are 500 nm.

Discussion

Our report presents the first human with a GOF mutation in KCC3, resulting from *de novo* substitution of Ala for Thr at amino acid position 991. This patient has an early-onset, severe, and progressive motor-predominant neuropathy. The regulated phosphorylation of Thr991 (in concert with Thr1048) is a key mechanism controlling KCC3 activity in heterologous expression studies (De Los Heros et al., 2014; Rinehart et al., 2009). KCC3 is normally inactive in isotonic conditions due to inhibitory phosphorylation at Thr^{991} and Thr^{1048} (De Los Heros et al., 2014; Rinehart et al., 2009). Cell swelling causes rapid dephosphorylation of these sites by protein phosphatase-1 (PP1) and PP2A to increase KCC3 activity (De Los Heros et al., 2014; Rinehart et al., 2009). When mutant KCC3 that cannot be phosphorylated at either Thr^{991} or Thr^{1048} due to alanine substitution is expressed in cultured cells, the mutant KCC3 exhibits constitutive activity (De Los Heros et al., 2014; Rinehart et al., 2009) Computer modeling predicted a close proximity of Thr^{991} to Thr^{1048} in KCC3 (**Fig. 2-2D**). Our patient's KCC3 T991A mutation recapitulates the constitutively active function found in KCC3 mutated and expressed in cultured cells. Furthermore, discovery of this mutation in human and reproducing the mutation in mouse provided a unique window to gain insight into the role of KCC3 function of the nervous system.

Our combined clinical, genetic, neurobehavioral, and physiological results implicate this *de novo* gain-of-function (GOF) mutation in KCC3 as the cause of the patient's progressive motor-predominant neuropathy. We have not yet identified additional alleles with this mutation in the human population, including patients suffering from peripheral nerve

disease. On the basis of the known importance of Thr^{991} in the regulation of KCC3 activity and the data we presented, we propose that this heterozygous mutation causes the symptoms of the disease: (i) this mutation is *de novo* and extremely rare (that is, this variant is not present in the patient's parents or the general unaffected population, as expected for an dominantly acting pathogenic allele); (ii) Thr^{991} is conserved in all KCC family members across evolution; (iii) modeling programs predict high pathogenicity scores for T991A; (iv) reversible phosphorylation of Thr^{991} is a key mechanism limiting KCC3 activity and regulating cell volume homeostasis (De Los Heros et al., 2014; Rinehart et al., 2009); (v) KCC3 activity is high and cell volume homeostasis is defective in the patient's fibroblasts, paralleling effects of this mutant protein expressed in HEK293 cells; and (vi) a homozygous mouse model of the T991A mutation exhibits motor nerve conduction and locomotor deficits. The importance of KCC3 in the nervous system is also supported by the abnormal, pathogenic central and peripheral phenotypes associated with KCC3 LOF in both humans and mice (Byun & Delpire, 2007; Howard, Mount, et al., 2002; Shekarabi et al., 2012).

Although our data with the $KCC3^{T991A/T991A}$ mice indicated that the pathology predominantly affected the hindquarters (tail and hindlimbs), we observed that homozygous mice required all 4 limbs with or without the tail to remain hanging on the wire. This indicates some forelimb weakness. In contrast to the human patient, we only observed locomotor deficits in the homozygous state in mice. Multiple precedents exist for dominant mutations causing human diseases, which can be only recapitulated in the homozygote state in the mouse. Such an example is lamin A (N195K), which in humans causes dilated

cardiomyopathy with conduction system disease (Heath, 1991) in the heterozygous condition but in mice requires homozygous loss to be pathogenic (Mounkes, Kozlov, Rottman, & Stewart, 2005). Differences between two species are not unexpected. While there is overall conservation in proteins and function between mouse and human, the precise contribution of each protein to a function is likely to be species-specific, as some factors in one species might better compensate for the loss of a protein than in the other species.

Importantly, our patient's clinical syndrome appears distinct from ACCPN, which features severe brain pathology and both sensory and motor peripheral neuropathies (nearly all ACCPN patients lack electrophysiological sensory responses and have only mildly reduced and slowed motor responses). ACCPN is due to recessive LOF KCC3 mutations commonly found in French Canadians (Boettger et al., 2003; Howard, Mount, et al., 2002; Salin-Cantegrel et al., 2007; Uyanik et al., 2006). In contrast, our patient has an early onset and severe predominantly motor peripheral neuropathy, lacks clinical or radiographic brain pathology, and harbors a *de novo* GOF mutation in KCC3. Although the neurological and physiological examination of the patient indicated the neuropathy to be predominantly affecting motor nerves, evidence from nerve conduction studies showed that peripheral sensory nerves are also involved, albeit to a lesser extent. We also detected a trend towards decreased sensory function in the nerves of the $KCC3^{T991A/T991A}$ mice. Interestingly, ACCPN patients and KCC3 KO mice exhibit axonal swelling of spinal nerve roots and cranial nerves (Boettger et al., 2001) This finding, our results with the T991A mutant patient and mice, along with the knowledge that Thr^{991} is dephosphorylated in response to cell swelling to

trigger regulatory volume decrease, suggests that either excessive (for example, T991A GOF mutation) or insufficient KCC3 activity (for example, the LOF mutation that causes ACCPN) – dysregulated KCC3 activity – results in peripheral nerve dysfunction, although with somewhat different consequences (**Fig. 2-8**). We show in human cells and in mice that KCC3 T991A abolishes the WNK1 kinase-dependent inhibitory phosphorylation at this site, resulting in a constitutively activated species of the transporter (**Fig. 2-4 & 2-5**). Dysregulation and constitutive transporter activation likely contribute to a failure of cell volume homeostasis in central or peripheral neurons with possible secondary axonal degeneration or loss. Consistent with this is the finding that KCC3-T991A patient cells exhibited significantly diminished cell swelling in response to acute hypotonic stress compared to that of the KCC3-WT parental cells. We propose this molecular mechanism defines a novel form of CMT type 2. Phosphorylation-dependent regulation of KCC3 could also affect and thus alter neuronal excitability. In central neurons, control of intracellular Cl^- concentrations is mostly accomplished by the related transporter KCC2, which is restricted to the brain and spinal cord (Blaesse et al., 2009; Kahle et al., 2013; Kahle & Delpire, 2016; Kahle et al., 2016; Kaila et al., 2014), but evidence exists for KCC2/KCC3 co-localization (Boettger et al., 2003; Pearson et al., 2001; Shekarabi et al., 2011), possible heterodimerization (Ding et al., 2013), and co-regulation of neuronal $[Cl^-]_i$ (Boettger et al., 2003) Whether the primary defect of the T991A mutation is dysregulation of cellular volume homeostasis or altered neuronal excitability due to altered intracellular Cl^- concentrations remains to be established.

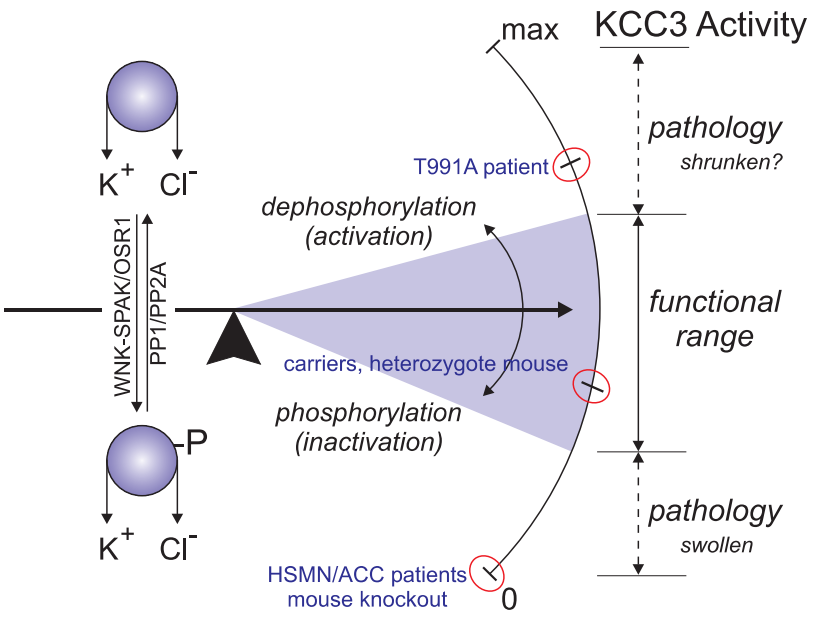

Figure 2-8. Finely tuned KCC3 activity is required for structure and function of the human peripheral nervous system (PNS). KCC3 activity, schematically represented on a scale from none (0) to maximal (max) activity, is contingent on the amount of KCC3 and a balance between the phosphorylated (inhibited) and dephosphorylated (activated) species of KCC3 in the neuronal plasma membrane. Insufficient KCC3 (for example as occurs in ACCPN, OMIM # 218000) due to LOF KCC3 mutations or as seen in KCC3-knockout mice) or excessive, unregulated KCC3 activity (as in the patient described here with a *de novo* GOF KCC3 T991A mutation that abolishes a WNK1 kinase-dependent inhibitory phosphorylation event) results in severe and progressive peripheral axonal neuropathy with secondary demyelinating features, likely from impaired cell volume regulation and subsequent neurodegeneration. Normal humans and mice, as well as ACCPN carriers and KCC3 heterozygous knockout mice, fall within a "functional range" that is free of significant pathology.

The precise mechanism by which KCC3 affects peripheral nerve integrity is still unknown. Disruption in the transport properties of the cotransporter are certainly the first and most logical explanation for the disorder and it seems now that both LOF and GOF of KCC3 lead to peripheral nerve disease. At this point, however, we cannot dismiss the possibility that substitution of Thr991 into alanine leads to pathologies through mechanisms that are unrelated to the transport function of the cotransporter, though this seems very unlikely given the known role of this residue for transport function. For instance, membrane proteins are not expressed in isolation but interact with many other proteins and disruption of the C-terminus of KCC3 might affect one of these interactions. Similarly, the central versus peripheral origin of the disorder has yet to be settled. The neuropathy/locomotor phenotype observed in the global KCC3 knockout mouse can be recapitulated by driving KCC3 deletion in neurons (Shekarabi et al., 2012) and more specifically in proprioceptive sensory neurons (Ding & Delpire, 2014). Furthermore, severe pathology is observed in parvalbumin-positive sensory fibers in both global and parvalbumin-specific KCC3 knockout mice. Thus, it is clear that KCC3 expression in sensory neurons is critical for PNS integrity. It remains to be tested whether a similar neuropathy/locomotor phenotype can be elicited by driving KCC3 deletion in motorneurons. If that is the case, we would conclude that both CNS and PNS neurons then contribute to the neuropathy. In the contrary, this would suggest that motor deficits observed in ACCPN patients and KCC3 KO mice are secondary to the sensory deficit.

It is also possible that loss of KCC3 function affects predominantly sensory neurons, whereas gain of KCC3 function affects mainly motor neurons. Because the PNS lacks KCC2

expression, PNS neurons would be particularly dependent on KCC3. PNS neurons have a relatively higher resting concentration of intracellular Cl^- compared with CNS (Alvarez-Leefmans et al., 1988; Sung et al., 2000). The presence of aquaporin water channels in PNS, but not CNS, neurons may also make PNS neurons more dependent on the volume homeostatic function of KCC3 (Kahle et al., 2015). In motorneurons, both KCC2 and KCC3 would be expressed with KCC2 function being predominant in lowering the intracellular Cl^- concentration (Boulenguez et al., 2010; Kahle & Delpire, 2016; Stil et al., 2011). Constitutive or unregulated KCC3 activity in the motorneurons would likely upset the balance of KCC2 and KCC3 function, enhancing Cl^- extrusion and GABA inhibition. Enhanced inhibition could negatively affect motor nerve conduction, thereby contributing to the neuropathy. Additional work will be required to fully establish all the neuronal cell types involved in the KCC3-mediated neuropathies.

Recognition of KCC3-mediated dysregulation as a disease mechanism identifies the transporter as a potential therapeutic target. KCC3, including the T991A mutant, is sensitive to inhibition by the loop diuretic furosemide, as we showed in our patient's fibroblasts. Identification of additional patients with activating KCC3 mutations may enable their treatment with clinically approved drugs. Dysfunctional kinase-mediated KCC3 regulation may also contribute to other forms of inherited or acquired neuropathies. For example, these findings may have relevance for diabetic peripheral neuropathy, a condition associated with accumulation of the intracellular organic osmolytes: sorbitol (Oates, 2002), which is a sugar alcohol derived from fruit, corn, and other vegetables that is slowly metabolized in humans

and is used as an artificial sweetener. Sorbitol is also an activator of WNK1 activity (Zagórska et al., 2007).

Conclusions

A T991A gain-of-function of KCC3 leads to the same peripheral neuropathy phenotype observed in patients with loss-of-function. This unique patient does not exhibit any cognitive abnormalities and has a fully developed corpus callosum. The T991A mouse model accurately recapitulates the locomotor phenotype observed in the patient, and demonstrates similar abnormal responses in nerve conduction studies. Our study concludes that KCC3 must exist in a homeostatic range in order to prevent disease.

CHAPTER 3

A Role for KCC3 in Maintaining Cell volume of Peripheral Nerve Fibers

Introduction

In the early 1970s, Andermann and colleagues first described an autosomal recessive anterior horn disease associated with agenesis of the corpus callosum (ACC) in a pair of brothers (Andermann et al., 1972). These siblings were brachycephalic and presented with partial syndactyly of the toes, poor muscle bulk, and generalized hypotonia. These brothers also suffered from severe intellectual disability as a result of their ACC. Initially, it was thought that these boys' parents may be closely related, but there was no evidence to support this claim. However, their parents were from Charlevoix and Saguenay Lac-Saint-Jean, regions located outside of Quebec City, known for their high consanguinity rate. Although it was unclear which gene was causing the disease or if this was actually the correct diagnosis, it was evident that both parents must be carriers of a mutated allele for both siblings to develop the disease. In 1996, Casaubon and colleagues mapped the disorder to human chromosome 15q13-q15 using a set of 120 microsatellite DNA markers in 14 families (Casaubon et al., 1996; Howard, Mount, et al., 2002). A few years later, the mapping of *SLC12A6*, the gene encoding the K-Cl cotransporter 3 (KCC3), to human chromosome 15q14 prompted geneticists to sequence the exons of individuals in Andermann syndrome families (Howard, Mount, et al., 2002). It is now well documented that a genetic mutation in KCC3 (2436delG, Thr813fsX813) causes a loss of function (LOF) resulting in Hereditary Motor Sensory

Neuropathy with Agenesis of the Corpus Callosum (HMSN/ACC) in this Canadian population (Howard, Mount, et al., 2002). Note HMSN/ACC in this population is also referred to as Agenesis of the Corpus Callosum with Peripheral Neuropathy (ACCPN) or sometimes Andermann Syndrome. For this review we will use the term HMSN/ACC. Other non-French Canadian families in other world regions were later identified with additional KCC3 LOF mutations (Uyanik et al., 2006).

KCC3 functions to efflux K^+ and Cl^-, forcing water molecules out of the cell. Although there have been several insights in understanding the presentation and pathology of HMSN/ACC using mouse models (Boettger et al., 2003; Byun & Delpire, 2007) it is still unclear how a disruption in KCC3 ultimately leads to HMSN/ACC. Interestingly, ongoing research on the role of KCC3 in disease has become more complex with the new human case of a gain of function (GOF) mutation in the cotransporter. The individual with the GOF mutation also presents with peripheral neuropathy (PN) but no corpus callosum nor cognitive abnormalities (Kahle *et al.* 2016). Although both of these diseases are rare, it is important to understand the role of KCC3 in both diseased and non-diseased states to shed light on related neuropathies and on the biology of KCC3. As such, the content of this review will focus on the biology and function of KCC3 as it relates to human health, as well as questioning its postulated role relative to isoforms of KCC3 and its transporter family.

The cloning of KCC3

When KCC3 was initially cloned, members of the *SLC12A* gene family were conventionally named in order of discovery. However, two unrelated groups were working simultaneously to clone KCC3 and KCC4, and the names and identities of these two co-transporters became confusing. To clarify the literature, we will provide a brief timeline of how these two transporters were discovered.

In 1999, the first paper published by Hiki and colleagues described a novel K-Cl cotransporter from human umbilical vein endothelial cells (Hiki et al., 1999). Since previous reports had already characterized two K-Cl cotransporters: KCC1 and KCC2 (Gillen et al., 1996; J. Payne et al., 1996) they named this transporter KCC3. Concurrently however, Mount and colleagues, unaware of the upcoming publication by Hiki, were also publishing a paper that reported the cloning of two new K-Cl cotransporters from human and mouse: KCC3 and KCC4 (Mount et al., 1999). Unfortunately, the KCC3 in the Hiki paper was not the same KCC3 of the Mount paper, but was actually KCC4. After the release of the Hiki paper, David Mount added a note in proof where he indicated that what was termed KCC4 in the paper should be read as KCC3, and vice-versa, what was termed KCC3 should be called KCC4 (Mount et al., 1999; Race et al., 1999) and the sequences were submitted with corrected names to NCBI. Following these two initial releases, a third paper by Race and coworkers also reported the cloning and characterization of KCC3 from a human placenta cDNA library (Race et al., 1999). In contrast to the KCC3 isoform cloned by Mount and Race which is driven by the most upstream gene promoter and contains exon 1a, Hiki's KCC3 originated

from a more proximal promoter and contained exon 1b (Race et al., 1999). KCC3a is mostly expressed in brain, whereas KCC3b is expressed in kidney (Pearson et al., 2001).

KCC3: Its function and expression

KCC3 is a member of the cation-chloride cotransporters (CCC) or *SLC12A* gene family. This is a family of electroneutral cotransporters that regulate the influx and efflux of ions across plasma membranes for trans-epithelial ion transport, maintaining intracellular Cl^- ($[Cl^-]_i$), and maintaining or regulating cell volume (Cruz-Rangel et al., 2011). This *SLC12A* gene family consists of Na^+-dependent and Na^+-independent transporters **(Figure 3- 1)**, all of which contain 12 transmembrane domains separating large intracellular termini. Two *SLC12A* members, CCC8 and CCC9, are proteins with no defined function. CCC9 might consist of 11 transmembrane domains and a possible extracellular C-terminus (Gerardo Gamba, 2005). The intracellular termini of SLC12A cotransporters contain important sites of phosphorylation involved in transport activation or inactivation. KCC3 has two major phosphorylation sites, T1048 and T991, that are located in the carboxyl-terminus (Rinehart et al., 2009). The major regulators of the cation-chloride cotransporters are the WNK-SPAK/OSR1 kinases (With No lysine (K), SPS1-related Proline/Alanine Kinase, Oxidative Stress-Responsive kinase 1) (De Los Heros et al., 2014; Moriguchi et al., 2005; Thastrup et al., 2012). The WNK kinases (WNK1-4) phosphorylate SPAK/OSR1, which in turn, phosphorylate key regulatory sites in KCC3 and in the N-terminal tail of NKCC1 (Hannemann & Flatman, 2011). These kinases have opposite effects on the Na^+-dependent and Na^+-independent cotransporters to modulate

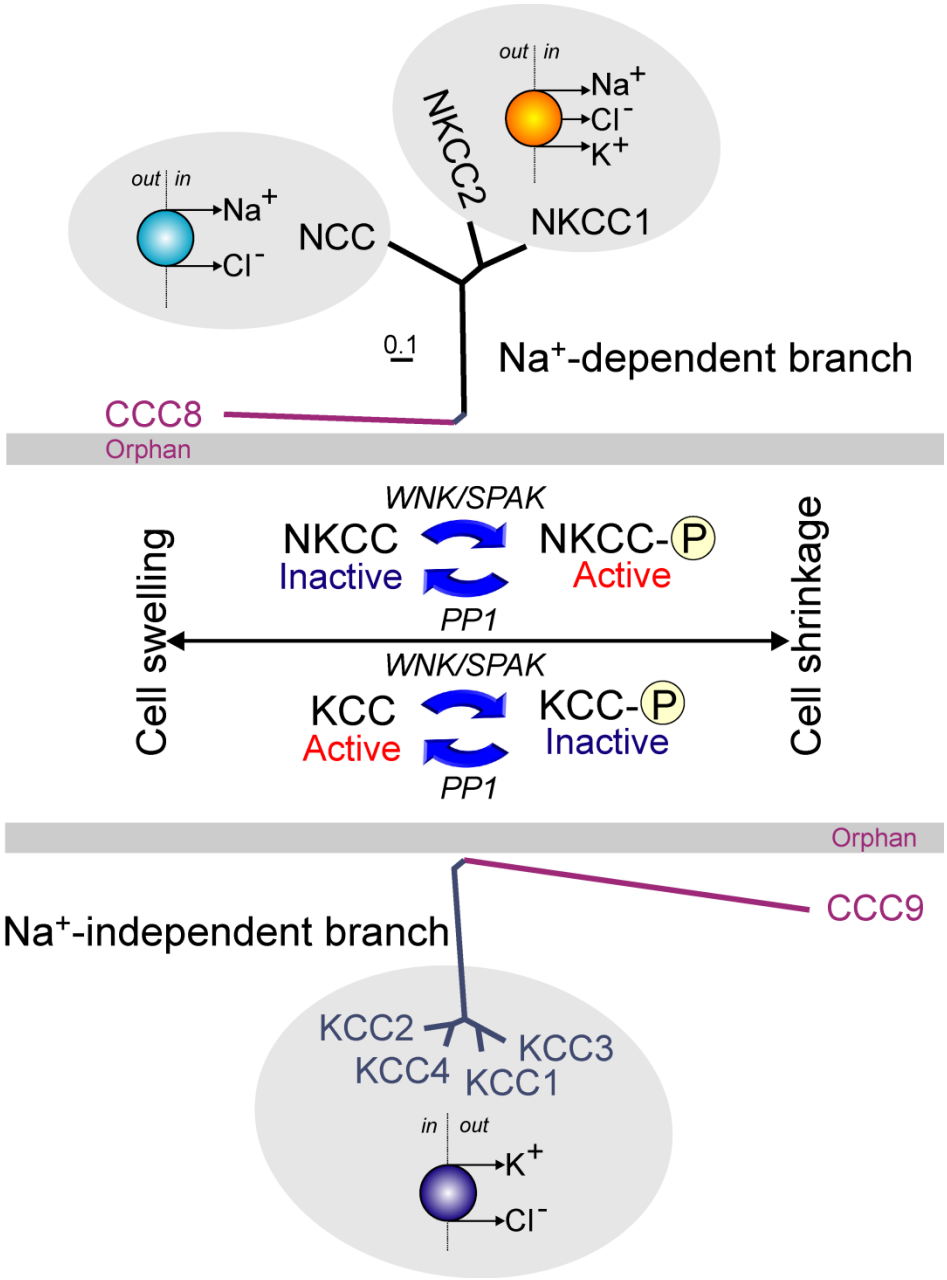

Figure 3-5. Regulation of cation-chloride cotransporters. The sodium dependent branch works to influx Na^+, Cl^-, and K^+ (NKCC) or Na^+ and Cl^- (NCC) into the cell. The sodium independent branch extrudes K^+ and Cl^- (KCC) from the cell.

ion transport and regulate cell volume. Specifically, phosphorylation of these active sites inactivates KCC3 and activates NKCC1, whereas conversely, dephosphorylation activates KCC3 and inhibits NKCC1 (**Figure 3-1**).

As a part of the Na^+-independent branch, KCC3 functions to transport one K^+ ion with one Cl^- ion out of the cell per transport cycle. This tightly coupled transport is electroneutral, meaning it does not directly affect neuronal membrane potential. K-Cl cotransport also drives the movement of obligatory water molecules. Whether water moves through the cotransporters or through other pathways is still a matter of debate. However, KCC4 is estimated to transport 500 water molecules per $1K^+$ and $1Cl^-$ (per cycle) (MacAulay, Hamann, & Zeuthen, 2004). Following cell swelling, K-Cl cotransport is activated, leads to the loss of K-Cl and water, thereby allowing the cell to regain its volume. In neurons of the central nervous system (CNS) and peripheral nervous system (PNS), KCC3 is thought to maintain cell volume. The cotransporter might also participate in the regulation of intracellular chloride $[Cl]_i$, although KCC2 predominately accomplishes this latter function in central neurons (DeFazio, Keros, Quick, & Hablitz, 2000; Pellegrino et al., 2011).

Initial localization of KCC3 was done in the mouse nervous system. KCC3 is expressed in multiple CNS and PNS cell types but at varying time points throughout development and through adulthood **(Table 3-1)**. In adulthood, KCC3 is widely expressed in the CNS (Pearson et al., 2001), but highest KCC3 expression has been documented in the amygdala and hypothalamus. In the hippocampus, KCC3 was also found localized in interneurons (Shekarabi et al., 2011). These data are consistent with *in situ* hybridization data

in the Allen mouse brain atlas, which show intense antisense oligo staining in neuronal layers of cortical, hippocampal and cerebellar structures. In the Allen spinal cord atlas, positive staining is seen in both dorsal and ventral grey matter. As for the adult PNS, KCC3 is expressed in extremely low amounts in the sciatic nerve and dorsal root ganglion (DRG) (Byun & Delpire, 2007); KCC3 is also expressed in parvalbumin positive (PV+) sensory neurons (Ding & Delpire, 2014). Parvalbumin is expressed in approximately 15-30% of sensory neurons (Zachařová & Paleček, 2009). In a first study published in 2001, we failed to detect KCC3 by Western blot analysis in isolated adult mouse DRG and peripheral nerves (Pearson et al., 2001). However, we later detected KCC3 transcript in DRG neurons isolated from P30 and adult rats using RT-PCR (Byun & Delpire, 2007). Interestingly, through RT-PCR and Western blot analysis of microsomal (or membrane) proteins, we detected KCC3 expression in early postnatal development (P2-P14) but not in adult in sciatic nerves.

The relatively broad expression of KCC3 throughout the brain, spinal cord, and periphery indicates that the cotransporter must play a key physiological role in neurons. Because the activity of the cotransporter is silent under isotonic conditions and activated upon cell swelling, we propose that this role is related to cell volume homeostasis. As shown below, this idea is strengthened by observations under disease conditions. Whether all neurons or only a subset of neurons expresses the cotransporter and whether KCC3 function is critical during the entire life of a neuron or during a defined developmental period are questions that remain to be answered.

	PNS	CNS
Adult	Dorsal Root Ganglion (Byun & Delpire, 2007) Nodes of Ranvier- Schwann Cell (Sun et al., 2010)	Hippocampus, Choroid Plexus, Piriform Cortex, Cerebellum (Allen Brain Atlas, Rouzic et al., 2006) Brainstem, spinal cord (Allen Brain Atlas, Pearson et al., 2001) Hippocampal interneurons (Shekarabi et al., 2011)
Postnatal	Sciatic nerve, Dorsal root ganglia (Byun & Delpire, 2007)	

Table 3-1 Variation of KCC3 expression: In the adult mouse CNS, KCC 3 expression appears in multiple structures/regions. In the adult PNS, KCC3 expression has thus far been observed in DRG and nodes of Ranvier. Post-natal expression of KCC3 has been observed in the sciatic nerve and DRG, but KCC3 expression has not been studied extensively in post-natal PNS.

Mapping of human KCC3

Mount and colleagues established that the *SLC12A6* gene maps to human chromosome 15q14 (Mount et al., 1999) within the 5 cM (5q13-15) interval that contains the gene(s) responsible for HMSN/ACC (Casaubon et al., 1996). As aforementioned, this led to the sequencing of the *SLC12A6* exons from HMSN/ACC patients and the discovery that KCC3 mutations are responsible for HMSN/ACC (Howard, Mount, et al., 2002). The affected individuals carry a homozygous deletion of a guanine in exon 18. This deletion (2436delG) leads to a frame shift and premature termination of the open reading frame, ultimately resulting in a loss of the KCC3-mediated transport. Interestingly, one individual was reported to be a compound heterozygote, carrying the 2436delG mutation in exon 18 in one allele and an additional mutation in exon 11 (1584_1585delCTinsG) that results in KCC3 LOF and therefore HMSN/ACC (Howard, Mount, et al., 2002).

KCC3 in disease

HMSN/ACC

HMSN/ACC is an autosomal recessive disease since both parents must be carriers of the 2436delG (Thr813fsX813) mutated allele. HMSN/ACC, although rare worldwide, exists at a frequency of 1 in 2,117 with approximately 1 in 20 individuals being carriers in the Charlevoix and Saguenay-Lac-Saint-Jean regions of Quebec (Howard, Mount, et al., 2002). Thus, it is likely that HMSN/ACC occurred as consequence of a founder mutation (Casaubon et al., 1996).

Defining characteristics of HMSN/ACC include a severe, progressive motor and sensory neuropathy with delays in motor milestones, severe intellectual disability, generalized hypotonia, areflexia, and most individuals losing their ability to walk and become bedridden (Casaubon et al., 1996; Howard, Mount, et al., 2002). What is most peculiar about HMSN/ACC is that individuals can range in agenesis severity, i.e., some individuals present with severe agenesis and no corpus callosum, while affected siblings have a partial or normal corpus callosum.

Post-mortem studies have attempted to classify whether HMSN/ACC is mainly an axonal or demyelinating neuropathy. It is important to note that HMSN/ACC is considered a sensorimotor neuropathy since patients exhibit severe locomotor and sensory deficits to the same degree (Auer et al., 2016). In the most recent post-mortem study examining eight patients with HMSN/ACC, Auer and colleagues discovered axonomas in both the CNS and PNS (Auer et al., 2016). Axonomas are small regenerative clusters of axons. The presence of axonomas usually indicates that the axon itself is degenerating as the cluster itself will remain around sites of lesion (Auer et al., 2016; J. Sung, 1987), hence defining HMSN/ACC as an axonopathy as opposed to a demyelinating neuropathy.

Interestingly, these studies have also revealed that on average, the brain mass of those with KCC3 LOF was significantly greater when compared to matched controls (Auer et al., 2016). This is a significant finding as it indicates that the brain as a whole is accumulating fluid or neuronal debris (Auer et al., 2016). This observation is consistent with the idea that KCC3 is involved in regulating cell volume. Post-mortem tissue studies have also pointed to

the fact that tissue swelling is often a pathological hallmark of KCC3-mediated disease in humans and mice. For instance, post-mortem reports have also noted swelling of cranial nerve fibers three and seven and of dorsal and ventral roots (A Larbrisseau, Vanasse, Brochu, & Jasmin, 1984; J Mathieu, Bédard, Prévost, & Langevin, 1990). In a global KCC3 knockout (KO) mouse, fluid filled axons in the sciatic nerves were observed (Byun & Delpire, 2007). A study published recently examined the nodes of Ranvier in the KCC3 knockout mouse; nodes of Ranvier are myelin sheath gaps that are located along a myelinated axon (Sun et al., 2016). Vacuoles and occasional myelin debris were observed by electron microscopy in the paranodal loops and microvilli of KCC3 KO sciatic nerve fibers. The paranodal loops with large vacuoles displayed detachment from the axon at the node with axon/Schwann cell adhesion underneath being damaged. Note that such damage was absent in the axon/Schwann cell adhesion at the juxtaparanode. These structural defects were shown to affect axon excitability (Sun et al., 2016). The origin of this pathology is difficult to assess. One possibility would be that KCC3 plays a role at the node of Ranvier itself and its disruption causes functional and morphological defects. There is evidence that the cotransporter is expressed at the node, outer mesaxon, and perinuclear nodes in Schwann cells but remains in absent in Schmidt Lanterman incisures (Sun, Lin, Tzeng, Delpire, & Shen, 2010). Interestingly, KCC4 expression is also found in the Schwann cell body and mesaxons (Karadsheh et al., 2004), but the knockout of KCC4 does not result in locomotor deficits (Boettger et al., 2002). Thus, it is possible that the pathology presents itself at the nodes

because these structures are finely organized and the presence of vacuoles and general axonal swelling might be sufficient to disrupt them.

Mouse models of HMSN/ACC

In efforts to understand HMSN/ACC and the biology of KCC3, multiple research groups have utilized mouse models that have recapitulated the HMSN/ACC-like phenotype **(Table 3-2)**. In 2002, we created the first global knockout of KCC3 by targeting exon 3, a 95 bp exon, which encodes a fragment of the NH_2-terminal tail of the cotransporter (Howard, Mount, et al., 2002). We were able to confirm early motor and locomotor dysfunction in the homozygous mouse model; heterozygous mice displayed no abnormalities. Gross anatomical analysis of the brain revealed no agenesis of the corpus callosum in either KCC3 heterozygous or homozygous mice (Howard, Mount, et al., 2002). Following this first report, Boettger and colleagues reported a KCC3 knockout mouse model where they targeted exons 3 and 4. In addition to the locomotor phenotype, they noted that their mice displayed deafness late in their lifespan, hypertension, as well as a reduced threshold for epileptic seizures (Boettger et al., 2003). They also observed that hippocampal pyramidal cells from KCC3 KO mice displayed an inability to restore their basal cell volume after swelling. Their data showing a shift in the chloride reversal potential (although small compared to the shift observed in the KCC2 knockout) and the inability to volume regulate are consistent with the basic transport function of KCC3 (i.e. intracellular chloride and cell volume homeostasis). Hypertension was later measured and confirmed in the first mouse model by using telemetric catheters to

continuously measure heart rate and mean arterial pressure in both light and dark phases. KCC3 deficient mice were characterized by a marked hypertension (30 mm Hg above controls) during both diurnal and nocturnal periods (N. C. Adragna et al., 2004). Hypertension in the KCC3 knockout mouse is neurogenic in origin (M. B. Rust et al., 2006). The main question that persists is how a disruption in KCC3 function, or rather, disruption in maintenance of cell volume and/or intracellular chloride lead to CNS deficits, nerve pathology and peripheral neuropathy.

References	KCC3 disruption	Behavior observed	Tissue pathology
Howard et al., 2002	Removal of exon 3: loss of function	- Dragging of hind limbs - Severe locomotor deficits - Defective paired pulse inhibition	- Hypomyelination - Axonal degeneration and swelling
Boettger et al., 2002	Disruption in open reading frame (exon 3): Global LOF of KCC3	- Severe locomotor deficits - Reduced seizure threshold - Deafness - Hypertensive	- Hypomyelination - Degenerating axons
Shekarabi et al, 2012	Deletion of Exon 18: Global LOF	- Dragging of hind limbs - Severe locomotor deficits	- Axon degeneration - Hypomyelination - Axonal swelling - Decreased brain masses
	Exon 18: KCC3 LOF in synapsin 1-expressing neurons		
Ding & Delpire, 2014	Exon 7: KCC3 LOF in Parvalbumin neurons	- Severe locomotor deficits - Hyperactivity	Tissue vacuolization in DRG
	Exon 7: KCC3 LOF in NaV1.8 neurons	No abnormalities	No abnormalities
	Exon 7: KCC3 LOF in Schwann cells	No abnormalities	No abnormalities
	Exon 7: KCC3 LOF in Enolase-2 neurons (all neurons?)	No abnormalities	No abnormalities
Kahle et al., 2016	Exon 22: T991A Gain of Function (point mutation)	- Inability to maintain balance on rotarod and balance beam	- Swollen nerve pathology - Hypomyelination

Table 3-2. KCC3 mouse models. Listed are all of the current mouse models of HSMN/ACC to date. Nearly all current mouse models except T991A observe the effects of a loss of function of KCC3

KCC3 gain of function

A young boy exhibiting a rare form of PN (peripheral neuropathy) was presented to the Neuromuscular and Neurogenetic Disorders of Childhood Section at the National Institutes of Health (NIH). The patient tested negative for all known mutations associated with Charcot Marie Tooth Disease, a well characterized inherited neuropathy. Neither of his parents presented with PN. Additionally, his motor neuropathy appeared greater than his sensory neuropathy, and he displayed no cognitive abnormalities. Whole exome sequencing demonstrated that the boy has a *de novo* heterozygous mutation in KCC3, which leads to the substitution of Thr991 for an alanine (T991A) (Kahle et al., 2016). Extraordinarily, the mutation occurs on one of the two most critical phospho-regulatory residues in KCC3 (Rinehart et al., 2009), resulting in a lack of phosphorylation at T991A and constitutive activity of the cotransporter. Thus, this heterozygous mutation is a gain of function (GOF) mutation. As indicated above, KCC3 activity is silenced upon phosphorylation of T991 and T1048. In the patient, T1048 is intact and still capable of being phosphorylated, yet this is not enough to compensate for the lack of phosphorylation at position 991.

To study this KCC3 GOF and recapitulate the young boy's phenotype, we created a T991A mouse model using CRISPR/Cas 9 technology (Kahle et al., 2016). We conducted locomotor tests with adult mice, comparing wild-type controls with heterozygous and homozygous cohorts. We observed that the homozygous T991A mice displayed severe locomotor deficits as they showed difficulty in maintaining balance on the rotarod and coordination on the balance beam (Kahle et al., 2016). In addition, nerve conduction

(compound nerve action potential) experiments were conducted to examine sensory and motor amplitudes and latencies. Homozygous mice displayed a significant decrease in motor amplitude and latency, and displayed a trend in decreasing sensory amplitude. The changes in sensory amplitude did not reach statistical significance (Kahle et al., 2016). The patient displayed a greater motor neuropathy than sensory neuropathy, therefore the T991A mouse model's phenotypes were consistent with the T991A patient. The nerve conduction phenotype observed in both homozygous and heterozygous mice established the deleterious effects of this single point mutation in KCC3 and confirmed causality of the T991A mutation to the patient's neuropathy.

Compound nerve action potential studies are useful in identifying the type of defect associated with a neuropathy (i.e., demyelinating versus axonal deficit). Indeed, in axonal neuropathies in which mainly axons degenerate, amplitudes in compound nerve action potential tend to decrease. In contrast, a decrease in latency is typically observed in demyelinating neuropathies as saltatory conduction is affected (Mallik & Weir, 2005). Thus, we utilized nerve conduction studies as a tool to further understand the T991A mutation. In dorsal caudal tail nerve conduction studies, homozygous mice displayed the lowest motor amplitudes and decreased latencies. These results suggested that both myelin and axons are affected in this GOF mutation. Importantly, individuals with HMSN/ACC (LOF of KCC3) have been characterized as having an axonopathy, based on post-mortem observations (Auer et al., 2016). It is noteworthy, however, that axon and myelin degeneration begin to confound each other as they progress, making it difficult to interpret the nerve conduction data.

Another factor to consider is the physiological impact of a GOF in KCC3. If KCC3 is continually working to efflux K^+, Cl^-, and water, one would expect the cells to shrink. Thus, just as the loss of KCC3 function results in axonal swelling (Byun & Delpire, 2007), it is likely that GOF of KCC3 leads to shrunken axons. Here, we tested this hypothesis by measuring axon diameters in the sciatic nerves of wild-type, KCC3-T991A heterozygous, and homozygous mice. Sciatic nerves from both genotypes were isolated, fixed, and prepared for electron microscopy **(Figure 3-2A-B).** To quantify nerve fiber diameters, we utilized the g-ratio (Byun & Delpire, 2007), which is calculated as the total axon diameter over fiber diameter **(Figure 3-2C).** For g-ratio analysis, nerve fibers are assumed to be perfect circles in order to estimate the diameter. We used Image J software to trace and measure the outer portion of the axon and the outer area of the myelin sheath **(Figure 3-2D**).

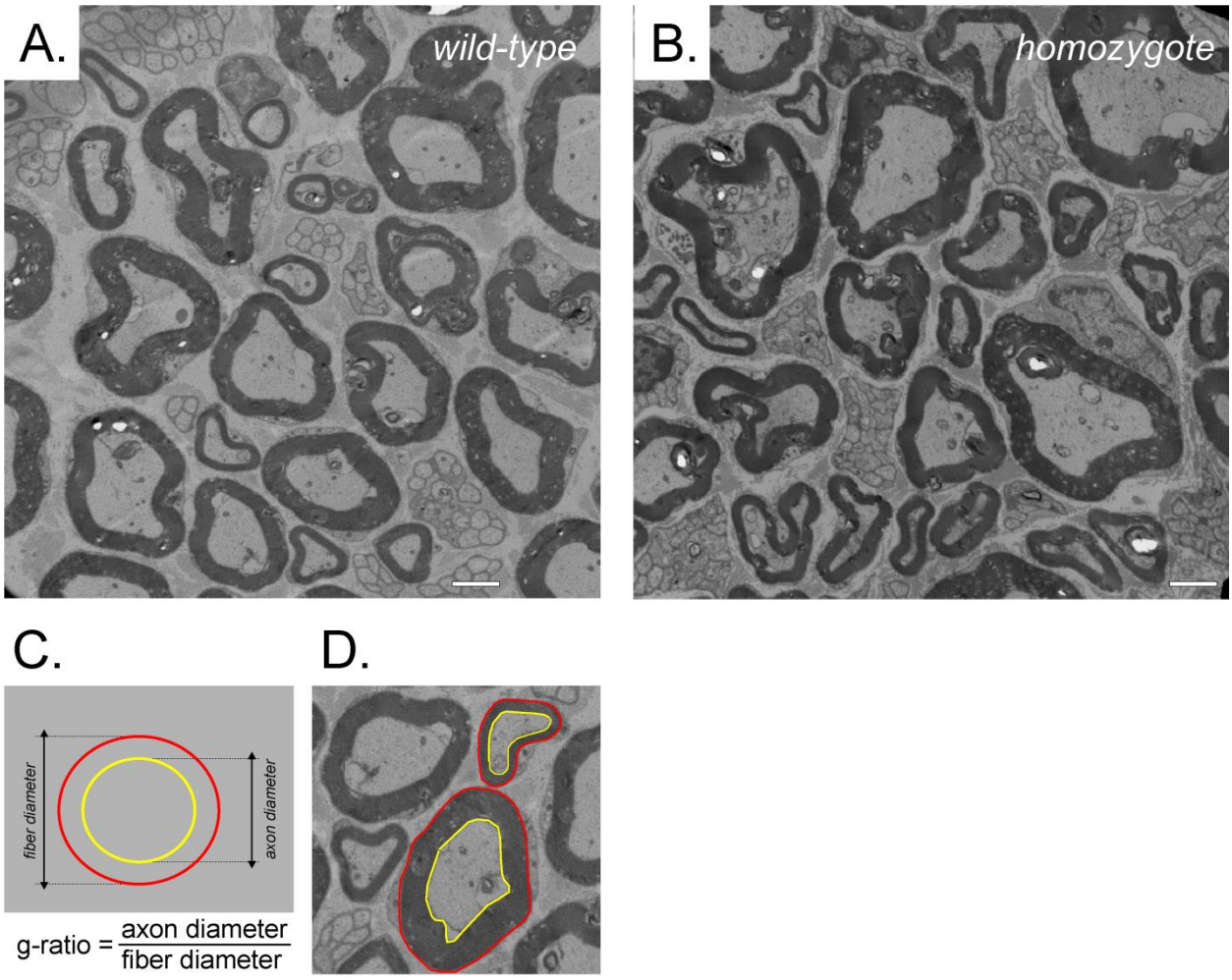

Figure 3-2. Electron micrographs of sciatic nerves. (A) wild-type, and (B) homozygous sciatic nerves taken at a direct magnification of 4400x display no overt phenotype. Size bars = 2 μM. C: calculated g-ratio is the ratio of axon diameter divided by whole fiber diameter, it assumes the nerve fiber to be a "perfect" circle. D: g-ratio of actual nerve fibers is obtained by outlining the circumference of the axon (i.e. yellow in this case) and the circumference of the total fiber (i.e. red in this case). The outlines are done within Image J software, which allows for precise circumference measurements from which the diameters and g-ratio can be calculated.

Interestingly, when plotting axon diameter versus g-ratio, control animals display a greater distributional spread of axon diameters; comparatively heterozygous and homozygous have a majority of their axon diameters concentrated in the smaller axon diameter range **(Figure 3-3A)**. Moreover, we observed an overall decrease in myelin thickness in both heterozygous and homozygous mice as well as decreased fiber diameters when compared to control animals **(Figure 3-3B & 3-3D)**. Interestingly, this change in distribution points towards cell shrinkage. An overall decrease in axon diameter is consistent with a gain of function mutation in KCC3 **(Figure 3-3D).**

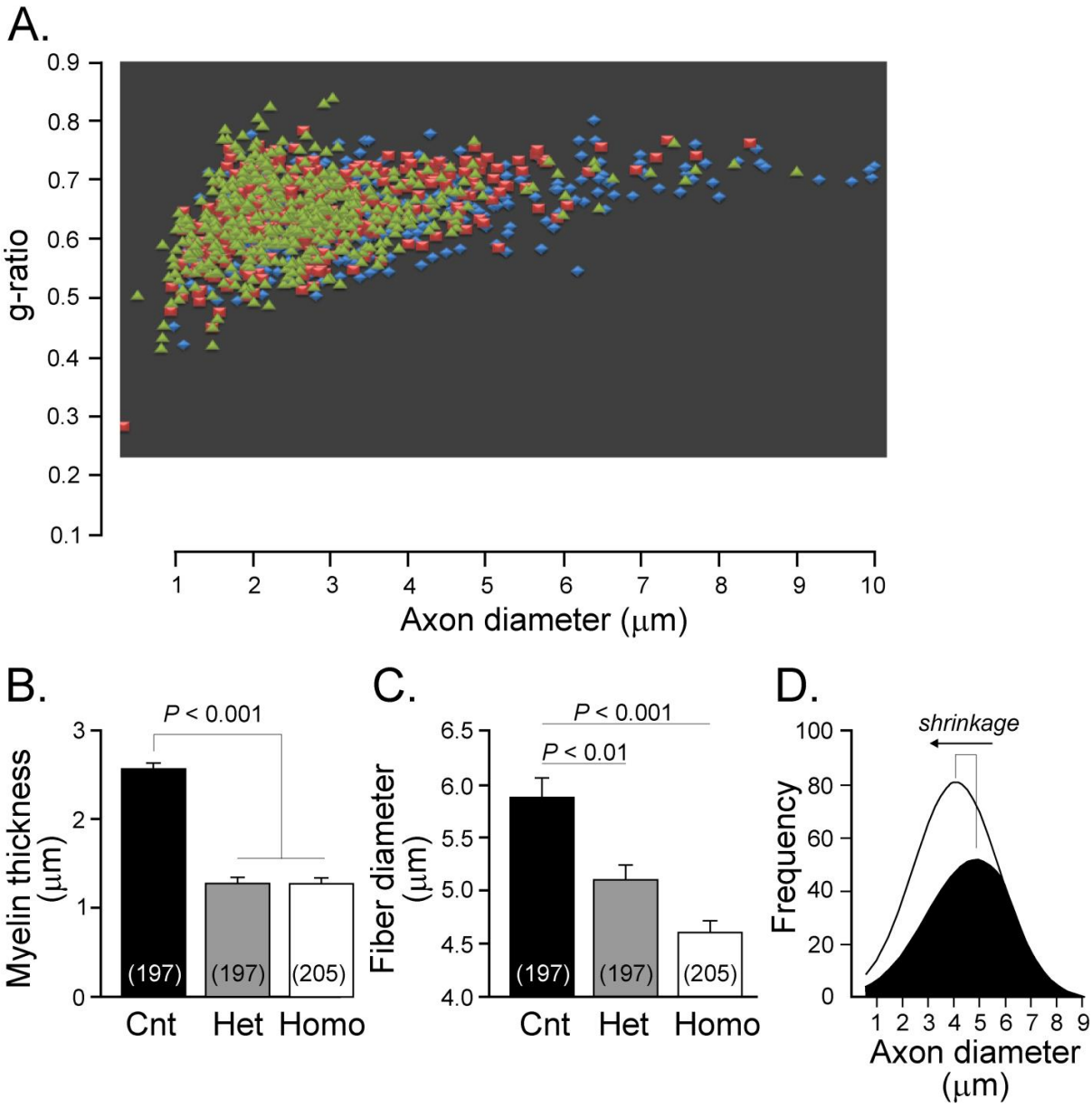

Figure 3-3. Shrinkage of axons and fibers in KCC3-T991A sciatic nerves. A: Graphing the axon diameter versus g-ratio reveals differences in spread (distribution) among homozygous (green triangles), heterozygous (red squares), and wild-type (blue diamonds) KCC3-T991A axon diameters. B: Myelin thickness is decreased in heterozygous and homozygous animals compared to controls ($P < 0.001$). C: When assessing total fiber diameter, both heterozygous and homozygous sciatic nerves displayed decreased diameters compared to controls. Bars represent mean ± S.E.M. (n, indicated within the bars). D: Distributions of sciatic nerve axon diameters of homozygous (white curve) and control (black curve) mice. A leftward shift of axon diameter (indicating shrinkage) is observed in the homozygous mice.

Alternative methods to assess sciatic nerves: Diffusion Tensor Imaging

Diffusion tensor imaging (DTI) is a quantitative magnetic resonance imaging technique used to assess tissue microstructure based on the rate and direction of water molecule movement, or diffusion, within that structure. DTI is used to assess diffusivity of water molecules in multiple directions and this data can be used to track fiber pathways in the CNS and PNS as diffusion is limited in certain directions in a nerve. We utilized DTI to assess water diffusion in mouse sciatic nerves. DTI takes advantage of the fact that water is sensitive to the barriers of tissue microstructure (i.e., myelin, intra- and extracellular components). In general, when water is in an unstructured space (e.g., sphere), there is equal diffusion in all directions; this concept is termed isotropic diffusion. However, when there are microstructural barriers in the tissue, such as a tube-like nerve, these barriers change the diffusion characteristics. In a normal myelinated axon, diffusion is limited perpendicular to the length of the axon while diffusion is greater in the direction parallel to the length of the axon. This concept is referred to as anisotropic diffusion. Therefore, the level of anisotropy describes diffusion characteristics. Changes in these diffusion characteristics can indicate differences in tissue microstructure and general organization of tissue. For this specific experiment the DTI parameters that we assessed were mean fractional anisotropy (FA), radial diffusivity (RD), and axonal diffusivity (AD). Each parameter indicates the degree and direction of diffusion in each sciatic nerve sample. Specifically, RD and AD can indicate changes in myelin (Winklewski et al., 2018), while FA is an indication of overall water

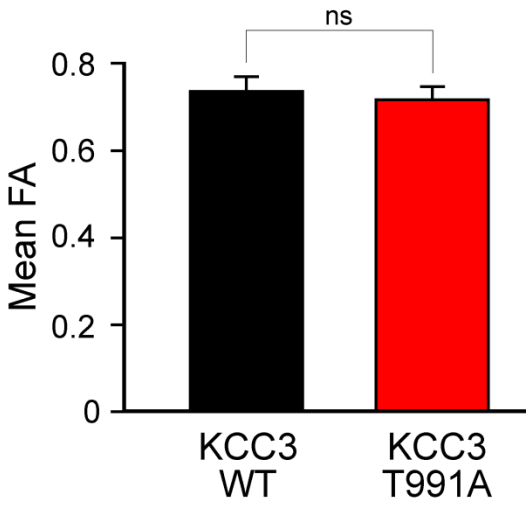

Figure 6-4. Mean Fractional Anisotropy. Comparison of mean fractional anisotropy between genotypes**.** There was no significant difference of mean FA between genotypes. Welch test two-sample t-test revealed, P = 0.670.

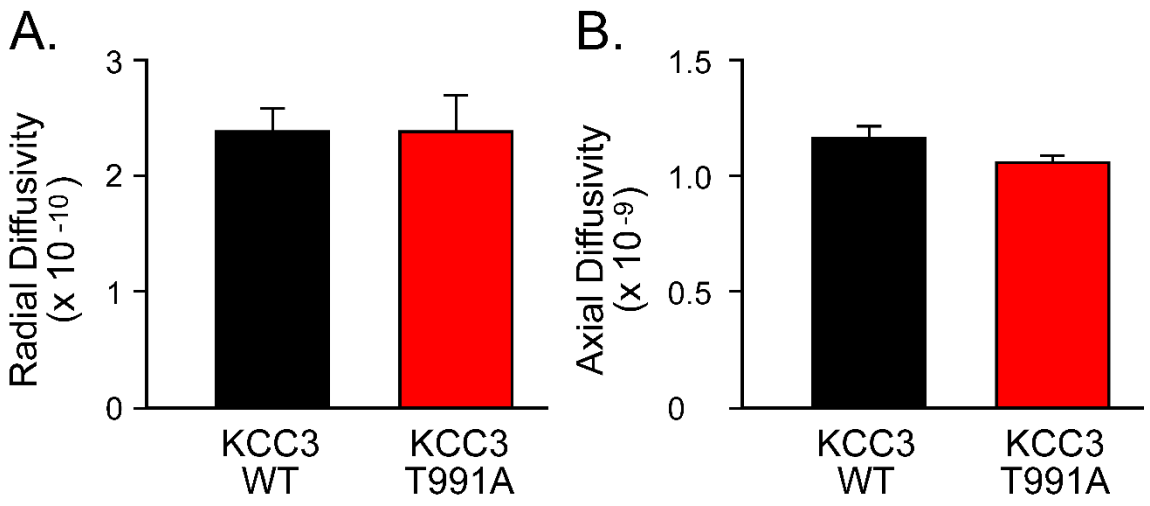

Figure 3-5. Radial and Axial diffusivity. Radial (A) and Axial (B) diffusivity differences between wild-type and homozygous T991A sciatic nerves.

diffusion. For example, when there is higher isotropic diffusion in unorganized tissue, FA values decrease.

The overarching goal of utilizing DTI was to re-confirm our results we observed in g-ratio experiments with the slice of the sciatic nerve. Specifically, we wanted to determine if there was a difference in water content and diffusivity of T991A homozygous sciatic nerves versus wildtype. Three nerves from three different samples of each genotype were prepared. The general advantage of DTI over histology is the ability to quantify the entire sciatic nerve as opposed to slices of it. Overall, there were no significant differences in FA between the two genotypes (**Figure 3-3**). Furthermore, there was no significant difference between RD (**Figure 3-4A)** or AD (**Figure 3-4B**).

KCC3 as a drug target

If KCC3 function is overactive in the T991A patient, could the neuropathy be treated with drugs that lead to cotransporter inhibition? One possibility would be to use a drug that directly interacts with and inhibits the cotransporter (Eric Delpire & Kahle, 2016). Currently, the only FDA approved drugs that inhibit the K-Cl cotransporters are the loop diuretics furosemide and bumetanide. Unfortunately, these drugs are poor inhibitors of the K-Cl cotransporters, with an IC50 for KCC above 500 μM in contrast to IC50s < 2 μM for NKCC1 or NKCC2 (Russell, 2000). A drug that acts as a weak inhibitor, might in fact, be a better strategy. Complete inhibition of KCC3 would mimic a LOF of the cotransporter and could be detrimental to the health of nerves. Whether or not the loop diuretics can reach CNS or PNS is

a question that still needs to be answered. In addition, a pharmacological approach also requires target specificity, which is an issue when dealing with four K-Cl cotransporters with different expression patterns and functions. In a large screening effort against KCC2 as a target, we identified inhibitory compounds that were 3-4 orders of magnitude more potent than the two loop diuretics (E. Delpire et al., 2009). However, these compounds were not ideal drug candidates as they were not specific to KCC2 but also inhibited KCC3, and they had poor pharmacokinetic properties (E. Delpire et al., 2009; Eric Delpire et al., 2012). Alternative to agents that bind to the cotransporter would be agents that affect proteins that modulate cotransporter activity. The most likely targets are the kinases that phosphorylate and inactivate KCC3 (SPAK and OSR1) or their upstream kinases (WNKs). This pathway also constitutes a major challenge as the same kinases which regulate KCC3 in neurons also regulate cation-chloride cotransporters such as KCC2 in neurons (De Los Heros et al., 2014), NKCC1 in neurons (Geng, Hoke, & Delpire, 2009) and other tissues, and NKCC2 and NCC in kidney (E. Delpire & Gagnon, 2006; Kenneth B E Gagnon et al., 2006; Grimm et al., 2012). Therefore, manipulating these kinases would likely create many off-target effects. Finally, whether the KCC3-mediated peripheral neuropathy can be reversed once it begins is also uncertain and should be further investigated before designing drugs to target KCC3 dysfunction.

The cellular basis of disease: KCC3

Neuronal by nature

The fact that both KCC3 LOF and GOF lead to peripheral nerve disease is indicative that the cotransporter must maintain homeostatic function. Initial studies of HMSN/ACC patients and LOF mouse model studies clearly indicated abnormalities in central and peripheral nervous systems. To further tease apart the cellular basis of HMSN/ACC, Shekarabi and colleagues created a neuronal specific knockout mouse model of KCC3 using the Cre/LoxP system. Deletion of KCC3 was accomplished by expressing CRE under the promoter for synapsin-1, a neuronal specific protein which is involved in synaptic vesicle release and thus modulation of neurotransmission (Cesca, Baldelli, Valtorta, & Benfenati, 2010). Thus, by crossing a synapsin-1-Cre mouse with a KCC3-flox mouse, they drove deletion of KCC3 in both CNS and PNS neurons. This neuronal specific knockout mouse presented with the same phenotypes as the global knockout, presenting the first piece of evidence that the KCC3-mediated neuropathy is neuronal in nature (Shekarabi et al., 2012). To determine if the neuronal-specific deletion had an effect on the corpus callosum, they utilized gold staining and MRI. When assessing changes in the corpus callosum, the neuronal-specific KCC3 KO mice displayed only slightly smaller corpus callosum lengths and smaller anterior commissure areas, compared to wild-type. In the global KO, the phenotype was enhanced with even smaller corpus callosum lengths, smaller anterior commissure areas, and overall decreased corpus callosum volumes. In spite of the more robust changes in the corpus callosum in the global KCC3 LOF, these brain abnormalities were not as visually apparent as

observed in the human HSMN/ACC cases. Therefore, it still remains to be resolved whether a) loss of KCC3 expression in additional cell types participates in this phenotype and b) if KCC3 is directly affecting these changes in the corpus callosum.

Concurrently, we also created a neuronal specific knockout of KCC3 using the neuronal specific enolase (NSE or enolase-2) promoter to drive deletion of KCC3 in all neurons (Ding & Delpire, 2014). NSE is one of three glycolytic enzymes expressed in brain metabolism (Rosenstein 1993) and hence ubiquitously expressed in all neurons. In humans, increased NSE expression correlates with brain injury or with stress, such as seizure episodes (Palmio et al. 2008). Surprisingly, this neuronal-specific KO displayed no locomotor deficits. As enolase-2 and synapsin-1 are expressed in all neurons, there should be a phenotype observed in the enolase-2-Cre x KCC3-flox mouse. There are several possible explanations for this discrepancy: First, the enolase-2 promoter might have been weak, and only a partial deletion of KCC3 might have occurred. Note that heterozygous KCC3 KO mice have no phenotype, indicating that expression has to be reduced at least below 50%. Second, it is possible that the expression of enolase-2 does not occur early enough, and KCC3 plays a critical role during development of the nerve. Indeed, enolase has been found weakly expressed in fetal brain, with expression increasing 1-2 weeks postnatal (Rosenstein, 1993). Furthermore, in one of the original NSE-Cre specific lines, it was found that NSE is restricted to fully differentiated neurons and is detected in DRG past postnatal day 0 (Kwon et al., 2006). Although the authors noted that NSE-driven Cre activity was detectable in the PNS at E13.5, the expression might be too low to affect KCC3 expression in early development.

Although KCC3 is expressed in adult DRG, its expression increases with gene maturation (Lucas et al., 2012).

An additional Cre line that our laboratory used to disrupt KCC3 was Nav1.8-Cre. Nav1.8 is a voltage-gated sodium channel that is predominately found in small diameter DRG and has been implicated in nociception, thermoception, and mechanoreception (M. Liu & Wood, 2011). These are three sensory modalities that are commonly affected in HSMN/ACC. Nav1.8 expression can be detected as early as E15 in dorsal root ganglia, with expression reaching approximately 25% of the DRG population by E17 and increasing up to 50% by adulthood (Benn, Costigan, Tate, Fitzgerald, & Woolf, 2001). Nav1.8 expression, therefore, precedes KCC3 expression during development, and Cre-mediated recombination and excision of KCC3 exon 7 likely occurred early. There was however no significant difference between genotypes in the response time of paw withdrawal following a heat-evoked (52^{o}C) nociceptive stimulus (Ding & Delpire, 2014). As anticipated for nociceptive fibers, disruption of KCC3 in Nav1.8 positive neurons also had no effect on locomotion.

Aside from the Enolase-2-Cre and Nav1.8-Cre, we also used a Parvalbumin-Cre (PV-Cre) line to mediate Cre recombination and excision of KCC3 exon 7 in all parvalbumin-containing cells, including parvalbumin-positive neurons. We chose PV to disrupt KCC3 as it is expressed in a subset of sensory neurons: the proprioceptive fibers, which transmit information about body position, motion, equilibrium, and limb posture to the CNS. In addition to these sensory neurons, PV is also expressed in a subset of interneurons (Celio, 1986, 1990). PV-positive interneurons have been implicated as gate-keepers that modulate

excitatory neurons to alleviate neuropathic pain (Petitjean et al., 2015). We observed severe locomotor deficits, swelling, tissue vacuolization, and fiber degeneration in dorsal root ganglia of PV-Cre x KCC3-floxed mice (Ding & Delpire, 2014).

Interestingly, the two gene promoters that drove Cre expression in the two lines of mice that recapitulated the HSMN/ACC phenotype (synapsin I and parvalbumin promoters) are active as early as E14 in both the CNS and PNS (Melloni & DeGennaro, 1994; J.-H. Zhang, Morita, Hironaka, Emson, & Tohyama, 1990); whereas the enolase promoter seems to be active later, as enolase expression is not detected before P7 (Rosenstein, 1993). These data suggest that the HSMN/ACC phenotype might be due to an early deficit in KCC3 function. KCC3 expression has been demonstrated in DRG as early as E14 by □-galactosidase activity, as the reporter gene was placed under the promoter of the Slc12a6 gene (Boettger et al, 2003). Additional studies are needed to address the precise timing of KCC3 deficit in HSMN/ACC.

A role for Schwann cells?

To further tease apart cell specificity in the development of HMSN/ACC, we also utilized a Desert hedgehog (Dhh)-Cre mouse to delete KCC3 specifically in Schwann cells, the cells that form and maintain the myelin sheaths in PNS. Desert Hedgehog is the protein that signals and initiates Schwann cell formation around peripheral nerves (Parmantier et al., 1999). While antibody studies have demonstrated a definite expression of KCC4 in Schwann cells and mesaxons along teased nerve fibers (Karadsheh et al., 2004), KCC3 transcript was also detected by RT-PCR in freshly isolated Schwann cells (Byun & Delpire, 2007;

Karadsheh et al., 2004). Interestingly, the Schwann cell specific mouse knockout of KCC3 displayed no locomotor deficits nor did it display any tissue abnormalities. At the time of this writing, this is the only KCC3 mouse model in literature that disrupts KCC3 in a glial cell subtype. Since KCC3 is involved in volume regulation, we initially hypothesized that KCC3 regulates volume in Schwann cells, but KCC3 does not appear to play a prominent role in the volume homeostasis of Schwann cells. Moreover, no attempts have been made to disrupt KCC3 function in oligodendrocytes, the cells that create the myelin sheath in the CNS. Since post-mortem autopsies of HMSN/ACC individuals and of mouse models appear to predominantly show abnormalities in axons (i.e., swelling), and the phenotype can be reproduced by deleting KCC3 in cells expressing synapsin-1 or parvalbumin, it is now clear that HMSN/ACC is primarily neuronal in nature (Auer et al., 2016; Byun & Delpire, 2007; Ding & Delpire, 2014; Shekarabi et al., 2012)

The next question that needs to be addressed is whether the phenotype is strictly related to proprioceptive fibers or if other neuronal cell types contribute to the development of HMSN/ACC. Since patients display severe sensorimotor neuropathy it seems logical that both sensory and motor neurons would play a role in the development of the peripheral neuropathy. It is also important to recall here that HMSN/ACC was first presented as an anterior horn disease (Andermann et al., 1972), questioning whether motor neurons also play a role. Do motor neurons also express KCC3, and would deletion of KCC3 in these neurons lead to a locomotor phenotype? This is yet to be determined.

The future of KCC3 and HMSN/ACC

Thus far, literature in the field indicates that KCC3 dysfunction in neurons, either GOF or LOF, leads to a HMSN/ACC phenotype. However, the nervous system is complex and multiple components are often involved in sophisticated physiological processes. The parvalbumin Cre/LoxP work, while a promising lead, must be further developed before concrete conclusions can be drawn among KCC3, parvalbumin positive neurons, and HMSN/ACC. Perhaps, then, it is prudent to reexamine the disease characteristics to guide future studies.

At first glance, the characteristics of HMSN/ACC seem discordant; some patients have corpus callosum malformation while others do not (Howard *et al.,* 2002; Casaubon *et al.,* 1996), and a patient with an intact corpus callosum can still suffer from intellectual disability. Therefore, the most consistent feature of the disease is the sensorimotor neuropathy, yet the neuropathy itself presents another layer of nuance. Is the phenotype caused by sensory neuron deficits, motor neuron deficits, or a combination of the two?

In the periphery, muscle contraction is accomplished by the action of primary motor neurons, with cell bodies residing in the ventral horn of the spinal cord, onto muscles (Stifani, 2014) **(Figure 3-4)**. In contrast, sensory neurons, specifically proprioceptive neurons, bring sensory information from the muscles back to the spinal cord, where they synapse onto both primary motor neurons and interneurons. Thus, sensory feedback influences motor neuron control of muscles at the level of the spinal cord. Proprioceptive feedback also travels to the CNS via the dorsal spinocerebellar and medial lemniscal tracts and eventually makes its way to the motor

cortex **(Figure 3-4).** In the motor cortex, proprioceptive information can be used to modulate the control of primary motor neurons, marking a second influence of sensory feedback on motor neurons, this time in the brain. Thus, motor neurons and sensory neurons are both connected to the motor cortex via descending and ascending pathways, respectively (Kandel et al., 2013).

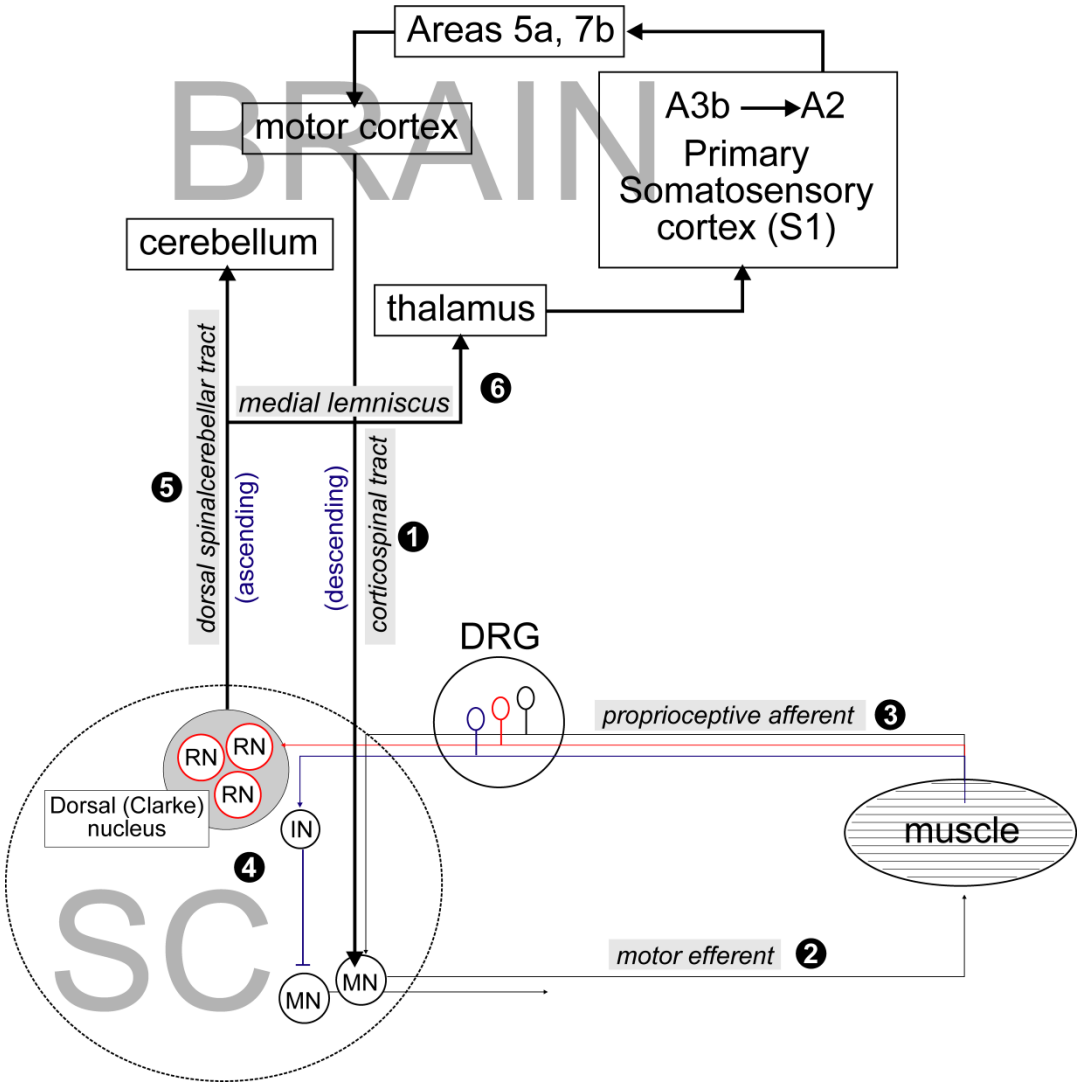

Figure 3-6 Structures of the PNS and CNS involved in locomotion. This connectivity diagram shows the flow of information within the spinal cord, muscles, and brain. (1) The motor cortex sends projections to the motor neurons via the corticospinal tract. (2) Motor neurons (MN) with their cell bodies in the ventral horn of the spinal cord send their axons to the periphery where they synapse onto muscles. (3) Sensory neurons, with their cell bodies in the dorsal root ganglia (DRG), bring proprioceptive information from muscles back to the spinal cord where they synapse onto both interneurons (IN) and relay neurons (RN). (4) IN synapse with some MN and inhibit them. (5) Some proprioceptive neurons, especially those from lower limbs, project to Clarke's nucleus in the lumbar spinal cord. Second order neurons from Clarke's nucleus then project to the cerebellum via the dorsal spinocerebellar tract. Some of these neurons give of collaterals (6) which join the medial lemniscus headed to the ventral posterior lateral nucleus (VPL) of the thalamus. The VPL projects to the primary somatosensory cortex (S1), which is composed of multiple Brodmann's areas. One area of S1, area 3b, carries proprioceptive information to Brodmann's area 2 within S1 before projecting to parietal areas 5a and 7b. Areas 5a and 7b then project to the motor and pre-motor cortex. Thus, proprioceptive information can be used to influence voluntary motor movements.

Considering the connectivity between the brain and the spinal cord, how can this information be used to investigate the HMSN/ACC pathology? The most salient clinical feature of HMSN/ACC patients is the severe locomotor deficit. Therefore, it seems logical that KCC3 dysfunction in motor neurons may be the cause. The neuromuscular junction (NMJ) of KCC3 KO mice was recently investigated by Bowerman and colleagues (Bowerman et al., 2017). When examining the tibialis anterior muscle, they found that some 20% of KCC3 global KO NMJs were partially denervated. Both KCC3 global KO and neuronal-specific KCC3 KO mice showed disorganized motor endplates. Additionally, the nerve terminals of KCC3 KO mice were shrunken compared to wild-type mice. However, they did not find a difference in the number of motor neuron cell bodies in the ventral horn of the spinal cord when comparing KCC3 KO to wild-type mice, indicating that the differences seen at the NMJ were not due to motor neuron death. Overall, the work by Bowerman and colleagues shows that KCC3 global KO mice have deficits at the NMJ, and considering the locomotor deficits seen before in this mouse line, it is likely that these NMJ deficits contribute to the phenotype of the mouse. However, it is still unclear whether these deficits are the primary reason behind the locomotor deficits or whether they are a secondary result of deficits in another area of the brain-spinal cord circuitry.

When Andermann and colleagues first described HMSN/ACC in 1972, they believed the patients may have been suffering from anterior horn cell disease, referring to the motor neurons of the anterior spinal cord. They suggested this diagnosis based on patient

electromyographs that displayed a decrease in the number of motor unit potentials, but with an increase in amplitude of the unit potentials that were present, and some polyphasic potentials (Andermann et al., 1972). This observation is consistent with the NMJ deficits that Bowerman observed; however, the authors of this latest study did not observe any differences in the amplitude or number of action potentials in motor neurons cultured from KCC3 global KO mice.

Yet there are still more locomotor characteristics to be considered in the HMSN/ACC phenotype. Locomotion can be broken down into initiation of motor movements, brief voluntary movements, and rhythmic sustained movements. Brief voluntary motor movements, such as raising an arm, are initiated in the primary motor cortex and pre-motor cortex. The primary motor cortex is involved in planning voluntary movements, and its neurons synapse onto motor neurons in the brainstem (corticobulbar tract) and the skeletal motor neurons in the ventral horn of the spinal cord (corticospinal tract) (Purves et al., 2001). The upper motor neurons of the pre-motor and motor cortexes are unlikely to be involved in the HMSN/ACC phenotype. Typically, upper motor neuron lesions result in muscle spasticity, hyperactive deep tendon reflexes, and abnormal big toe behavior upon sole stimulation or pressure (i.e., Babinski's sign) in patients, but do not result in amyotrophy (Purves et al., 2001). Traditionally, a disease that has been considered a purely upper motor neuron disorder is primary lateral sclerosis (PLS), and PLS patients present with hyper-reflexia and increased muscle tone (Wias et al., 2017).

After the action potential for a voluntary movement has left the upper motor neurons and reached the lower motor neurons of the ventral horn of the spinal cord, these neurons send signals to skeletal muscles to contract. Patients with lower motor neuron lesions can present with muscle wasting, limb weakness, hypoactive tendon reflexes, and decreased muscle tone (Purves et al., 2001). Additionally, patients with spinal muscular atrophy (SMA), a disease of the alpha motor neurons, display hypotonia in infancy, progressive weakness (especially in the legs), and progressive muscle atrophy (Mercuri et al., 2017). The symptoms of lower motor neuron lesions and SMA appear more like the phenotype of HMSN/ACC patients than those of upper motor neuron diseases, suggesting that lower motor neurons may play a role in HMSN/ACC.

Lower motor neurons do not affect voluntary movement in isolation. Other neurons, such as proprioceptive sensory neurons and interneurons also play key roles in body movement, including locomotion. Locomotor activity is a complex behavior that involves rhythmic activation of motor neurons for the flexor and extensor muscles of the limb. Both proprioceptive (type Ia) sensory neurons and interneurons also contribute to the rhythmic activation of flexor and extensor muscles around a joint (Kiehn, 2016). Here, it is important to note that the HMSN/ACC patient phenotype does not offer a clear indication of which pathway is predominantly affected. HMSN/ACC patients experience degrading ambulation as they age, but it is unknown if they experience this symptom because of a sensory deficit, a motor deficit, or both. Our study with the parvalbumin-specific KCC3 KO mouse suggests a significant role for proprioceptive fibers (Ding & Delpire, 2014). This, however, does not

exclude a role for motor neurons as well. Could the motor neuropathy observed in HMSN/ACC patients be secondary to a deficit in proprioceptive fibers? In the absence of proper sensory feedback, the motor neurons might be unable to affect muscle contraction at an appropriate time. In this case, the KCC3 disruption might not directly affect motor neurons, but the end result would be the same, with motor neurons unable to convey proper signals to enable locomotion. Future studies should examine KCC3 dysfunction directly in lower motor neurons and further tease apart the role of KCC3 in proprioceptive fibers.

Conclusion

Despite nearly two decades of research and the creation of multiple mouse models, we are still left with many more questions than answers regarding the biology of KCC3 and how its dysfunction can cause HMSN/ACC. This review has clearly demonstrated that both LOF and GOF mutations in KCC3 result in peripheral neuropathy, but it is still unclear how the cotransporter is involved. Moreover, it is still uncertain how ACC may be related to a loss of function of KCC3, but not necessarily a gain of function. It is important to note, however, that complete absence of the corpus callosum is never observed in mouse models. Compared to the various degrees of ACC observed in human patients, the changes observed in the mouse are relatively minor, missed in the analyses of the first two mouse knockout models (Howard et al., 2002; Boetger et al., 2003), but detected upon more rigorous analyses by Shekarabi and colleagues (Shekarabi et al., 2012).

The LOF and GOF mouse models as well as the documented clinical cases all point toward disruption in cell volume. Indeed, nerve fibers are swollen in the KCC3 knockout mouse (and HMSN/ACC patients), while shrunken in the constitutively active KCC3-T991A mouse. When added to our knowledge that the cotransporter is activated by cell swelling and then extrudes water out of the cell, this suggests a role for KCC3 in cell volume maintenance of peripheral nerve fibers. The time point when KCC3 function is critical for neurons or their axons is unknown. Is it needed only during a defined developmental period, or is it required during the entire life of the nerve fibers? Because the transporter is otherwise functionally silent under isotonic conditions, is it possible that KCC3 would be required in developmental processes that lead to cell volume changes, or upon situations like inflammatory or injury conditions that lead to cell swelling? If the transporter is maintaining a key parameter such as cell volume and integrity of a nerve fiber, could it be that its function is also affected in other cases of peripheral nerve disease? Finally, there is the question of disease reversibility and possibility of targeted therapeutic agents. Currently there are no drugs or therapies that specifically target KCC3 function. The challenges that exist with drug targets are twofold. First, there is a list of unknown cell types that could also be affected upon KCC3 disruption. Second, there are other isoforms of the K-Cl cotransporter differentially expressed throughout the body that will also likely be targets of KCC3 therapies; it will be difficult to target KCC3 specifically with the level of conservation existing among isoforms. The challenge with targeting KCC3 will be to effectively change its function without disrupting or affecting any of its other isoforms or proteins it may interact with.

CHAPTER 4

Osmotic Response of Dorsal Root Ganglion Neurons Expressing Wild-Type and Mutant KCC3 Transporters

Introduction

KCC3 loss of function is well established as the primary cause of Hereditary Sensorimotor Neuropathy with Agenesis of the Corpus Callosum (HSMN/ACC) found in a French Canadian population (Howard et al., 2002). Patients with HSMN/ACC exhibit severe sensory and motor deficits with edema in their extremities (Andermann & Andermann, 1994; Howard, et al., 2002; Jean Mathieu et al., 1990). Mouse models of a LOF of KCC3 recapitulate the peripheral neuropathy phenotype, sharing similarities in tissue pathology (Boettger et al., 2003; Howard et al., 2002). Electron micrographs of sciatic nerves of the mouse model displayed axonal swelling and degeneration (Byun & Delpire, 2007). Furthermore, tissue vacuolization has been observed in dorsal root ganglion of mice that target KCC3 deletion in parvalbumin positive neurons (Ding & Delpire, 2014). The aforementioned tissue pathology has also been observed in autopsies of individuals with HSMN/ACC from the French-Canadian population, where carriers of the truncation of KCC3 exist in about 1 of 20 individuals (Howard et al., 2002). Due to KCC3's ability to extrude K^+ and Cl^- ions and water, the cotransporter is involved in cell volume maintenance and regulation (Lauf & Adragna, 2000). Thus, we hypothesized that the phenotypes observed were linked to a disruption in cell volume regulation. The logic underlying this hypothesis is

strengthened by the knowledge that KCC3 activity is enhanced under swelling conditions (Mount et al., 1999; Rinehart et al., 2009). Therefore, the cells' inability to lose K^+ and Cl^- could lead to cell swelling upon slight osmotic perturbations.

Patients with HMSN/ACC suffer not only from peripheral nerve deficits, but also exhibit severe cognitive disabilities and schizophrenia-like symptoms, indicating both peripheral and central origins. KCC3, a swelling-activated K-Cl cotransporter, participates in the efflux of K^+, Cl^-, and water from cells that are exposed to swelling under hypotonic conditions (Lauf et al., 1992). The loss of ions and water helps the cells return to their original volume, through a process known as regulatory volume decrease. It is unclear exactly how LOF of KCC3 results in severe sensory and locomotor deficits, (Boettger et al., 2003; Howard et al., 2002; Salin-Cantegrel et al., 2007; Shekarabi et al., 2012) except to say that complete absence of KCC3 in mice leads to axonal swelling and some degree of axonopathy in both central (Boettger et al., 2003) and peripheral nervous systems (Auer et al., 2016; Byun & Delpire, 2007). Disruption of KCC3 specifically in parvalbumin positive neurons, resulted in tissue vacuolization in dorsal root ganglion (DRG) (Ding & Delpire, 2014).

Interestingly, we also documented the case of a young boy who carried a gain of function (GOF) mutation in KCC3 that led to a constitutively active cotransporter. The patient exhibited severe sensory and motor neuropathy, but was cognitively normal (Kahle et al., 2016). The GOF was caused by the substitution of threonine residue at position 991 into an alanine. The T991A mutation also resulted in severe locomotor deficits and nerve damage in homozygous mice (Kahle et al., 2016). Residues T991 and T1048 are the most critical sites in

the phospho-regulation and activation of KCC3 (Rinehart et al., 2009), as the transporter only becomes active upon dephosphorylation of those sites (Adragna et al., 2015b; De Los Heros et al., 2014) .

It is unclear how LOF and GOF in KCC3 both result in peripheral nerve disease. Electron microscopy of the sciatic nerve of LOF mice revealed axonal swelling, whereas the same analysis in GOF mice revealed significant axonal shrinkage, in addition to some myelin defects (Byun & Delpire, 2007; Flores et al., 2019). Thus, our working model considers that volume homeostasis is critical to peripheral nerve integrity and function.

Cell volume regulation studies were previously conducted comparing cell swelling in T991A and control fibroblasts. Surprisingly, almost no swelling was observed in response to hypotonic challenges in the mutant cells (Kahle et al., 2016). This is clearly an abnormal behavior as the swelling phase following a hypotonic shock is typically regarded as a rapid re-equilibration of water across the plasma membrane with little participation of ions, which are far less permeable. Fibroblasts adhere tightly to their substrate, as their main function is to synthesize and provide extracellular matrix forming connective tissues in animals. In addition, they are not an adequate cell model system to assess the role of neuronal KCC3 in maintaining/regulating cell volume. In this study, we take advantage of our KCC3 knockout (KO) and KCC3-T991A mouse models to address the role of KCC3 in cell volume regulation. We utilized a large, rounded, and barely adherent, primary cell type: the dorsal root ganglion (DRG) neuron. DRG neurons have their cell bodies located in dorsal root ganglia. They

transmit sensory information from the periphery (e.g. muscles, skin) to the spinal cord and central nervous system.

In both HSMN/ACC patients and KCC3 knockout mice sensory perception is impaired. In parvalbumin (PV)-driven KCC3 knockout mice, DRGs demonstrate tissue vacuolization and degeneration. Currently, we hypothesize that KCC3 cotransporter expression in sensory neurons participates in the maintenance of cell volume. We show that control DRG neurons (DRG neurons that have native KCC3 expression) volume regulate. Comparatively, DRG neurons lacking KCC3 are no longer able to undergo regulatory volume decrease following hypotonic swelling. In addition, we show that when KCC3 is constitutively active (T991A GOF), the cells exhibit significantly reduced swelling compared to wild-type cells upon a hypotonic challenge. This observation not only solidifies the view that the cotransporter is important in the cell volume maintenance and regulation of sensory fibers but also questions the nature of the swelling phase of the cell that results from the osmotic challenge.

Materials and Methods

Reagents

Phosphate Buffered Saline (Sigma P7059-1L), Calcein AM ThermoFisher Scientific (C1430), Boric Acid (Sigma Aldrich, 10043-35-3), NaCl (RPU, S23020-1000.0), Sodium tetraborate Decahydrate (Fisher chemical, S246-500), Fisherbrand Microscope cover glass (12-545-CIR -1.5.), Matek 35 mm Dish, 14 mm glass diameter (P35G-1.5-14-C),

Polyethylenimine (PEI) (*Sigma P3143*), Gibco Laminin Mouse protein (Gibco, 23-017-015), Collagenase (Roche Diagnostics, 11088882001), Trypsin (Sigma T-4665), DNase I (Roche Diagnostics, 10104159001), Trypsin Inhibitor (T-9128), Tween 20 (Sigma, P7949), Triton x-100 (Sigma, T-8787), Dulbecco's Modified Eagle Medium Nutrient Mixture F-12 (Gibco 11320-033).

Animals

All animal handling and experimental procedures were approved by Vanderbilt's Institutional Animal Care and Use Committee and done in accordance with guidelines provided by the National Institutes of Health. The KCC3 knockout and KCC3-T991A mouse lines were previously described by us (Howard, Mount, et al., 2002; Kahle et al., 2016).

Coverslip preparation

Prior to plating the DRG neurons, coverglass slips were placed on 35 mm Matek glass bottom dishes. Glass coverslips were plated overnight with 1% Polyethylenimine (PEI) diluted in borate buffer (100 mM boric acid, 75 mM NaCl, and 25 mM Na-tetraborate) and incubated at 37°C, 5% CO_2. PEI was then washed 3 times with autoclaved water the next day. Laminin (30 µg/ml) was then placed on the glass coverslips and incubated overnight at 37°C., 5% CO_2. Laminin was aspirated prior to cell plating.

Dorsal root ganglion (DRG) extraction and cell culture

Adult mice were euthanized with isoflurane and were immediately dissected to remove T1-L5 DRGs. As described in (Sleigh, Weir, & Schiavo, 2016), the vertebrae column was extracted, placed on ice, and then cut in half, ventral side facing upwards to remove the spinal cord and extract the DRGs. Once removed, DRGs were placed in a T-25 flask containing complete culture media, and then transferred to culture media containing collagenase, DNAse I, and Trypsin. The flask was placed in a 37ºC heated water bath and gently shaken for one hour. After incubation, the DRGs were vigorously shaken to disintegrate clumps and Trypsin inhibitor was added. The cells were then spun down at 900 rpm for 4 min, resuspended 200 µl of control media. Cells were plated at a concentration of 200,000 cells per coverslip, in 2 ml of culture media per plate. Neurons were cultured on the PEI and laminin coated coverslips. The neurons were left to incubate and settle for two hours at 37°C prior to adding additional complete media and were imaged approximately 24 hours later.

Solutions

The isotonic solution contained 80 mM NaCl, 3 mM KCl, 1 mM $CaCl_2$, 1 mM $MgCl_2$, 5 mM glucose, and 10 mM HEPES, pH. 7.4. The osmolarity was adjusted to 300 mOsM through the addition of 115 mM sucrose. Hypotonic (180, 240 mOsm) solutions were obtained by reducing the amount of sucrose, and hypertonic solutions (420, 240 mOsm) were adjusted with increasing concentrations of sucrose.

Cell volume measurements

We utilized the Nikon Multi Excitation Tirf in wide field mode to measure changes in fluorescent intensity. These changes in intensity are used as a proxy for cell volume as previously described (Altamirano, Brodwick, & Alvarez-Leefmans, 1998; Alvarez-Leefmans, Herrera-Pérez, Márquez, & Blanco, 2006). Fluorescence intensity was measured using Plan Apo VC 20x/0.75 magnification. DRG neurons were incubated with calcein-AM (0.03 μM) diluted in isotonic media for 25 minutes at 37°C and washed three times with isotonic media prior to placing the coverslip in the chamber. Calcein AM is a single excitation dye with a good signal to noise ratio (Crowe et al., 1995). Each glass coverslip of neurons was placed in an open-top chamber platform (Warner instruments P-1, 64-0277) in a perfusion chamber (RC-26GLP). Solutions were perfused by gravity columns to ensure even flow of changing solutions. Images were captured using an Andor Zyla sCMOS camera, a Lumencor Spectra X light engine (with filters) as the light source, and with the Perfect Focus System turned on to avoid focus drifting. Cells were continuously perfused and imaged every 15 seconds for 16 min (3 min in isotonic media, followed by a 10 min osmotic challenge, and a final return to isotonic media for 3 min). calcein was excited at 470 nm and emission was collected at 525 nm ± 50 nm.

Changes in fluorescence intensity were measured using region of interest pinhole measurements placed in the middle of the cell utilizing the Time Lapse imaging setting in NIS Elements. Background was subtracted from fluorescent intensity measurements. Note that in

graphs denoting changes in volume, have their Y axis denoted FΔ/F0 (change in Fluorescence/Initial fluorescence).

The area of the cells (**Figure 4-3**) was measured using NIS elements software region of interest area detection. Volume was then extrapolated from the measured area assuming a perfect sphere, as DRG keep a round shape under all osmolarities.

Immunostaining

DRG cell culture was prepared as aforementioned and allowed to sit for 24 hours before staining. Cells were briefly washed with Hank's Balanced Salt Solution (HBSS), without calcium, nor magnesium. An ice cold 1:1 methanol acetone mixture was then added for cell culture fixation for 20 minutes. The fixation solution was removed, and cells were treated with 5% BSA, 1% goat serum, 0.5% Tween 20, 0.5% Triton X-100 in 1X PBS for two hours. Primary rabbit polyclonal KCC3 antibody (1:200) was applied in the blocking buffer for 90 minutes at room temperature and transferred to 4°C overnight. The following day, fixed cells were washed with 1X PBS, 3 x 10 minutes. For secondary antibody, goat anti-rabbit IgG H&L (FITC) secondary antibody (1:200, Abcam, ab6717) was resuspended in blocking buffer and placed on the fixed cells for 2 hours at room temperature. Cells were then washed 3 x 10 min in 1X PBS and mounted with Prolong Gold antifade reagent with DAPI. The fixed cells were imaged on a Zeiss LSM 880 microscope. The same procedure was done for staining with the KCC2 antibody (1:200, Abcam, ab49917).

For staining, dorsal root ganglia were extracted as described above. They were then fixed in 10% formalin at room temperature, overnight. Once fixed, the tissue was embedded in paraffin and 10 micron thick sections were prepared. The paraffin was dissolved using Citrisolv (Thermo Fisher Scientific) and the tissue was rehydrated in 5 min consecutive washes of 100%, 95%, 70% ethanol, followed by a 10 min wash in 1X PBS. Antigen retrieval was performed on the slides using Citra Plus (BioGenex, Freemont, CA). Sections were then blocked with a buffer consisting of 5% bovine serum albumin, 1% goat serum, and 0.5% Triton X-100, for two hours. Sections were incubated with a rabbit polyclonal KCC3 antibody (1:200, Byun et al., 2007) at room temperature for 1.5 hours, and then placed overnight at 4°C. The primary antibody was then washed in 1X PBS for 10 minutes (3X), and subsequently placed in secondary FITC antibody (1:200, Abcam, ab97063) at room temperature for 2 hours. Tissues were then washed in 1X PBS, mounted with and mounted with ProLong Gold antifade reagent with DAPI (Life Technologies, Grant Island, NY), and imaged on a Zeiss LSM 880 microscope.

Data analysis and statistics

Cell water volume was determined using the arbitrary fluorescent measurements from the NIS elements timelapse tool to measure intensity. Cells were chosen based on whether they responded to the final osmotic challenge of returning to isotonic solution. Leak of calcein over time can cause fluorescent changes that are independent of cell volume. Therefore, the fluorescent signal from cells that appeared to have dye leakage was corrected as previously

described (Muallem, Zhang, Loessberg, & Starr, 1992). GraphPad Prism8 was used for all statistical analysis. All data are reported as means ± SEM. One-way ANOVA tests for generally followed by post-hoc Tukey tests to determine significance among specific groups.

Results

Use of primary sensory neurons as a model for cell volume regulation

We utilized two available KCC3-targeted mouse lines to assess the role of KCC3 in cell volume regulation: a loss- of-function (LOF) line (Howard, Mount, et al., 2002) and a gain-of-function (GOF) mouse line (Kahle et al., 2016). We compared these two lines to control littermates (mice with no mutations in KCC3) and also compared neurons from wild-type animals with neurons pharmacologically treated with the potent KCC2/KCC3 inhibitor, ML077 (E. Delpire et al., 2009). Careful preparation of primary neurons on coverslips was critical in creating consistent, standardized results. First, glass cover slips were prepared two days prior to plating with an overnight incubation in 1% polyethylenamine (PEI), followed by an additional overnight incubation with laminin (50 µg/ml). DRG were then extracted and plated as described in the method section. KCC3 has been shown previously to be expressed in sensory neurons (Byun & Delpire, 2007; Howard, Mount, et al., 2002; Pearson et al., 2001). To confirm KCC3 expression in our isolated DRG neurons, we fixed the cells the day after plating and co-stained the neurons with anti-KCC3 antibody and DAPI and observed strong KCC3 signal (**Figure 4-1A-B**). No signal was observed when the cells were exposed to

secondary antibody alone (**Figure 4-1C**). Importantly, we observed no expression of KCC2, the central nervous system-specific K-Cl cotransporter (**Figure 4-1D-F**).

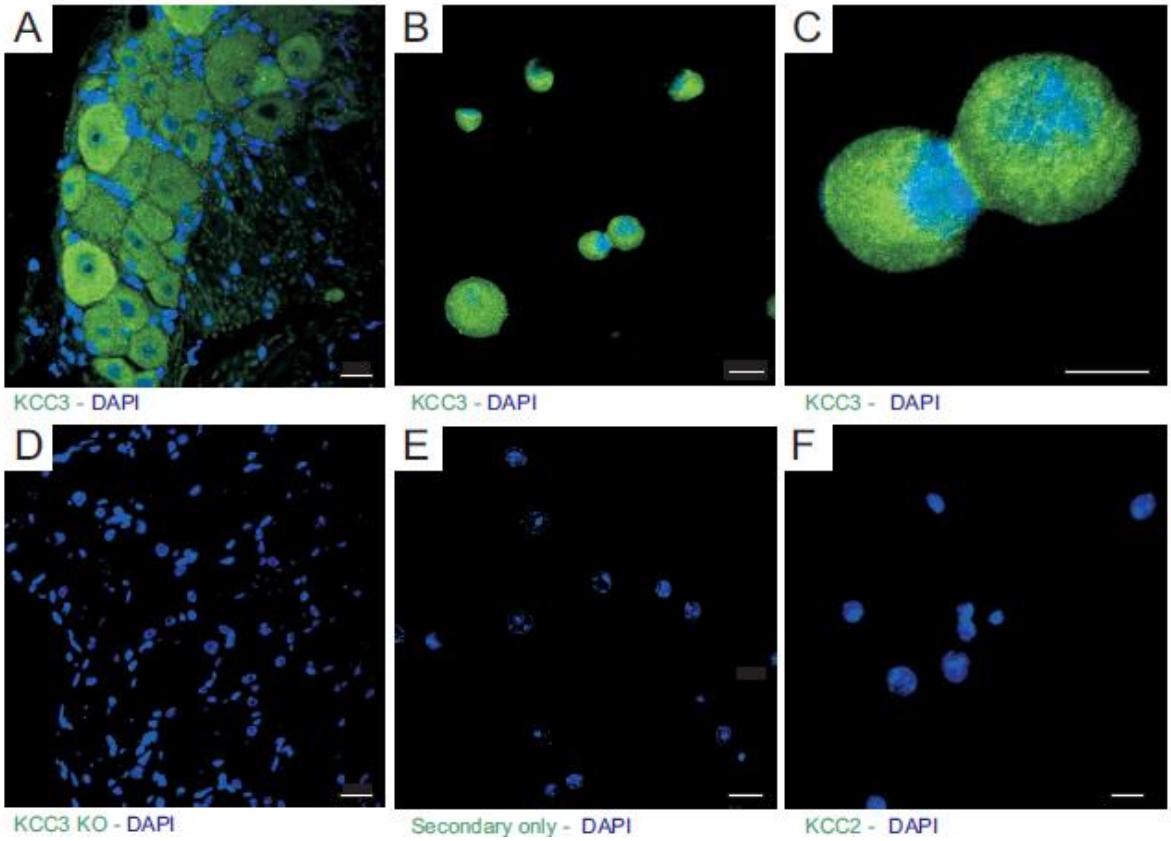

Figure 4-1. Expression of KCC3 in mouse DRG neurons. (A) Section of dorsal root ganglion isolated from wild-type mice stained with rabbit anti-KCC3 polyclonal antibody, followed by FITC-conjugated anti-rabbit antibody. **(B-C)**, DRG neurons isolated from wild-type mice stained with rabbit anti-KCC3 polyclonal antibody followed by FITC-conjugated anti-rabbit antibody. **(D)**, Section of dorsal root ganglion isolated from KCC3 knockout mice, stained with rabbit anti-KCC3 polyclonal antibody, followed by FITC-conjugated anti-rabbit antibody. **(E)**, Isolated dorsal root ganglion neurons stained with secondary antibody only. **(F)** wild-type DRG neurons stained with rabbit anti-KCC2 polyclonal antibody show absence of KCC2 expression. All slides were mounted with DAPI-containing mounting reagent to stain nuclei. Bars: 20 mm for A, B, D-F and 10 mm for C.

DRG cell volume was determined through calcein fluorescence measurements

All volume measurement experiments were also performed one day after plating. Experimental set up included a 25 min incubation period with Calcein-AM (0.03 μM) in isotonic medium (300 mOsm), a baseline period under isosmotic solution, followed by an osmotic challenge. For our first set of experiments, we analyzed our data by placing the pinhole to different regions of the cell (**Figure 4-2**). The data was highly variable as some pinholes gave the typical decrease in fluorescence due to dye dilution during cell swelling, while others gave either no change or an increase in fluorescence signals.

The data were, however, highly consistent when the pinholes were selected around the center of the cell (**Figure 4-3A**). In all cases, a significant decrease in fluorescence signal was observed with a tight average and a small signal variation (**Figure 4-3B-C**). The fluorescence signal traced well with the measured volume of the neurons, based on the area of the cell (**Figure 4-3D**). **Figure 4-3E** provides the typical response of a control DRG neuron when baseline fluorescence is recorded in isotonic solution for 3 min, followed by a 10 minute 40% hypotonic challenge, and a return to isotonic solution for 3 min. The cell swelled rapidly, followed by a period of regulatory volume decrease. When the cells are returned to isosmotic conditions, the volume overshoots as the cells have lost osmolytes. The perfusion bath system was designed in such a way that the open chamber refills with the new solution in a matter of seconds, allowing rapid changes in fluorescence (volume) to be detected. The extent of swelling (1), rate of swelling (slope, 2), rate of RVD (3), the rate of shrinkage upon return to

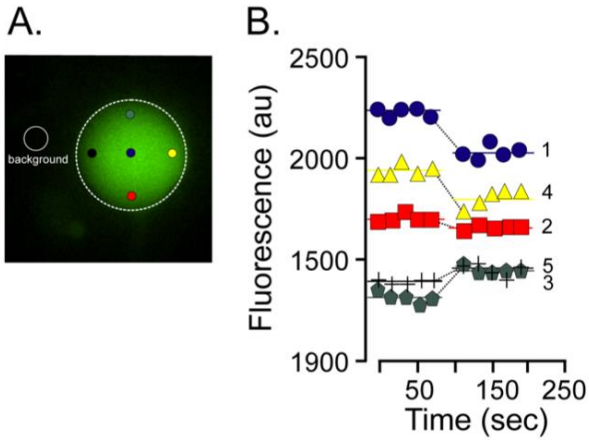

Figure 4-2. Calcein fluorescence measurements in dorsal root ganglion neurons. (A) Micrograph showing an isolated neuron loaded with calcein and background surrounding signal. Colored circles provide the position of the small "pinholes" that were used to acquire fluorescent signal during the swelling phase of the neuron during a hypotonic treatment. **(B)** variability of signals with only blue and yellow pinholes showing anticipated decrease in fluorescence, whereas no fluorescence or even increased fluorescence were observed at the red and green pinholes, respectively.

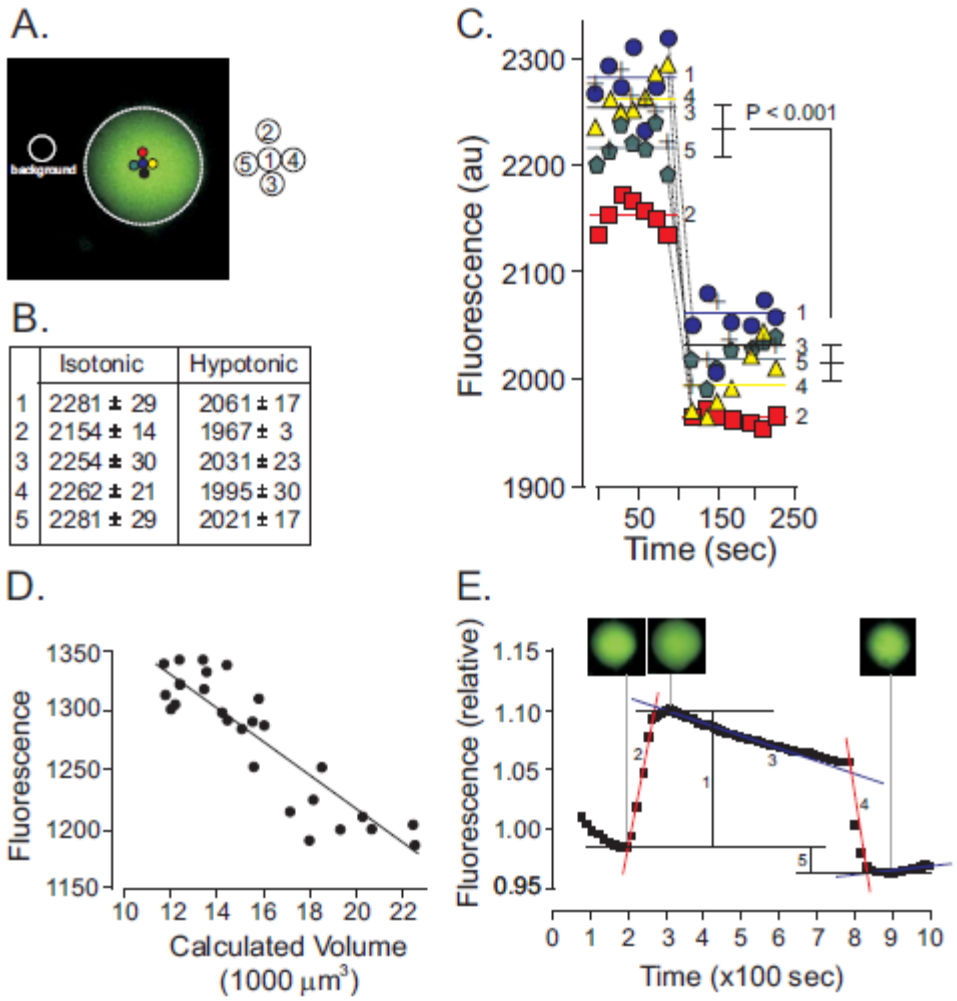

	Isotonic	Hypotonic
1	2281 ± 29	2061 ± 17
2	2154 ± 14	1967 ± 3
3	2254 ± 30	2031 ± 23
4	2262 ± 21	1995 ± 30
5	2281 ± 29	2021 ± 17

Figure 4-3. Calcein fluorescence measurements in dorsal root ganglion neurons. (A) Micrograph showing an isolated neuron pre-loaded with calcein-AM and background surrounding signal. Several pinholes, indicated by colored circles, were positioned around the center of the neuron. **(B)** Average fluorescence values obtained under isotonic (0 – 100 sec) and hypotonic (100 – 250 sec) conditions. **(C)**, same data presented in graph form with average fluorescence decreasing significantly upon cell swelling. **(D)**, Linear relationship between fluorescence signal and cell volume measured through the area of the neuron. **(E)** Typical curve of fluorescence over time of neurons exposed to a hypotonic solution. The graph can be divided into a swelling phase (extent of swelling: 1, and rate of swelling: 2), regulatory volume decrease phase (3), a shrinkage phase when the cells are returned to isosmotic conditions (4) and possible volume overshoot (5). Neuron insets show larger neuron at peak of swelling with decreased fluorescence.

isosmotic conditions (4), and the extent of overshoot (5), are all parameters measured in this type of experiment (**Figure 4-3E**).

Neurons from wild-type (with or without KCC3 inhibitor), loss of KCC3 function, or gain of KCC3 function display different responses to the osmotic challenge.

For this set of experiments, we isolated DRG neurons from 2-3 mice per genotype and recorded the response of a large number of neurons per preparation. All neurons were subjected to the 3 min isotonic baseline recording. At 3 min, the perfusion solutions were rapidly changed from isotonic to a 40% hypotonic osmotic shock and the cells were monitored for 10 minutes. The cells were then returned to isotonic media to assess the ability of the neurons to return to baseline. If a cell did not properly respond to the return under isosmotic solution, this cell was eliminated from further analysis.

As neurons were exposed to hypotonic solution, they all swelled, but surprisingly to different degrees. Control neurons swelled by 11.5%, and with a rate of 0.0011 sec^{-1} (**Figure 4-4, 4-5A-B**). Cells that lacked KCC3 increased their volume by 13.6% with a slower rate of 0.0007 sec^{-1}, whereas cells that express the constitutively active transporter demonstrated a blunted swelling response: 9%, and also with a slower rate of 0.0006 sec^{-1}. Finally, control neurons exposed to the KCC-specific ML077 inhibitor also showed an increased swelling over no inhibitor (although statistically not significant) with a rate of 0.0010 sec^{-1} (**Figure 4-4, 4-5A-B)**. The slopes amongst genotypes and treatment differed significantly ($P = 0.0001$).

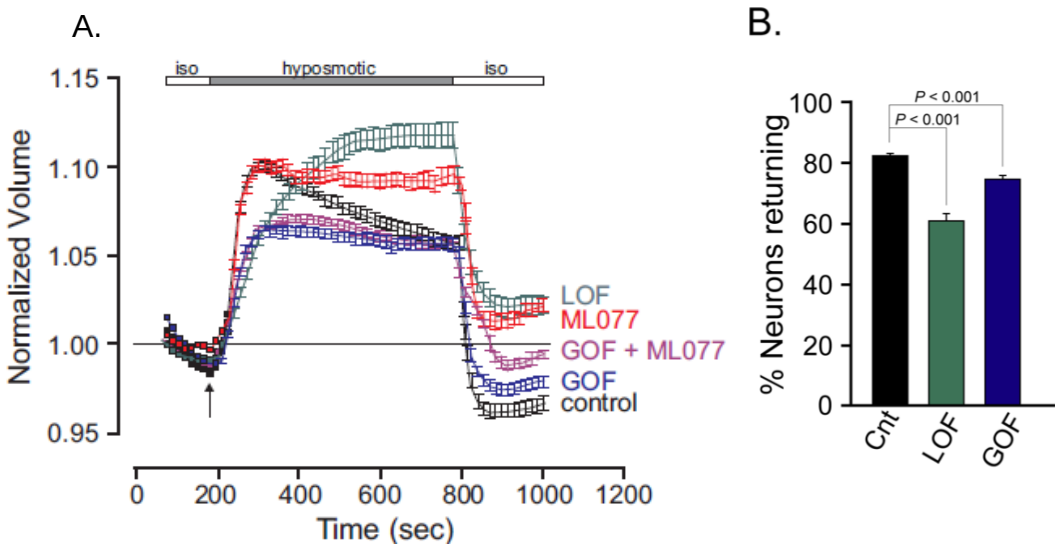

Figure 4-4. Osmotic behavior of neurons exposed to a hypotonic challenge. (A) Neurons from wild-type (black), KCC3 knockout (green), KCC3-T991A (blue), wild-type exposed to ML077 (red), KCC3-T991A exposed to ML077 (purple) were exposed to a 40% hypotonic shock. Fluorescence signals were averaged from 3 mice, 152 neurons for controls, 3 mice, 98 neurons for loss of function, 3 mice, 229 neurons for gain of function (T991A), and 3 mice, 134 neurons for the ML077 condition. Values are means ± SEM. **(B)** Percentage of cells that failed to shrink (return towards baseline) when re-exposed to isosmotic solution. The non-responsive cells were deemed unviable and eliminated from the analysis. Statistical significance was calculated using one-way ANOVA with Tukey post-test.

When the data were calculated by using time to half-peak rather than peak swelling, the data were similar (data not shown).

Following the swelling phase, most cells undergo regulatory volume decrease through a process that involves the loss of K^+ and Cl^- ions, and obligatory water. Control DRG neurons exhibited such a behavior (**Figure 4-4, 4-5C**). Interestingly, no regulatory volume decrease phase was observed in DRG neurons lacking KCC3 expression, expressing a constitutively active transporter, or exposed to the KCC-specific inhibitor, ML077. In fact, DRG neurons lacking KCC3 kept swelling for a few more minutes without reaching a true plateau. Statistical analysis confirmed that the slopes were significantly different between conditions ($P = 0.001$).

When the neurons were returned to isosmotic solution, they all shrunk. As seen in **Figure 4-6A**, the slopes were not significantly different ($P = 0.05$). What was statistically significant was the position of the curves ($P = 0.0001$), which reflects the differences in swelling and RVD that the cells have experienced during the hypotonic phase. To determine the ability of the DRG neurons to return their volume to baseline, we calculated the difference between the volume reached by the neurons following their return under isosmotic solution and the original volume of the cells. As seen in **Figure 4-6B**, both control and constitutively active KCC3 neurons reached a new volume that was significantly lower than the original volume, whereas neurons lacking KCC3 expression (LOF) or function (ML077) did not fully return to their original volume. A one-way ANOVA showed an overall significant difference among means of osmotic recovery for all genotypes ($P = 0.0001$), with also significance at P

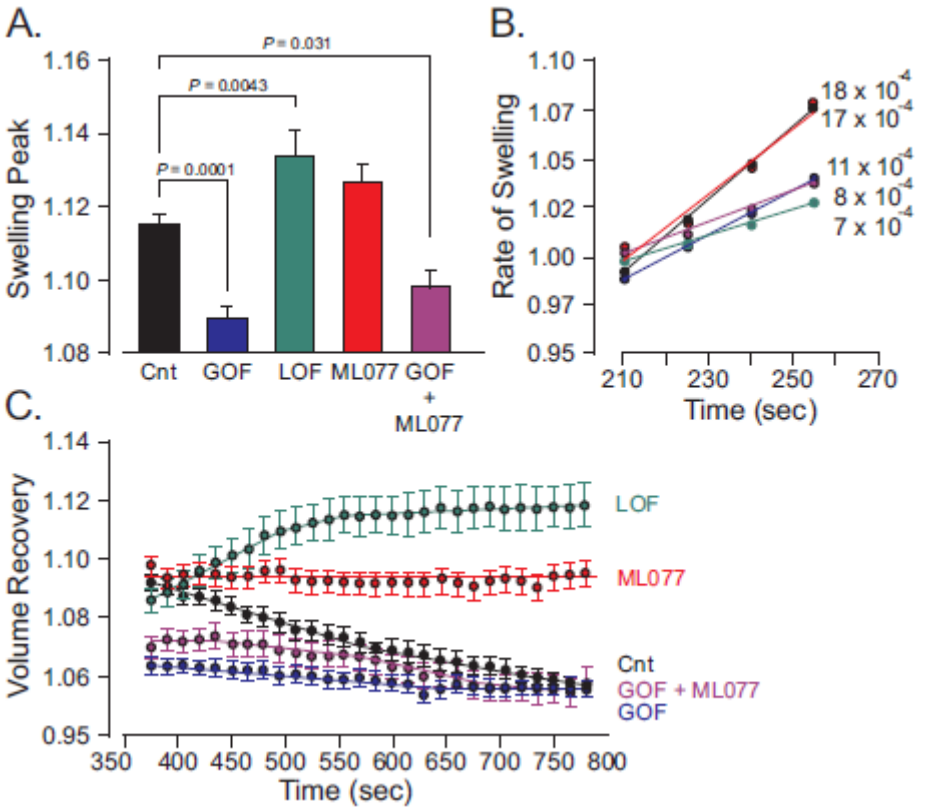

Figure 4-5. Osmotic behavior broken-down by components. (A) Extent of swelling of control neurons (black bar), KCC3 gain-of function (T991A) neurons (blue bar), KCC3 loss-of-function (knockout) neurons (green bar) and wild-type neurons exposed to 10 µM ML077 (red bar). Note the significant (One-way ANOVA) reduction in swelling elicited by the neurons expressing the constitutively active transporter and significantly increased swelling elicited by neurons lacking KCC3 expression. Treatment with ML077 showed no significant difference compared to control (P = 0.06). Bars represent means ± SEM (the number of neurons per genotype is listed in the legend of Figure 4). **(B)** Rate of swelling as calculated by the slope of volume increase. Control neurons: y = 0.0011 x + 0.7596; control neurons with ML077: y = 0.0010 x + 0.7984; neurons expressing KCC3 gain-of-function: y = 0.0007 x + 0.8448; and neurons lacking KCC3: y = 0.0006 x + 0.8178. **(C)** Regulatory volume decrease phase as measured over a 10 min period with only untreated wild-type neurons showing a negative slope**.**

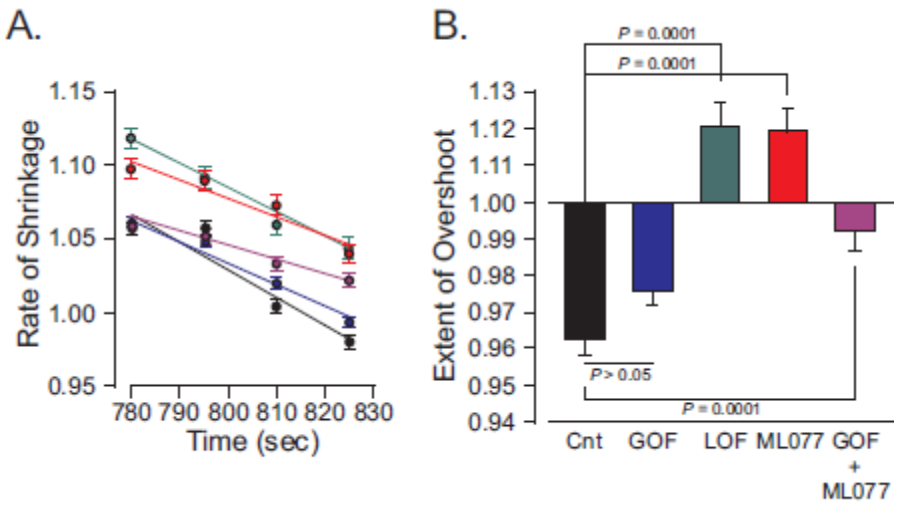

Figure 4-6. Osmotic behavior of neurons broken-down by components. (A) rate of shrinkage of neurons when they are returned to isosmotic saline following a 10 min exposure to hypotonicity. Note that the slopes are not very different amongst genotypes. **(B)** Extend of cell shrinkage. The Y axis represents relative fluorescence where 1 represents the original fluorescence of the cells under isosmotic solution prior to the osmotic shock. A negative bar (as for control neurons and KCC3 T991A neurons) represents a volume overshoot, whereas a positive bar (as KCC3 knockout neurons and wild-type neurons treated with 10 μM ML077) represents a volume still larger than the original volume of the neurons. Bars represent means ± SEM (3 mice, 98-229 neurons). Significance was calculated using one-way ANOVA followed by Tukey Post-hoc analysis test.

= 0.0001 when comparing individually LOF with control neurons or ML077-treated neurons with control neurons. In contrast, there was no statistical difference between GOF and control ($P = 0.05$).

Osmotic behavior of DRG neurons: the Van't Hoff plot

The osmotic phase of a cell depends primarily upon the water permeability of the membrane and the extent of the osmotic pressure verb upon the cell. As we have seen in **Figure 4-4**, the extent of swelling in response to a 40% osmotic shock was highly dependent on the genotype condition. To analyze further the osmotic behavior of the neurons, we exposed cells to milder hypotonic shock and to hypertonic shock and plotted the ratio of volumes versus ratio of osmotic pressures. The Van't Hoff plots are depicted in **Figure 4-7**. It can be seen that the relationship of volumes versus pressures is linear over the range of applied pressure, but that the slopes differed significantly. Indeed, statistical analysis revealed a significant difference among the slopes ($P = 0.04$). Note that the Van't Hoff slope of neurons expressing the constitutively active KCC3 transporter was significantly reduced compared to wild-type neurons, consistent with the reduced swelling of the LOF cells under the 40% hypotonic shock, whereas the slope of neurons lacking KCC3 expression is increased, again consistent with the increased swelling observed with these cells. We also produced van't Hoff plots for the volume changes observed when the cells are returned under isosmotic conditions after the original osmotic perturbation. As seen in Figure **4-7B**, there was no significant slope difference among the different groups of neurons ($P = 0.7$).

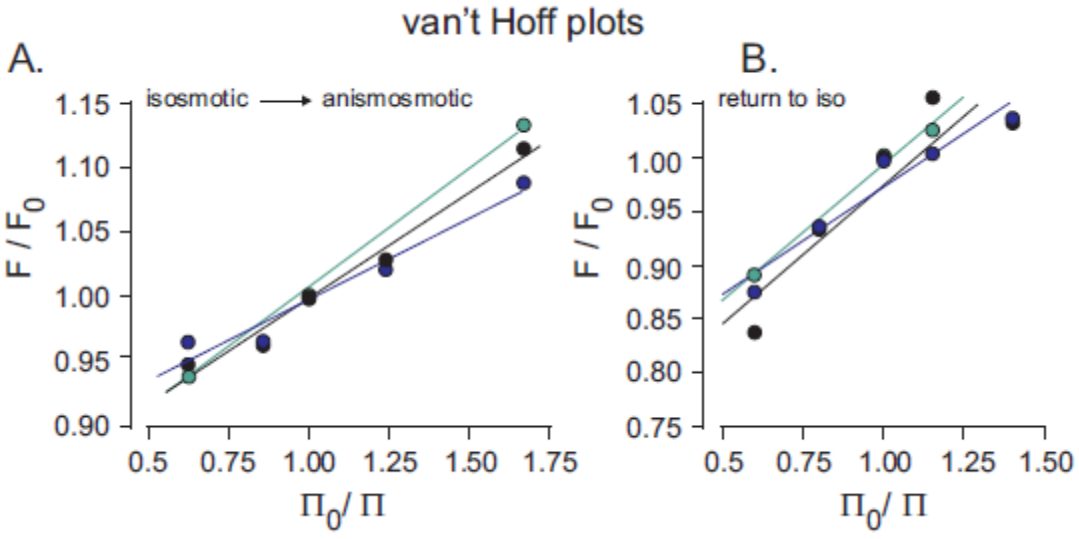

Figure 4-7. Osmotic sensitivity of neurons. (A) Van't Hoff plot showing fluorescence ratio versus osmotic pressure ratio of neurons exposed to 40% and 15% hypotonic and hypertonic shock. Note that the slope of the KCC3 gain-of-function neurons (blue dots and line, y = 0.126 x ± 0.8715) is lower than the slope of wild-type neurons (black dots and line, y = 0.1651 x ± 0.8330); whereas the slope of the KCC3 knockout neurons (green dots and line, y = 0.1861 x ± 0.8211) is bigger that for wild-type neurons. **(B)** van't Hoff plot of neurons returning to isosmotic conditions. There was no significant difference among the slopes (P = 0.7) nor intercepts (P = 0.6). All slopes appear similar (control, y = 0.2563 x ± 0.7187; GOF y = 0.1984 ± 0.7742; LOF y= 0.2515 x ± 0.7419).

Discussion

We previously documented the first human case of a gain of function of KCC3 (Kahle et al., 2016). Similar to the patients with a loss of KCC3 function, this unique patient with the constitutive Thr991Ala mutation also exhibited sensorimotor neuropathy. In this case, however, there was no agenesis of corpus callosum or cognitive impairment. Experiments performed with fibroblasts isolated from the patient surprisingly demonstrated an inability to swell upon hypoosmotic challenges, when compared to control fibroblasts (Kahle et al., 2016). Interestingly, analysis of nerve fibers from the KCC3-T991A mice revealed shrunken fibers (Flores et al., 2019b). Thus, it is clear that cell volume disturbance is a common feature in both KCC3 knockout and KCC3-constitutively active peripheral neuron and this implicates volume homeostasis as a critical factor for the health of peripheral nerve fibers.

The overarching goal of our experiments was two-fold. First, we wanted to assess the ability of sensory neurons from KCC3 wild-type, LOF and GOF mice to regulate their volume upon a hypotonic challenge. Second, we wanted to re-confirm with another native cell type, more relevant to the neuropathy, the unusual data that were observed with human fibroblasts expressing the overactive KCC3 transporter (Kahle et al., 2016).

Overall, there were clear differences in the osmotic responses of GOF, LOF, and neurons treated with the KCC inhibitor ML077, when compared to control neurons. We assessed these difference by utilizing a fluorescent marker as a proxy for cell volume (Altamirano et al., 1998). Our data confirm that using changes in the fluorescence signal of a

dye was a reliable method to follow changes in cell volume as fluorescence signal has an inverse relationship with cell volume.

The swelling phase of cells during hypotonic treatment is typically regarded as strictly mediated by rapid water movement across the membrane to equilibrate the osmotic pressure. Cell membranes are indeed typically regarded as semi-permeable membranes, i.e. far more permeable to water than ions and other osmolytes. In fact, the estimated water permeability of biological membranes (Stein & Litman, 1990) ranges from 0.5 (as for water tight membranes, i.e. the bladder) – 40 (as for water permeable membranes, i.e. red blood cell) x 10^{-4} cm/s. Comparatively, the intrinsic ion permeability of a membrane to ions like Na^+ and K^+ is many orders of magnitude smaller (4-5 x 10^{-14} cm/s, (Hauser et al., 1972). As the water permeability of a membrane is only dependent on the lipid composition of this membrane and the presence or absence of water channels, one would assume that the water permeability of DRG neurons is identical amongst the different KCC3 genotypes and the cells would at least exhibit similar swelling behavior, even if they exhibit different volume regulation behaviors.

Indeed, control DRG neurons exposed to a 40% hypotonic shock exhibited the typical swelling phase, followed by a regulatory volume decrease phase. Although the cells did not return to their original volume over the 10 minute hypotonic shock, they clearly underwent regulatory volume decrease. The fact that the volume of these cells reached a volume smaller than the original volume when the cells were returned to isosmotic solution, confirmed that the RVD process was due to a loss of intracellular osmolytes. When control neurons were exposed to the KCC-specific inhibitor, they swelled to the same degree than wild-type cells,

but did not volume regulate. The cells remained swollen for the duration of the hypotonic shock. This data indicates that the cotransporter is involved in the RVD process and may be responsible for the volume set point for activation of the cotransporter that exists under hypotonic conditions (Hoffmann et al., 2009).

The behavior of the KCC3-knockout neurons and the KCC3-constitutively active neurons was surprising. As shown with fibroblasts isolated from the KCC3-T991A patient (Kahle et al., 2016) and HEK293 cells transfected with a KCC3-T991A + T1048A mutant transporter (Adragna et al., 2015), DRG neurons isolated from KCC3-T991A mice failed to properly swell under the 40% hypotonic shock. The extent of swelling was significantly reduced compared to wild-type cells.

The fact that DRG neurons isolated from KCC3-T991A mice did not swell to the same degree indicates that some of our assumptions are incorrect. First, we need to consider that the KCC3-T991A neurons already start with a smaller volume under isosmotic conditions. Indeed, on average, T991A neurons have a volume of approximately 10,000 μm^3 (N = 2 mice, n = 107 neurons) whereas control neurons are 10% larger with a baseline volume of 11,000 μm^3 (N = 1, n = 94). The mutant cells therefore have already a reduced amount of water and osmolytes. However, if they start with a smaller volume, and the swelling phase is purely osmotic, they should swell in the same proportion than wild-type cells.

Second, the explanation for the swelling discrepancy might be related to the assumption that the swelling is purely osmotic. It might possible that the constitutive activity of KCC3 allows for a rapid loss of K^+ and Cl^- ions during the swelling phase, possibly large

enough to reduce the extent of cell swelling. Unusually high ion permeability might indeed be possible as in human red blood cells, for instance, the Cl^- permeability is in the same order of magnitude than the water permeability of water-tight epithelia (Hauser et al., 1972). This high Cl^- permeability results from high expression levels of AE1 (formally band 3), a Cl^-/HCO_3^- exchanger.

Note that in contrast to the T991A mutant cotransporter that would have a constitutively high K^+ and Cl^- permeability, the wild-type cotransporter needs a few minutes to activate when the cells are exposed to hypotonic stimuli. This lag phase, first described in red blood cells, was demonstrated to be due to swelling-induced inhibition of transporter phosphorylation, i.e. inhibition of a kinase (Jennings & Al-Rohil, 1990). Thus in wild-type cells, KCC3 would be silent during the swelling phase and allow for the full osmotic effect. The explanation of a rapid loss of ions, however, was rejected when DRG neurons isolated from KCC3-T991A mice were exposed to the 40% hypotonic shock in the presence of ML077. The inhibitor failed to restore the swelling extent to its original value.

Third, assumption that K-Cl cotransporters transport only K^+ and Cl^- ions was challenged by the work of Zeuthen who provided evidence for a direct KCC-mediated transport of water. He estimated a stoichiometry of about 500 water molecules for each K^+ and Cl^- ion (Zeuthen, 1994). Part of the evidence was that water movement could occur against an osmotic gradient. Whether this phenomenon is at play in KCC3-T991A neurons during their swelling phase is currently unknown. The recent cryo-EM structure of KCC1

(Liu et al., 2019) does not provide any hint that direct water movement through the K-Cl cotransporter protein is possible.

As mentioned above, in their 2015 paper, Adragna and coworkers observed a similar reduction in swelling of fibroblasts transfected with constitutively active KCC3 (Kahle et al., 2016). They argued that NKCC1 in these conditions was activated as the extent of swelling could be restored by inhibiting the cotransporter with low doses of bumetanide. These data suggests that the transport of salt and water during the swelling phase is able to affect the extent of swelling. Indication that a rapid transport of ions and water during the swelling phase is supported by the demonstration that the intrinsic water permeability of the GOF neurons is, in fact, not different than control cells. Indeed, the rate of cell shrinkage when cells are returned to isosmotic conditions, as evidenced by the slopes (see **Figure 4-6A**), was identical between genotypes.

Indication that the constitutive activity of KCC3 leading to a counteractive loss of ions (osmolytes) during the swelling phase might be at play comes from the demonstration that the intrinsic water permeability of the GOF neurons is in fact not different than control cells. Indeed, the rate of cell shrinkage when cells are returned to isosmotic conditions, as evidenced by the slopes (see **Figure 4-6A**), was identical between genotypes.

When neurons isolated from KCC3 knockout mice were exposed to the 40% hypotonic shock, the cells swelled to a higher degree than wild-type cells (**Figure 4-4**). This is also consistent with the idea that that transport mechanisms can affect the swelling phase. However, the rate of swelling (slope to peak or to ½ peak) was reduced when compared to

wild-type neurons, a phenomenon that we cannot fully explain. No RVD process was then observed in the KCC3 knockout neurons, consistent with the notion that loss of K^+ and Cl^- through the cotransporter mediates regulatory volume decrease in DRG neurons. These data also confirm previous data obtained with hippocampal pyramidal neurons and renal tubule proximal cells from KCC3 knockout mice versus wild-type mice. Both neurons and epithelial cells from knockout increased their volume to the same extent than wild-type cells, but the regulatory volume decrease phase was significantly blunted in the KCC3 knockout cells (Boettger et al., 2003).

Another piece of evidence that KCC3 activity in wild-type neurons is involved in RVD comes from the overshoot observed when cells are returned to isosmotic conditions (**Figure 4-6B**). The fact that the neurons shrank to a volume lower than the original volume indicates that the cells had lost osmolytes during their time under hypotonicity and the fact that neurons lacking KCC3 did not overshoot but instead showed a positive volume (**Figure 4-6B**) confirmed the participation of KCC3 in the process. Interestingly, wild-type neurons exposed to ML077 during the hypotonic phase also failed to RVD and accordingly failed to overshoot when placed back under isotonic conditions. The fact that KCC3-T991A neurons exhibited a volume overshoot also implies that osmolytes were lost under the hypotonic phase. In this case, however, no RVD phase was observed, possibly indicating that the loss of ions/osmolytes instead occurred during the swelling phase.

In agreement with the lack of swelling of KCC3-T991A DRG neurons with a 40% hypotonic shock, the slope of the van't Hoff volume/osmolarity relationship was also

significantly reduced when compared to wild-type neurons. The fact that the volume versus osmolarity relationship is linear is in agreement with the osmotic behavior of most cells studied in the range of experimental osmolarities tested (Delpire & Gagnon, 2018). The reduced slope is indicative of a reduced ability of GOF neurons to swell under hypotonic conditions. The intercept of a typical Van't Hoff plot on the Y axis provides the osmotically inactive volume, which in any cells ranges from 5-20%. The observation that the intercept of our Van'Hoff lines in our experiments provides values of about 85% reflects the fact that a ratio of fluorescence is plotted as a proxy of volume. From the data of **Figure 4-3E**, one can calculate that an 8% increase in fluorescence, in fact, corresponds to a 67% increase in cell volume. Thus, the intercept on the Y axis in our van't Hoff plots hardly represents the osmotically inactive volume.

The inability of KCC3 LOF neurons to volume regulate and inability of KCC3 GOF neurons to swell clearly indicate that these cells are unable to maintain volume homeostasis. This is in fact in full agreement with demonstration that nerve fibers from KCC3 knockout mice are swollen (Byun & Delpire, 2007), whereas nerve fibers from KCC3-T991A mice are shrunken compared to the fibers of control littermates (Flores et al., 2019b). The inability of neurons to properly volume regulate likely accounts for the vacuolization and related pathology observed in the central nervous system (Boettger et al., 2003) and peripheral nervous system (Auer et al., 2016; Byun & Delpire, 2007; Ding & Delpire, 2014). The fact that a greater number of neurons (40% LOF and GOF versus 10% for controls) failed to "survive" the osmotic challenge (as evidenced by lack of shrinkage when returned under

isotonicity, see **Figure 4-4B**), validates the *in vivo* studies. Similarly, the number of DRG neurons that were isolated per mouse was significantly lower for KCC3 knockout mice, indicating the fragility of these neurons. It is likely that this inability to maintain volume integrity is at the basis of the nerve pathology and the inability of the nerve fibers to properly function. Ultimately, further work needs to be done to further understand the discrepancies we observe in cell swelling amongst mutations in KCC3, and how these disruptions ultimately lead to peripheral neuropathy in both humans and mice.

Conclusions

Compared to wild-type, loss of KCC3 function in sensory neurons leads to inability of the cells to cell volume regulate following a hypotonic challenge. Comparatively, gain of KCC3 function in sensory neurons led to an unexpected blunted swelling response to hypotonicity. Differences in swelling rates amongst all three genotypes suggest a potential role for KCC3 in facilitating water transport.

CHAPTER 5

Physiological relevance of the temporal expression of KCC3

Introduction

The physiological importance of KCC3 has been clearly demonstrated in the population located in the Saguenay Lac-St-Jean region outside of Montreal, Quebec. These individuals of French-Canadian origin with a LOF of KCC3 suffer from hereditary sensorimotor neuropathy with agenesis of the corpus callosum (HSMN/ACC) (Casaubon et al., 1996; Howard, Mount, et al., 2002; Salin-Cantegrel et al., 2007). As basic science researchers, we have observed and recapitulated the debilitating and life-threatening effects of a loss of function LOF of KCC3 (Howard et al., 2002; Boettger et al., 2003; Ding et al. 2014; Shekarabi et al., 2012), we are no closer to finding an actual cure or remedy for this population. However, what has taken place has been primarily preventative with individuals from this population undergoing genetic counseling. As mentioned in chapter 3, HSMN/ACC (formerly Andermann Syndrome), was not reported until the 1970s when Eva and Frederick Andermann visited this area to assess these individuals (Andermann et al., 1972). Furthermore, it would be another 30 years until scientists directly linked a LOF of KCC3 to Andermann Syndrome (HSMN/ACC) (Howard, Mount, et al., 2002).

Part of why it has been so difficult to find a standard pharmacological treatment is multi-fold. First, although the disruption in KCC3 protein is considered a “LOF”, it leads to a

truncated protein, due to a frameshift resulting from one base (guanine) deletion in exon 18 (2436delG, Thr813fsX). Therefore, it is not simply a matter of "re-activating" the protein or a related transporter, but "fixing" the DNA to restore proper translation of the full-length protein. Secondly, we have also established in Chapters 2-3 that KCC3 function is required within a specific functional range for proper health of nerve fibers. For example, if KCC3 is over-active, humans and mouse models display peripheral neuropathy phenotypes (Kahle et al., 2016) as when KCC3 is inactive. Finally, despite the past decades of research on the cotransporter, we still do not fully understand its physiological relevance. Our work in Chapter 4 strongly suggests a role in cell volume maintenance and regulation, as it was intimated by previous studies (Boettger et al., 2003; Byun & Delpire, 2007). All of these considerations raise the question of whether *SLC12A6* could be considered for gene therapy. HSMN/ACC individuals display neurodevelopmental deficits (e.g. variable agenesis of the corpus callosum, edema) and deficits in motor function relatively early in life (Andermann & Andermann, 1994). The disease also significantly worsens as the individual ages. Thus, there seems to be both developmental and neurodegenerative components to the disease. In this chapter, I present studies that were designed to temporally control expression of KCC3 by using a tamoxifen inducible system linked to CRE-mediated recombination. The studies focus on two time periods: adult mice (as many individuals with HSMN/ACC are currently now adults) and the younger, juvenile, period of postnatal day 20 (P20).

As mentioned in previous chapters, the global knockout of KCC3 recapitulates HSMN, but not ACC, a phenotype which in humans does not display 100% penetrance

(Howard et al., 2002; Boettger et al., 2003; Shekarabi et al., 2012). It has also been established that this phenotype is neuronal in origin, as neural-specific deletion of KCC3 in mice reproduces the entire phenotype (Shekarabi et al., 2012). In addition, our laboratory also demonstrated that a subset of neurons, the parvalbumin expressing neurons, accurately recapitulated locomotor deficits and the neuropathology observed in dorsal root ganglia (DRG) (Ding & Delpire, 2014; Auer et al., 2016). It should be noted that the mouse models generated by Boettger and Shekarabi sought to replicate Quebec mutation (within exon 18, Boettger et al., 2003; Shekarabi et al., 2012); whereas our laboratory generated mouse models that disrupted earlier exons (exon 3, Howard et al, 2002 and exon 7, Ding et al, 2014). All mouse models generated nicely recapitulated the human peripheral nerve disease. Therefore, the design of our two mouse models is based on the targeting of exon 7 and the use of a PV-Cre^{ERT2} tamoxifen-inducible system, as discussed further below.

Materials and Methods

ES cell targeting

The targeting vector of the rescue mouse was constructed by dropping via recombineering a 2526 bp fragment (5' recombination arm) from BAC clone bMQ-302F12 between unique sites located upstream of the first loxP site of a vector containing 3 loxP sites, 2 FRT sites, and a PGK-driven neomycin resistance gene cassette. A small DNA fragment consisting of two exons 7 surrounded by short intronic sequences was then ligated downstream of the first loxP site. Note that although not necessary, a stop codon was placed in the second exon 7 sequence. Then, a 7.5 kb fragment (3' recombination arm) was dropped from the BAC, downstream of the last loxP site. The construct was verified by map digest and partial sequencing. To target the *SLC12A6* gene for homologous recombination, 129/SvEvTac embryonic stem cells were electroporated with the construct linearized with *Not*I and grown on fibroblast feeder cells in Dulbecco's Modified Eagle Medium (D-MEM) medium supplemented with 15% fetal bovine serum, 50 mg/ml gentamicin, 1000 U/ml LIF, 90 mM β-mercaptoethanol, and 0.2 mg/ml G418. Forty independent neomycin-resistant colonies were picked and grown in 96-well plates on feeder layer, expanded, and their genomic DNA was analyzed for the presence of the mutant gene by Southern blot analysis. One clone (2A10) was identified and further characterized by long range PCR followed by sequencing. The validated clone was then injected into C57BL/6J blastocysts and two chimeric animals (one male and one female, with >90% brown fur) were produced. The chimeric male was mated to

C57BL/6J females and pups demonstrated germline transmission. The F1 mice were then crossed to FLPeR mice to eliminate the neomycin-resistance gene cassette and produce the designed mouse with loxP sites flanking the second exon 7. The mice were then backcrossed for 10 generations in C57BL/6J background prior to use.

Mouse models

All animal handling and experimental procedures were approved by Vanderbilt's Institutional Animal Care and Use Committee and done in accordance with guidelines provided by the National Institutes of Health. B6(Cg)-Pvalb$^{tm1(CreERT2)Zjh/j}$ mice (Stock No: 021189) were obtained from Jackson laboratories. The KCC3-flox mouse was previously described (Ding & Delpire, 2014). The two lines were crossed to obtained animals expressing one copy of the PV-Cre^{ERT2} allele and two copies (homozygous) of the KCC3-floxed exon 7 allele (mouse A). For the rescue experiment, we generated a mouse line that expressed a duplicated exon 7 flanked by loxP sites. This mouse was also bred to the PV-Cre^{ERT2} mouse to obtain animals expressing one copy of the PV-Cre^{ERT2} allele and two copies (homozygous) of the KCC3-stop allele (mouse B).

Genotyping

Mice were genotyped using two sets of oligonucleotide primers: one set identifying the presence of CRE, the other establishing the status of the Slc12a6 allele. For CRE, primers 5' CTGCATTACCGGTCGATGCAAC 3' and 5' CCGGTTATTCAACTTGC ACC 3' were

used to amplify a 149 bp fragment. For Slc12a6, oligonucleotide primers flanking the loxP site located upstream of exon 7 were: forward primer: 5′ TGTGACAGACA CTTCCTACAAGCC 3′ and reverse primer: 5′ TCAGACTTTGGGAAATTGAACGTAAC 3′. PCR amplification yielded a 294 bp fragment from the mutant allele and a smaller 254 bp fragment from the wild-type allele.

Tamoxifen preparation and administration

For adult mice, tamoxifen (Sigma, T5648-1G) was prepared at a concentration of 37.5 mg/mL in pharmaceutical grade corn oil (Sigma, C-8267). The concentration was halved to 18.75 mg/ml for juvenile mice. To ensure that the tamoxifen was fully dissolved, the tamoxifen-corn oil mixture was left to shake overnight at 37°C. Tamoxifen was given through oral gavage to adult mice at age P60 for mouse models A&B. In a second cohort of mice (model A), tamoxifen was also administered at postnatal day 20. Each mouse was given 100 μl tamoxifen per day for 3 consecutive days. Mice were given a 10-day rest period and then subjected to a week of behavioral tests. Mice were also retested 30 days later.

Accelerated rotarod assay

A neuromotor coordination task was performed using an accelerating rotating cylinder (model ENV-574M: Med associates Inc) in two cohorts of mice: 7 wild-type and 7 KCC3-PV-Cre^{ERT2} positive mice. The rotating drum was 3.18 cm in diameter. Mice were confined to a 7.62 cm-wide sections of the cylinder and divided by white Plexiglas dividers.

Two to five mice were placed on the cylinder at once. The rotation rate of the cylinder increased over a 4 min period from 4 to 40 rpm. The latency of each mouse to fall off the rotating cylinder was automatically recorded by the device. Mice that remained on the rotarod during the 300 sec trial period were removed and given a score of 300 sec. The test was performed for three trials daily for 3 consecutive days with an inter-trial interval of at least 30 min.

Balance beam

To assess motor coordination and balance, we utilized a 1-meter long, steel balance beam. We utilized two beams of varying thickness: a standard-sized beam (12 mm), and a thinner beam (6 mm), both of which had square cross sections to assess finer motor movements. The beam was placed approximately 50 cm from the ground and positioned between two pillars. For mice that fell, empty cages with bedding were placed underneath the balance beams. Mice were acclimated to the balance beam by rubbing bedding from their cage prior to them crossing. At the start of the balance beam, mice began on an open, square platform and ended in an enclosed, black box with bedding as motivation for the mice to cross. We trained the mice for two days (three trials per day for each beam) beginning with the thicker beam (12 mm) and progressing to the thinner beam (6 mm). The mice were tested consecutively on each beam with ten-minute relief periods between each trial. The third day was used as a test day with three trials for each beam. The mice had approximately 60 seconds to traverse the beam and were scored on the neurological scoring system for beam

walking adapted from Feeney and Colleagues (Feeney et al., 1982). This scoring system is based on the ability of the mouse to cross the beam and accounts for the number of paw slips. The mice received a score ranging from 1-7 based on their ability to complete the task, to place affected limbs on beam, and on the number of paw slips. This neurological scoring system considers a high score of 7 to be indicative of a wild-type mouse phenotype with no coordination deficits and a low score of 1 indicative motor defects [score of 7: mouse crosses beam with no more than two paw slips; 6: is able to cross beam but uses affected limbs more than halfway along beam; 5: is able to cross beam but uses affected limbs less than halfway along beam; 4: crosses beam and is able to place affected limbs at least once on horizontal beam; 3: crosses beam but drags (affected) hind limbs; 2: is unable to cross beam, but is able to hold horizontal balance for at least 5 seconds; 1: is unable to cross beam].

Hot plate Assay

Mice were placed individually on a hot plate heated to 55°C for a maximum of 15 seconds (Hot-Plate Analgesia Meter; Columbus Instruments, Columbus, OH). Mice were confined to the hot plate by a plastic cylinder measuring 15 cm (diameter) and 20 cm (height). Mice are observed and immediately removed from the hot plate if they displayed withdrawal behaviors (i.e. licking paws or jumping; Richardson et al., 1998). As this is potentially a stressful test for the mice, this assay was done on the last day of the behavioral testing period and was only performed once.

Immunohistochemistry of Dorsal Root Ganglia (DRG)

Adult mice were euthanized with isoflurane and immediately dissected to remove T1-L5 DRGs. As described in (Sleigh et al., 2016), the vertebrae column was extracted, placed on ice, and then cut in half, ventral side facing upwards to remove the spinal cord and extract the DRGs. DRGs were then fixed in 10% formalin at room temperature overnight. Once fixed, tissue was embedded in paraffin and 10 micron thick sections were prepared. The paraffin was dissolved using Citrisolv (Thermo Fisher Scientific) and the tissue was rehydrated in 5 min consecutive washes of 100%, 95%, 70% ethanol, followed by a 10 min wash in 1X PBS. Antigen retrieval was performed on the slides using Citra Plus (BioGenex, Freemont, CA). Sections were then blocked with a buffer consisting of 5% bovine serum albumin, 1% goat serum, and 0.5% Triton X-100, for two hours. Sections were incubated with a rabbit polyclonal KCC3 antibody (1:200, Byun et al., 2007) at room temperature for 1.5 hours, and then placed overnight at 4°C. The primary antibody was then washed in 1X PBS for 10 minutes (3x), and subsequently placed in secondary FITC antibody (1:200, Abcam, ab97063) at room temperature for 2 hours. Tissues were then washed in 1X PBS and incubated with a Fab unconjugated antibody (1:20, Jackson Immunoresearch Laboratories, 111-007-003,) for 1 hour. After an additional washing, the process was repeated to be double stained with a parvalbumin antibody (1:750, Abcam, ab11427), and secondary Cy 3 (1:200, Abcam, ab6939)

Statistical analysis

For all behavioral experiments One-way ANOVA was performed utilizing GraphPad Prism (Version 8.3.1).

Results

To temporally manipulate KCC3 expression, we designed two separate mouse models (**Figure 5-1**). The first mouse starts with a normal expression of KCC3 from conception to adulthood. Then, upon tamoxifen treatment (**Figure 5-2**), the gene is disrupted and KCC3 expression is reduced or eliminated in cells expressing parvalbumin. This mouse model will allow us to determine if the deficit is developmental, i.e. if disruption of KCC3 in adulthood fails to reproduce the phenotype. The second mouse starts with a defective gene and a diseased mouse. Upon tamoxifen injection, the gene is repaired and KCC3 expression is restored. Through the use of this mouse, we should be able to assess if there is a point in time at which the development of the disease can be prevented or reversed.

As KCC3-flox mice develop with a functional cotransporter prior to administration of tamoxifen at P60, they should initially perform as wild-type mice on the rotarod assay. As seen in Figure 5-3, mice performed as anticipated with increased performance per trial each day and increased performance over the 3 day test. Importantly, when we re-tested the mice 10 days after tamoxifen administration and there was no significant difference in performance (**Figure 5-3)**. To determine if there was an earlier time point at which the disease could be triggered, we administered tamoxifen at P20 in a separate cohort of mice. As these mice were

too young to be subjected to behavioral analyses, we conducted the behavior at P60. Again, no differences were observed in the performance of mice treated with tamoxifen at P20. One-way ANOVA showed no significant differences ($P = 0.05$) for mice given tamoxifen at either

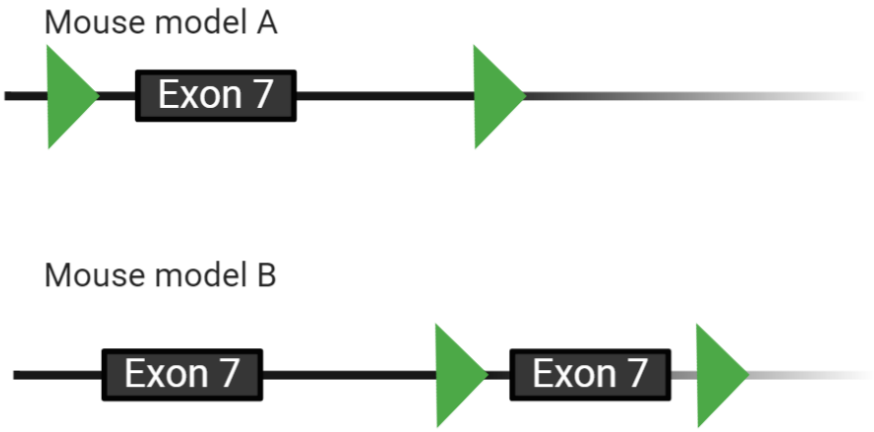

Figure 5-1. Design of mouse models to induce disruption or recovery of KCC3 expression. Mouse model A consists of a fully functional exon 7 flanked by loxP sites. The mouse has a functional KCC3 and develops properly. Disruption of KCC3 can then be induced later in life. Mouse Model B carries a Slc12a6 allele with two exons 7, the second flanked by loxP sites. Insertion of 2 exons 7 in the transcript disrupts KCC3 translation and produces a knockout. Thus, the mice develop like a KCC3 knockout animal. Once tamoxifen is administered, the duplicated exon 7 is excised and a fully functional KCC3 is expressed.

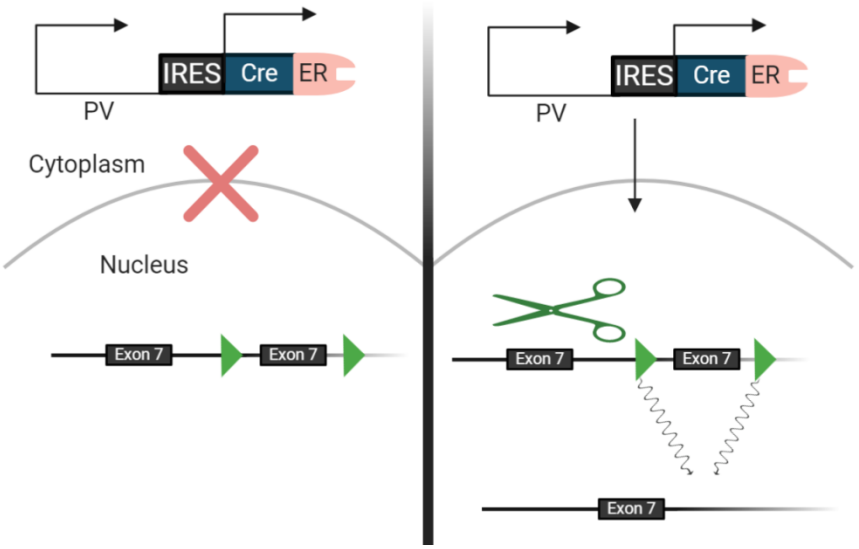

Figure 5-2. Inducible PV-Cre^{ERT2} system. As CRE^{ERT2} is located within the 3'UTR of the parvalbumin gene, its expression is driven by the parvalbumin promoter. The Slc12a6 gene with exon 7 surrounded by loxP sites will undergo recombination following administration of tamoxifen. Without tamoxifen, the CRE recombinase cannot enter the nucleus.

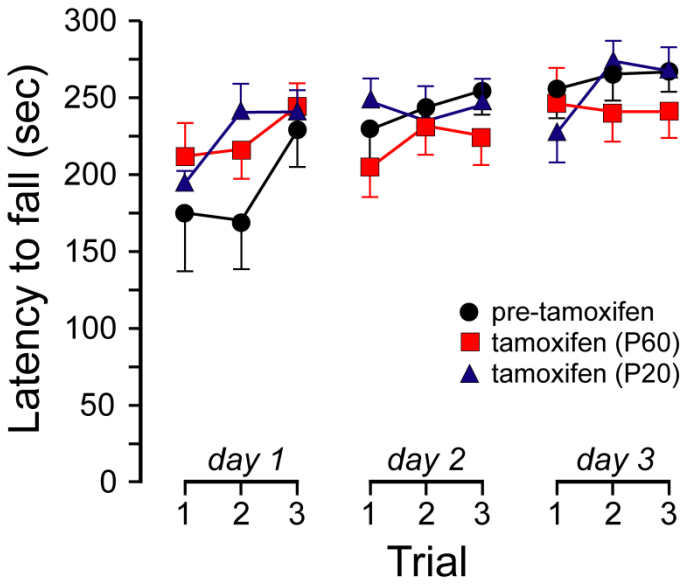

Figure 5-3. Rotarod performance of mice expressing inducible Pv-CRE x KCC3-flox mice. Mice treated with tamoxifen at P60 were first tested with roratod assay at P55 and re-tested at P70. Mice treated with tamoxifen at P20 were tested with rotatod assay at P60. There are no significant differences in performance on the rotarod (P = 0.5, n = 7 per cohort, one-way ANOVA).

P60 (cohort 1) or P20 (cohort 2), when compared to mice of cohort 1, pre-tamoxifen treatment.

As no significant differences were observed in the rotarod test, we performed the balance beam task, which can detect more subtle deficits in locomotor coordination (Luong et al., 2011). Balance beam performance can be quantified with time (seconds it takes each mouse to traverse the suspended beam) and by a "neuro-score", or assessment of how well each mouse traverses the beam without paw slips or falling. As described in Chapter 2, the test is performed first with a wide 12-mm beam then a more challenging 6-mm wide beam. For the 12 mm beam, animals treated with tamoxifen at P20 and behaviorally tested at P60 were significantly faster than mice tested at P50 prior to their tamoxifen treatment at P60 (p = 0.03, one-way ANOVA, **Figure 5-4A**). However, there was no significant difference in their neuro-score (p = 0.6, **Figure 5-4B**). When the mice were tested on the more challenging 6 mm beam, the P20 treated animals also took less time to traverse the beam (p = 0.2, one-way ANOVA, **Figure 5-5A**). While the neuro-score was a bit smaller, it did not reach statistical significance (p = 0.7, one-way ANOVA, **Figure 5-5B**).

Mice were also subjected to the hot plate assay to assess sensory perception, as HSMN/ACC patients experience both motor and sensory deficits. Mice treated with tamoxifen at P60 and tested at P70 on the hot plate or treated with tamoxifen at P20 and tested at P70 displayed a marked decrease in the latency to respond to a heat-evoked (55^{o}C) noxious stimulus, compared to pre-treatment. One-way ANOVA showed that mice administered with tamoxifen at P20 responded significantly faster than control mice (p = 0.04, **Figure 5-6)**.

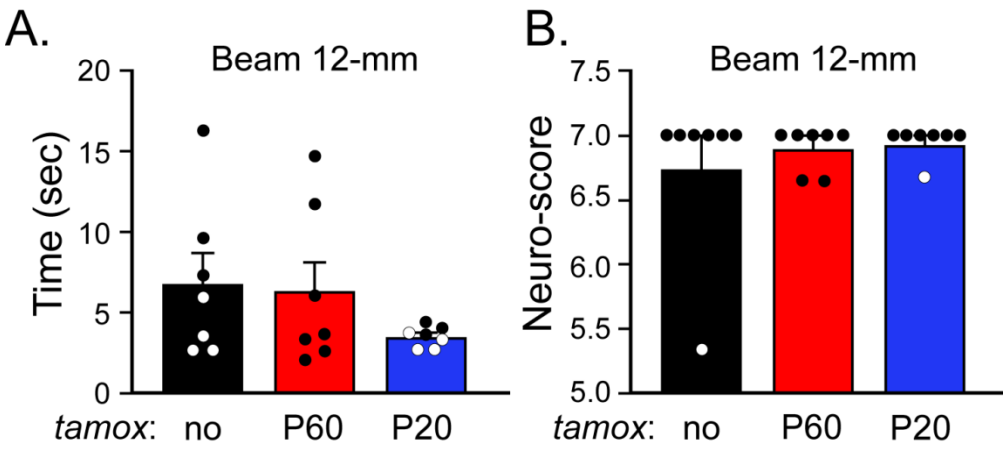

Figure 5-4. Balance beam (12-mm) performance of Pv-CRE^{ERT2} x KCC3-floxed mice. (A) Mice treated with tamoxifen at P20 displayed a shorter time interval to cross the beam. In contrast, mice treated at P60 displayed similar behavior than mice prior to treatment. **(B)** The neuro-scores, while slightly higher are not statistically different between groups (p = 0.6).

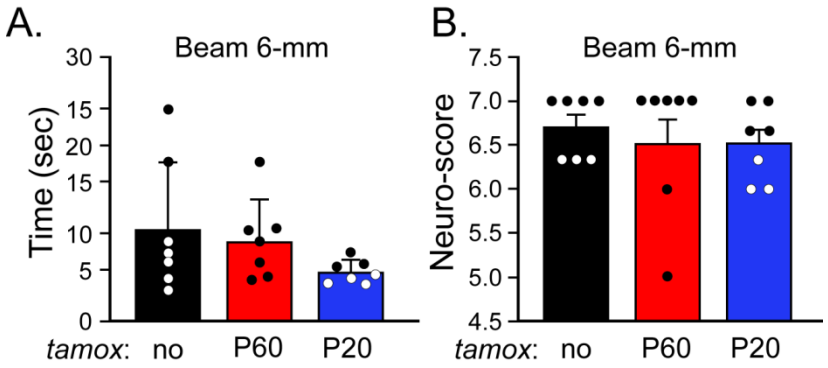

Figure 5-5. Balance beam (6-mm) performance of Pv-CRE^{ERT2} x KCC3-floxed mice. Mice treated at P20 with tamoxifen displayed faster times in traversing beam (P = 0.02). The neuro-scores, while slightly higher are not statistically different between groups (p = 0.7).

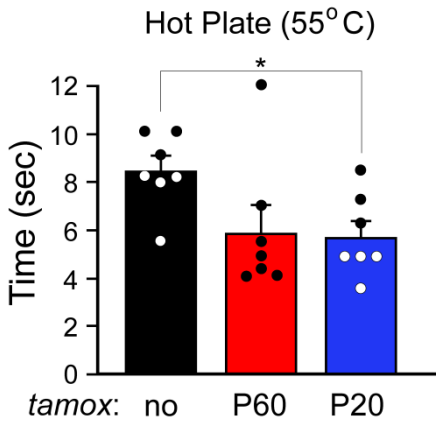

Figure 5-6. Hot plate assay in Pv-CRE^{ERT2} x KCC3-flox mice. Mice treated with tamoxifen (18.75 mg/ml) at P20 displayed increased sensitivity to a noxious heat stimulus, $P = 0.04$, one way ANOVA.

To ensure that the tamoxifen administration led to the excision of exon 7 in Slc12a6 and absence of protein expression, we conducted immunofluorescence studies of dorsal root ganglia immediately following the behavior experiments. Because KCC3 was specifically disrupted in parvalbumin expressing neurons, we used double staining of KCC3 and parvalbumin. As seen in **Figure 5-7**, overlapping parvalbumin and KCC3 signals can be seen in the mouse DRGs prior to tamoxifen treatment, while complete absence of KCC3 signal is observed after tamoxifen treatment.

Due to complicated breeding scheme and mice dying prior to our behavioral analyses, we only obtained and studied two mice that were Pv-CRE^{ERT2} positive on the background of the KCC3-exon 7-stop mice (model B). The two mice were assessed by rotarod analysis prior to tamoxifen administration and only one mouse was alive for the 10-day post tamoxifen re-test. As seen in **Figure 5-8**, mice tested very poorly on the rotarod, falling well before 50 sec in the first day and close to 50 sec on the third day of testing.

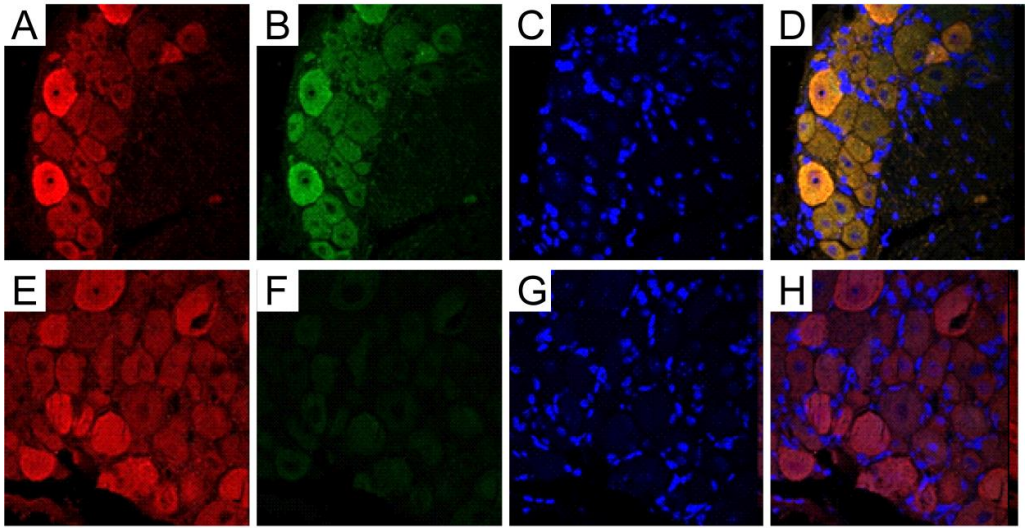

Figure 5-7. Immunofluorescence analysis of DRGs isolated from Pv-CRE^{ERT2} x KCC3-flox mice pre- and post- tamoxifen treatment. (A-D) DRGs prior to tamoxifen treatment displayed parvalbumin (red, A) and KCC3 (green, B) immunoreactivity. Dapi (C, blue) is used to stain nuclei. Overlay of panels A-C (in D) gives an orange color. **(E-H)** DRGs isolated from mice treated with tamoxifen. While the parvalbumin staining is visible (red, E), there is no expression of KCC3 (absence of green, F). Dapi (G, blue) and overlay (red, H) panels are also shown for the tamoxifen condition.

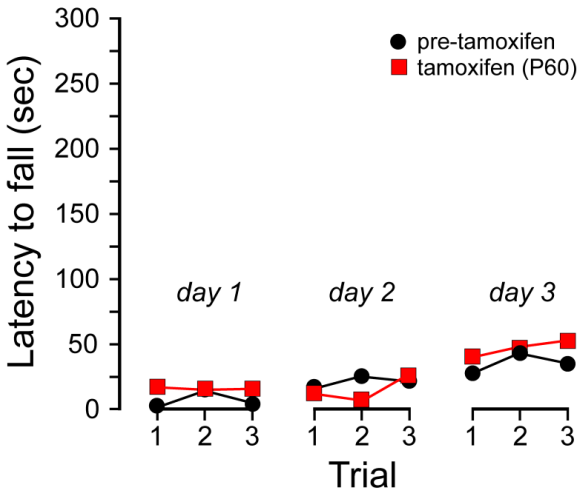

Figure 5-8. Poor rotarod performance of Pv-CRE^{ERT2} x KCC3-stop mice. Note that mice performed slightly better on day 3 than day 1, indicating an ability to learn. There are no error bars, as statistics could not be done on this cohort: n = 2 for pre-tamoxifen condition (back circles), and n = 1 for post-tamoxifen condition (red squares).

Discussion

In two regions of Quebec, Canada, the prevalence of HSMN/ACC has been recorded as 1 in 2,117 (De Braekeleer, Dallaire, & Mathieu, 1993), whereas the carrier mutation is estimated to about 1 in 23 individuals (Howard, Mount, et al., 2002). Currently, the means of combating these statistics has been through means of preventive medicine, like genetic counseling. Although this may affect prevalence of individuals with HSMN/ACC, it does not solve the health outcomes with those currently affected with this severe disease. As we have previously demonstrated, KCC3 remains a critical cotransporter in the nervous system, as a either a loss or gain of its function results in peripheral neuropathy (Howard, Mount, et al., 2002; Kahle et al., 2016). We know that KCC3 is likely important in development, as affected individuals display severe locomotor deficits at very young age. In addition, as the motor and sensory abilities of these patients deteriorate over time, leaving them with an average life-span of 33 years, there also seems to be a neurodegenerative component to the disease (Howard, Mount, et al., 2002). Whether the patients could be treated by re-introducing a functional cotransporter by gene therapy is unknown and in need of experimental testing. This was the goal of our studies and the design of two novel mouse models.

To assess whether there is a developmental component to the disease, we used an inducible system to completely bypass the developmental period and disrupt KCC3 in the adult mouse. The design took advantage of the fact that deletion of KCC3 in parvalbumin positive neurons results in significant locomotor deficit and sensory nerve pathology (Ding & Delpire, 2014). The mice were first tested as young adults (P55), then treated with tamoxifen

and retested still in their young adult phase (P70-P80). Overall, they displayed no locomotor deficits, as established by the rotarod and balance beam tasks. To ensure that enough time had elapsed between the tamoxifen administration and the neurobehavioral tests, we re-tested the mice 30 days later and obtained with similar data (data not shown). Because we established that KCC3 expression was eliminated in DRGs 10 days after the tamoxifen treatment, we conclude that it is during an earlier period that KCC3 function is critical to the peripheral nervous system. Interestingly, we observed a small decrease in the latency to respond to a noxious heat signal, although it did not reach statistical significance.

To assess whether the disease can be triggered earlier, we administered tamoxifen at age P20, which corresponds to a 3-4 month old human baby (Dutta & Sengupta, 2016). When the mice were tested at P60, we observed no difference in locomotor coordination, and again a small increase in thermo-sensitivity. Absence of any locomotor deficit clearly indicates that KCC3 function must be critical during the developmental period. Why the mice responded faster to the heat-evoked noxious stimuli (although barely significant when tamoxifen was administered at P20) is still unknown. While parvalbumin is expressed in afferent type Ia proprioceptive and not in nociceptive fibers (Medici & Shortland, 2015), the fact that parvalbumin is also expressed in interneurons in brain and spinal cord could provide a link between nociception and parvalbumin neurons. However, the knockout of KCC3 resulted in a delayed response to heat stimulus on the hot plate, indicating reduced ability to sense and/or respond to pain stimulus and here if anything, the mice responded better to the stimulus. Thus,

our data clearly indicate that locomotion and nociception were not impaired when KCC3 expression was knocked out in parvalbumin-positive neurons after birth.

Examining KCC3 during development will require additional studies and a change in approach. Indeed, mouse dorsal root ganglion neurons are born at E11.5-E12.5 (Lawson & Biscoe, 1979) and KCC3 expression is observed as early as E14 (Boettger et al., 2003). In contrast, the parvalbumin transcript is barely detectable at postnatal day 4 in both brain and spinal cord but present at P14 and P28 (Allen Developing Mouse Brain and Spinal Cord atlases). Thus, a different promoter system would be required to induce KCC3 deletion during early development.

Whether KCC3 is involved in processes such as neuronal migration, differentiation, and maturation during the developmental period is still unknown. The proprioceptive sensory afferents fibers for instance start reaching the spinal cord at E10.5 and enter the dorsolateral portion by E11.5-E12.5. Some fibers over the next few days descend to deeper portions and by E17, some axons form connections with motor neurons (Ozaki & Snider, 1997; Mears & Frank, 1997). Prior to E13.5, primary afferent axons are smooth in appearance, but at that stage, many clear “swellings” are observed with the appearance of elaborate collateral branches (Ozaki & Snider, 1997). We postulate that KCC3 might have a role to play during this critical period. In contrast, when sensory neurons and motor neurons are fully developed and connected in the adult mouse, they no longer dependent on KCC3 to maintain these connections.

A role for KCC3 in cell migration has been demonstrated in cancer cells (Gagnon, 2012). To migrate, cells need to extend filopodia at the leading edge while retracting the trailing edge. These processes are likely to be facilitated by water intake at the leading edge and water loss at the trailing edge (Watkins, 2011). As KCC3's main function is cell volume homeostasis (Chapter 4, Byun & Delpire, 2007; Flores et al., 2019; Kahle et al., 2016; Shen et al., 2001) it seems reasonable to postulate that KCC3 might play a role in neuronal migration during development.

As anticipated, PV-CRE^{ERT2} x KCC3-stop mice displayed very severe locomotor deficits and many of these mice did not survive. The fact that the mice fell from the rotating rod well below 50 seconds is reminiscent of the original KCC3 knockout mice (Howard et al., 2002). It is unknown why the survival of the mice seems to be more affected in this model versus the other KCC3 knockout mouse models. Additional breeding is required to obtain enough mice to administer tamoxifen at P20 and see if the rescue is possible. However, based on our data with the PV-CRE^{ERT2} x KCC3-flox model, the rescue is likely to be needed during embryonic development instead of the postnatal time period.

If the critical period is truly during embryonic development, re-introducing an active KCC3 after birth will not repair what seems to be irreparable damage to motor and sensory nerves. This suggests that therapy is unlikely for patients that are diagnosed during their first few months after birth. Developmental studies should help pinpoint the precise time period and clarify the precise developmental deficit caused by absence of KCC3 expression. These will be pre-requisite for the design of therapeutic strategies to help HSMN/ACC patients.

Conclusions

Disruption of KCC3 in an adult mouse or in a young mouse at weaning did not induce locomotor or sensory phenotypes. In addition, inducing KCC3 expression in an adult KCC3 knockout mouse did not rescue the locomotor phenotype. Thus, KCC3 function seems to be critical during an earlier, likely prenatal, developmental period. Therefore, experiments need to be done in the global knockout during embryonic ages 10.5-17.7 when sensory fibers projects to the dorsal spinal cord and migrate to the ventral part to connect with motor-neurons. Alternatively, disruption of KCC3 expression could be done using a Cre line that expresses during early development.

CHAPTER 6

Future directions and conclusions

Throughout this dissertation, I have sought to: I) characterize a gain-of-function (GOF) mutation of KCC3, II) assess nerve fiber diameters from the KCC3 GOF mouse model, III) determine differences in cell volume regulation among wild-type and mutant KCC3 sensory neurons and IV) assess whether the peripheral neuropathy can be induced by deleting KCC3 in adult or very young mice.

(I) T991A: Characterization of a gain-of-function mutation of KCC3

Characterizing a GOF of KCC3 in a mouse model proved to have similar phenotypes to that of a LOF. The patient with a GOF demonstrated a HSMN phenotype like the patients in the Saguenay/Lac St. Jean region, but with no agenesis of the corpus callosum. Similarly, a GOF mutation resulted in rapid muscle deterioration starting early in infancy. Furthermore, nerve conduction studies of our T991A mouse model accurately recapitulated similar disruptions in speed and latency compared to the patient (Chapter 2, Kahle et al., 2016). On a cellular level, the patient's fibroblasts also displayed an inability to swell, confirming the constitutive activity of KCC3. Thus, this indicates that KCC3 must exist in some homeostatic range to prevent disease. Unfortunately, there is no clear remedy for how to mitigate the phenotypic effects of an overactive KCC3, as completely inhibiting its activity is also toxic

and results in the same peripheral neuropathy phenotype. Hence, Chapters 3 and 4 focused on further assessing the GOF mutation in sciatic nerves and sensory neurons.

(II) Characterizing sciatic nerves from the T991A (GOF) mouse

Previously, it had been confirmed that a LOF results in axonal swelling and myelin debris in sciatic nerves (Byun & Delpire, 2007). In LOF mice, without proper efflux transport of K^+ and Cl^-, and ultimately water, this would result in cell swelling. Therefore, it seemed likely that with an overactive KCC3, the opposite phenotype would be observed, i.e. shrunken axons. We sought to determine this by using previous methods from Byun and Delpire, i.e. by extracting sciatic nerves and observing them through cryo-electron microscopy (EM). We utilized a G-ratio to determine size of axons in adult mice. Ultimately, when comparing the GOF to wild-type nerves nerve fiber diameters appeared shrunken. However, because G-ratio only provides a fixed image in time, the next logistical step was to assess if this phenomenon happened in primary sensory cells.

(III) Cell volume regulation of wild-type, LOF, and GOF sensory dorsal root ganglion (DRG) neurons

Isolated DRG neurons cultured for up to 24 hours are large rounded cells highly suitable for cell volume measurements. In addition, these cells express KCC3 and are affected by deletion of the cotransporter in both HSMN/ACC patients and the KCC3 knockout mouse model. Importantly, sensory DRG neurons do not express KCC2, the neuronal-specific K-Cl

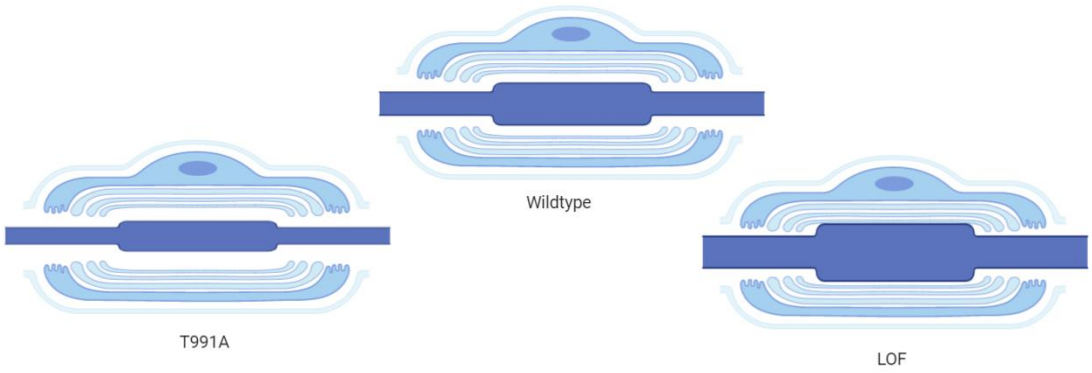

Figure 6-7. Differences in axonal size in KCC3-T991A, wild-type, and KCC3 knockout mice. Gain of function mice exhibit shrunken axons (dark blue) compared to wild-type, whereas LOF mice exhibit swollen axons.

cotransporter, eliminating the possibility of compensation when KCC3 activity is manipulated.

To study cell volume, I utilized Calcein as fluorescent proxy for cell volume. This is a well-established method pioneered by Alvarez-Leefmans (Altamirano et al.,1998) and utilized in Chapter 2 to assess cell volume properties of fibroblasts isolated from the KCC3-T991A patient and in Chapter 4 to assess cell volume in DRG neurons isolated from wild-type and KCC3 mutant mice. Overall, we made four key findings: (i) LOF DRG neurons displayed an inability to volume regulate during a hypotonic challenge, continuing to swell until returned to baseline (ii) GOF neurons displayed an inability to swell to the same degree as wild-type neurons (as observed in the patient's fibroblasts, (iii) the rates of swelling (changing from isotonic to hypotonic) for wild-type, GOF, and LOF were different, (iv) the rates of shrinkage following the return to isosmotic solution was identical among all conditions.

With the exception of KCC2, KCC-mediated transport of K^+ and Cl^- is silent under isosmotic conditions and activated by cell swelling. Thus, KCC only becomes active once cell swelling has occurred and the activated transport of K^+ and Cl^- and obligatory water out of the cells now participates in regulatory volume decrease. Thus, observing regulatory volume decrease in DRG neurons isolated from wild-type neurons and absence of RVD in DRG neurons isolated from KCC3 knockout mice clearly demonstrated the importance of KCC3 activity in the RVD process of sensory neurons. Difference in the rate of swelling was however unexpected as this process is believed to be purely osmotic and dependent upon the water permeability of the plasma membrane. Our data suggest that an overactive KCC3

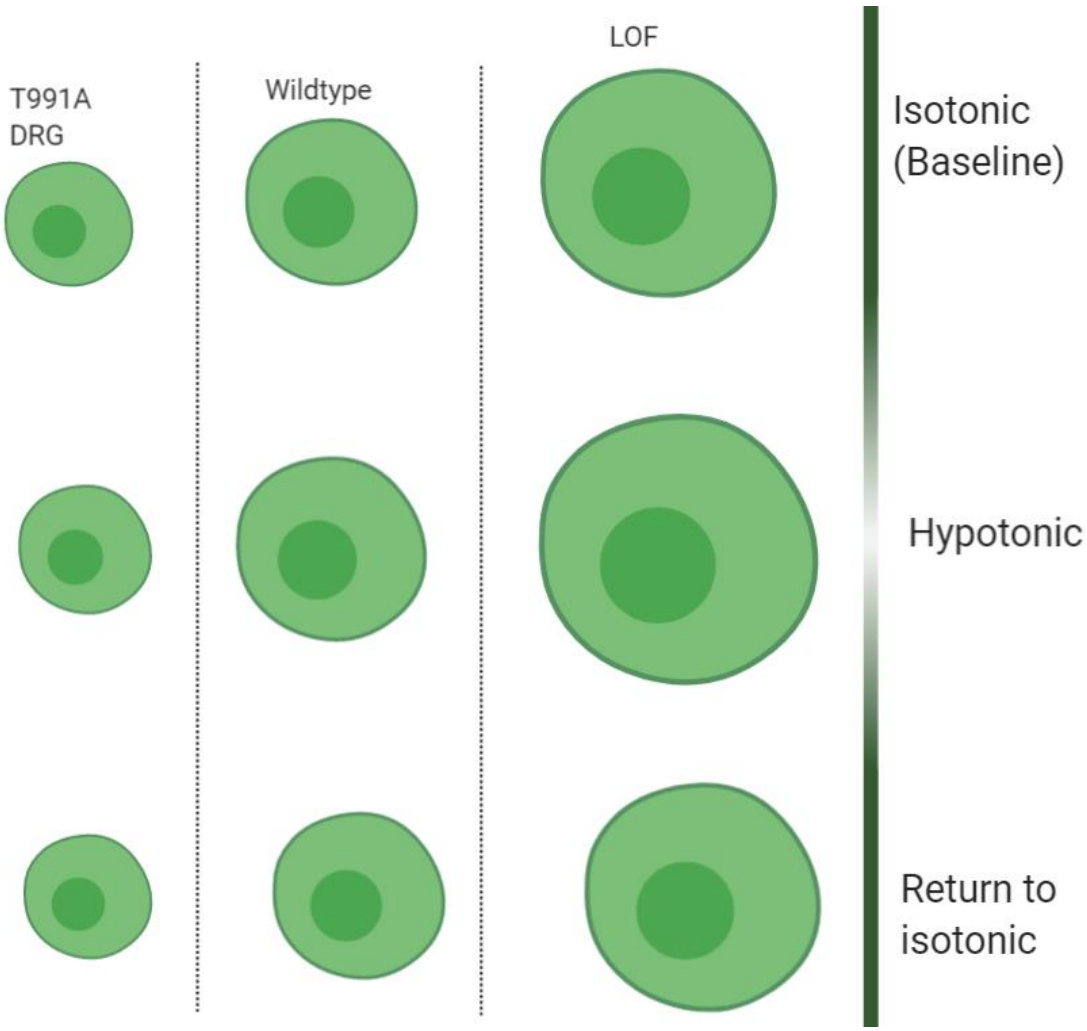

Figure 6-2. Cell volume response in sensory neurons isolated from KCC3-T991A, wild-type, and KCC3 knockout mice. At baseline, LOF and GOF sensory neurons exhibit different sizes. Upon hypotonic challenge, neither GOF nor LOF can volume regulate. LOF neurons do not return to their initial baseline once returned to isotonic solution.

significantly affects the water permeability properties of the cell membrane. Future work should test the effect of expressing different amount of overactive transporters in the membrane, or exposing cells expressing a certain amount of overactive KCC3 to different amount on KCC inhibitor and measure the rate of swelling. Future work should also address the possibility that KCC3 'actively' transports water alongside K^+ and Cl^- ions during transport cycle and address the significance of such a property.

(IV) Assessing temporal expression of KCC3

As most of the HSMN/ACC patients exhibit signs of peripheral neuropathy early in infancy, they endure a lifetime of debilitating symptoms. The fact that preventative measures (such as genetic counseling) are now in place is not a help to patients already diagnosed with LOF mutations in KCC3. A possible avenue of research to help these patients is gene therapy. One main question we addressed in this work was whether disruption of KCC3 in adult of very young mice is able to produce the phenotype. In addition, we asked the question as whether re-introducing KCC3 expression in the KCC3 knockout mouse would rescue the peripheral neuropathy phenotype. As discussed in Chapters 2 and 5, because GOF of KCC3 also results in HSMN, the cotransporter needs to be re-expressed to the right expression level for proper health of the peripheral nerve.

When adult mice expressing PV-CRE^{ERT2} x KCC3flox were administered tamoxifen to disrupt the KCC3 gene, we observed normal locomotor and sensory phenotypes, despite the fact that KCC3 expression was eliminated in DRG neurons. Similar results were obtained

when tamoxifen was administered much earlier (P20), indicating that KCC3 expression must be critical to peripheral nerves during an earlier developmental period. Unfortunately, we were not able to successfully complete our studies of re-introducing KCC3 in KCC3 knockout mice, as the mice did not survive long enough to complete behavioral assays. Only one mouse survived long enough to complete the rotarod task pre- and post-tamoxifen administration at P60 and the mouse did not display any significant improvements in locomotor performance. This again supports the notion that KCC3 function is important earlier in development.

Effort should be placed on completing the rescue experiments by producing and analyzing more mice and by shifting the administration of tamoxifen to earlier time points. For instance, tamoxifen could be given through gavage to the mother and delivered to the pups through milk. Repeated gavage of tamoxifen to the mother starting at P10-P14 would not only move the window earlier but also would solve the issue of having to gavage very young pups. Future work should also focus on the role of the cotransporter during development. As discussed in Chapter 5, KCC3 expression is observed in DRG neurons as early as E14 (Boettger et al., 2003). One set of studies should examine the connections between the sensory fibers and motorneurons between E10.5 and E17.5 in the KCC3 knockout. This is the period where proprioceptive fibers enter the spinal cord on the dorsal side of the spinal cord and move progressively towards the ventral side to ultimately synapse with motor-neurons. This process might be disrupted in the absence of KCC3. Another set of studies should examine expression of KCC3 in motor-neurons and assess whether deletion of KCC3 in motor-neurons also lead to a locomotor phenotype. Finally, if KCC3 deletion was to be

induced at different stages of development, an inducible system (other than the parvalbumin-CRE^{ERT2}) would have to be used, as parvalbumin expression in the nervous system increases during the second and third weeks of postnatal life in rodents.

While our studies are not yet complete, they so far indicate that the time window where KCC3 is critical is likely to be during development, and thus, gene therapy might not be possible unless it occurs early during embryonic development.

REFERENCES

Adragna, N. C., Di Fulvio, M., & Lauf, P. K. (2004). Regulation of K-Cl cotransport: From function to genes. *Journal of Membrane Biology*, *201*(3), 109–137. https://doi.org/10.1007/s00232-004-0695-6

Adragna, N., Ravilla, N. B., Lauf, P. K., Begum, G., Khanna, A. R., Sun, D., & Kahle, K. T. (2015a). Regulated phosphorylation of the K-Cl cotransporter KCC3 is a molecular switch of intracellular potassium content and cell volume homeostasis. *Frontiers in Cellular Neuroscience*, *9*, 255. https://doi.org/10.3389/fncel.2015.00255

Adragna, N., Ravilla, N., Lauf, P., Begum, G., Khanna, A., Sun, D., & Kahle, K. (2015b). Regulated phosphorylation of the K-Cl cotransporter KCC3 is a molecular switch of intracellular potassium content and cell volume homeostasis. *Frontiers in Cellular Neuroscience*, *9*, 255. https://doi.org/10.3389/fncel.2015.00255

Adzhubei, I. A., Schmidt, S., Peshkin, L., Ramensky, V. E., Gerasimova, A., Bork, P., … Sunyaev, S. R. (2010). A method and server for predicting damaging missense mutations. *Nature Methods*, *7*(4), 248–249. https://doi.org/10.1038/nmeth0410-248

Alessi, D. R., Zhang, J., Khanna, A., Hochdörfer, T., Shang, Y., & Kahle, K. T. (2014). The WNK-SPAK/OSR1 pathway: Master regulator of cation-chloride cotransporters. *Science Signaling*, *7*(334), re3. https://doi.org/10.1126/scisignal.2005365

Altamirano, J., Brodwick, M., & Alvarez-Leefmans, F. (1998). Regulatory volume decrease and intracellular Ca2+ in murine neuroblastoma cells studied with fluorescent probes. *The Journal of General Physiology*, *112*(2), 145–160. https://doi.org/10.1085/JGP.112.2.145

Alvarez-Leefmans, F., Herrera-Pérez, J., Márquez, M., & Blanco, V. (2006). Simultaneous measurement of water volume and pH in single cells using BCECF and fluorescence imaging microscopy. *Biophysical Journal*, *90*(2), 608–618. https://doi.org/10.1529/biophysj.105.069450

Alvarez-Leefmans, F. J., Gamiño, S. M., Giraldez, F., & Noguerón, I. (1988). Intracellular chloride regulation in amphibian dorsal root ganglion neurones studied with ion-selective microelectrodes. *The Journal of Physiology*, *406*, 225–246. https://doi.org/10.1113/jphysiol.1988.sp017378

Ammendola, A. (2001). Peripheral neuropathy in chronic alcoholism: a retrospective cross-sectional study in 76 subjects. *Alcohol and Alcoholism*, *36*(3), 271–275. https://doi.org/10.1093/alcalc/36.3.271

Andermann, F., & Andermann, E. (1994). Callosal Agenesis: A Natural Split Brain? In M. Lassonde & M. Jeeves (Eds.), *Advances in Behavioral Biology* (Vol 42, pp. 19–26). Montreal: Springer.

Andermann, F., Andermann, E., Joubert, M., Karpati, G., Carpenter, S., & Melancon, D. (1972). Familial Agenesis of the Corpus Callosum with Anterior Horn Cell Disease: A Syndrome of Mental Retardation, Areflexia, and Paraparesis. *Trans. Amer. Neurol. Ass.*, *97*, 242–244.

Arroyo, J. P., Kahle, K., & Gamba, G. (2013). The SLC12 family of electroneutral cation-coupled chloride cotransporters. *Molecular Aspects of Medicine*, *34*(2), 288–298. https://doi.org/10.1016/j.mam.2012.05.002

Auer, R., Laganière, J., Robitaille, Y., Richardson, J., Dion, P., Rouleau, G., & Shekarabi, M. (2016). KCC3 axonopathy: neuropathological features in the central and peripheral nervous system. *Modern Pathology*, *29*(9), 962–976. https://doi.org/10.1038/modpathol.2016.90

Ben-Ari, Y. (2002). Excitatory actions of gaba during development: the nature of the nurture. *Nature Reviews Neuroscience*, *3*(9), 728–739. https://doi.org/10.1038/nrn920

Ben-Ari, Y. (2017, September 1). NKCC1 Chloride Importer Antagonists Attenuate Many Neurological and Psychiatric Disorders. *Trends in Neurosciences*. Elsevier Ltd. https://doi.org/10.1016/j.tins.2017.07.001

Benn, S. C., Costigan, M., Tate, S., Fitzgerald, M., & Woolf, C. J. (2001). Developmental expression of the TTX-resistant voltage-gated sodium channels Nav1.8 (SNS) and Nav1.9 (SNS2) in primary sensory neurons. *The Journal of Neuroscience : The Official Journal of the Society for Neuroscience*, *21*(16), 6077–6085. Retrieved from http://www.ncbi.nlm.nih.gov/pubmed/11487631

Blaesse, P., Airaksinen, M. S., Rivera, C., & Kaila, K. (2009). Cation-Chloride Cotransporters and Neuronal Function. *Neuron*, *61*(6), 820–838. https://doi.org/10.1016/j.neuron.2009.03.003

Boettger, T., Hübner, C. A., Maier, H., Rust, M. B., Beck, F. X., & Jentsch, T. J. (2002). Deafness and renal tubular acidosis in mice lacking the K-Cl co-transporter Kcc4. *Nature*, *416*(6883), 874–878. https://doi.org/10.1038/416874a

Boettger, T., Rust, M., Maier, H., Seidenbecher, T., Schweizer, M., Keating, D., … Jentsch, T. (2003). Loss of K-Cl co-transporter KCC3 causes deafness, neurodegeneration and reduced seizure threshold. *EMBO Journal*, *22*(20), 5422–5434. https://doi.org/10.1093/emboj/cdg519

Boulenguez, P., Liabeuf, S., Bos, R., Bras, H., Jean-Xavier, C., Brocard, C., … Vinay, L. (2010). Down-regulation of the potassium-chloride cotransporter KCC2 contributes to spasticity after spinal cord injury. *Nature Medicine*, *16*(3), 302–307. https://doi.org/10.1038/nm.2107

Bowerman, M., Salsac, C., Bernard, V., Soulard, C., Dionne, A., Coque, E., … Scamps, F. (2017). Neurobiology of Disease KCC3 loss-of-function contributes to Andermann syndrome by inducing activity-dependent neuromuscular junction defects. *Neurobiology of Disease*, *106*, 35–48. https://doi.org/10.1016/j.nbd.2017.06.013

Brown, F. C., Conway, A. J., Cerruti, L., Collinge, J. E., McLean, C., Wiley, J. S., … Curtis, D. J. (2015). Activation of the erythroid K-Cl cotransporter Kcc1 enhances sickle cell disease pathology in a humanized mouse model. *Blood*, *126*(26), 2863–2870. https://doi.org/10.1182/blood-2014-10-609362

Byun, N., & Delpire, E. (2007). Axonal and periaxonal swelling precede peripheral neurodegeneration in KCC3 knockout mice. *Neurobiology of Disease*, *28*(1), 39–51. https://doi.org/10.1016/j.nbd.2007.06.014

Caron, L., Rousseau, F., Gagnon, É., & Isenring, P. (2000). Cloning and functional characterization of a cation-Cl-cotransporter-interacting protein. *Journal of Biological Chemistry*, *275*(41), 32027–32036. https://doi.org/10.1074/jbc.M000108200

Casaubon, L. K., Melanson, M., Lopes-Cendes, I., Marineau, C., Andermann, E., Andermann, F., … Rouleau, G. A. (1996). The gene responsible for a severe form of peripheral neuropathy and agenesis of the corpus callosum maps to chromosome 15q. *American Journal of Human Genetics*, *58*(1), 28–34. Retrieved from http://www.ncbi.nlm.nih.gov/pubmed/8554065

Castañeda-Bueno, M., Vázquez, N., Bustos-Jaimes, I., Hernández, D., Rodríguez-Lobato, E., Pacheco-Alvarez, D., … Gamba, G. (2010). A single residue in transmembrane domain 11 defines the different affinity for thiazides between the mammalian and flounder NaCl transporters. *American Journal of Physiology - Renal Physiology*, *299*(5), F1111–F1119. https://doi.org/10.1152/ajprenal.00412.2010

Celio, M. R. (1986). Parvalbumin in most gamma-aminobutyric acid-containing neurons of the rat cerebral cortex. *Science (New York, N.Y.)*, *231*(4741), 995–997. Retrieved from http://www.ncbi.nlm.nih.gov/pubmed/3945815

Celio, M. R. (1990). Calbindin D-28k and parvalbumin in the rat nervous system. *Neuroscience*, *35*(2), 375–475. https://doi.org/10.1016/0306-4522(90)90091-H

Cesca, F., Baldelli, P., Valtorta, F., & Benfenati, F. (2010). The synapsins: Key actors of synapse function and plasticity. *Progress in Neurobiology*, *91*(4), 313–348. https://doi.org/10.1016/j.pneurobio.2010.04.006

Chew, T. A., Orlando, B. J., Zhang, J., Latorraca, N. R., Wang, A., Hollingsworth, S. A., … Feng, L. (2019). Structure and mechanism of the cation–chloride cotransporter NKCC1. *Nature*, 1–5. https://doi.org/10.1038/s41586-019-1438-2

Chowdhury, J. A., Liu, C. H., Zuber, A. M., & O'Shaughnessy, K. M. (2013). An inducible transgenic mouse model for familial hypertension with hyperkalaemia (Gordon's syndrome or pseudohypoaldosteronism type II). *Clinical Science*, *124*(12), 701–708. https://doi.org/10.1042/CS20120430

Clayton, G. H., Owens, G. C., Wolff, J. S., & Smith, R. L. (1998). Ontogeny of cation-Cl-cotransporter expression in rat neocortex. *Developmental Brain Research*, *109*(2), 281–292. https://doi.org/10.1016/S0165-3806(98)00078-9

Crowe, W. E., Altamirano, J., Huerto, L., & Alvarez-Leefmans, F. J. (1995). Volume changes in single N1E-115 neuroblastoma cells measured with a fluorescent probe. *Neuroscience*, *69*(1), 283–296. https://doi.org/10.1016/0306-4522(95)00219-9

Cruz-Rangel, S., Melo, Z., Vazquez, N., Meade, P., Bobadilla, N. A., Pasantes-Morales, H., … Mercado, A. (2011). Similar effects of all WNK3 variants on SLC12 cotransporters. *AJP: Cell Physiology*, *301*(3), C601–C608. https://doi.org/10.1152/ajpcell.00070.2011

Daigle, N. D., Carpentier, G. A., Frenette-Cotton, R., Simard, M. G., Lefoll, M. H., Noël, M., … Isenring, P. (2009). Molecular characterization of a human cation-Cl - cotransporter (SLC12A8A, CCC9A) that promotes polyamine and amino acid transport. *Journal of Cellular Physiology*, *220*(3), 680–689. https://doi.org/10.1002/jcp.21814

De Braekeleer, M., Dallaire, A., & Mathieu, J. (1993). Genetic epidemiology of sensorimotor

polyneuropathy with or without agenesis of the corpus callosum in northeastern Quebec. *Human Genetics*, *91*(3), 223–227. Retrieved from http://www.ncbi.nlm.nih.gov/pubmed/8386695

De Los Heros, P., Alessi, D., Gourlay, R., Campbell, D., Deak, M., Macartney, T., … Zhang, J. (2014). The WNK-regulated SPAK/OSR1 kinases directly phosphorylate and inhibit the K+ -Cl- co-transporters. *Biochemical Journal*, *458*(3), 559–573. https://doi.org/10.1042/BJ20131478

DeFazio, R. A., Keros, S., Quick, M. W., & Hablitz, J. J. (2000). Potassium-coupled chloride cotransport controls intracellular chloride in rat neocortical pyramidal neurons. *The Journal of Neuroscience : The Official Journal of the Society for Neuroscience*, *20*(21), 8069–8076. Retrieved from http://www.ncbi.nlm.nih.gov/pubmed/11050128

Deleu, D., Bamanikar, S. A., Muirhead, D., & Louon, A. (1997). Familial progressive sensorimotor neuropathy with agenesis of the corpus callosum (Andermann syndrome): a clinical, neuroradiological and histopathological study. *European Neurology*, *37*(2), 104–109. https://doi.org/10.1159/000117419

Delpire, E., Days, E., Lewis, L. M., Mi, D., Kim, K., Lindsley, C. W., & Weaver, C. D. (2009). Small-molecule screen identifies inhibitors of the neuronal K-Cl cotransporter KCC2. *Proceedings of the National Academy of Sciences*, *106*(13), 5383–5388. https://doi.org/10.1073/pnas.0812756106

Delpire, E., & Gagnon, K. B. (2006). SPAK and OSR1, key kinases involved in the regulation of chloride transport. *Acta Physiologica*, *187*(1–2), 103–113. https://doi.org/10.1111/j.1748-1716.2006.01565.x

Delpire, E., & Guo, J. (2020). The cryo-EM structures of Dr NKCC1 and hKCC1 : a new milestone in the physiology of cation-chloride cotransporters. *Am J Physiol Cell Physiol.*, *318*(2), C225–C237.

Delpire, E., Wolfe, L., Flores, B., Koumangoye, R., Schornak, C. C., Omer, S., … Adams, D. R. (2016). A patient with multisystem dysfunction carries a truncation mutation in human SLC12A2, the gene encoding the Na-K-2Cl cotransporter, NKCC1. *Cold Spring Harbor Molecular Case Studies*, *2*(6).

Delpire, E, Cornet, M., & Gilles, R. (1991). Volume regulation in rat pheochromocytoma cultured cells submitted to hypoosmotic conditions. *Archives Internationales de Physiologie, de Biochimie et de Biophysique*, *99*(1), 71–76. https://doi.org/10.3109/13813459109145906

Delpire, Eric, Baranczak, A., Waterson, A. G., Kim, K., Kett, N., Morrison, R. D., … Lindsley, C. W. (2012). Further optimization of the K-Cl cotransporter KCC2 antagonist ML077: Development of a highly selective and more potent in vitro probe. *Bioorganic & Medicinal Chemistry Letters*, *22*(14), 4532–4535. https://doi.org/10.1016/j.bmcl.2012.05.126

Delpire, Eric, & Gagnon, K. B. (2018). Water Homeostasis and Cell Volume Maintenance and Regulation. In *Current Topics in Membranes* (Vol. 81, pp. 3–52). Academic Press Inc. https://doi.org/10.1016/bs.ctm.2018.08.001

Delpire, Eric, & Kahle, K. (2016). The KCC3 cotransporter as a therapeutic target for

peripheral neuropathy. *Expert Opinion on Theraputic Targets*, *21*(2), 113–116. https://doi.org/10.1080/14728222.2017.1275569
Delpire, Eric, Lu, J., England, R., Dull, C., & Thorne, T. (1999). Deafness and imbalance associated with inactivation of the secretory Na- K-2Cl co-transporter. *Nature Genetics*, *22*(2), 192–195. https://doi.org/10.1038/9713
Ding, J., & Delpire, E. (2014). Deletion of KCC3 in parvalbumin neurons leads to locomotor deficit in a conditional mouse model of peripheral neuropathy associated with agenesis of the corpus callosum. *Behavioural Brain Research*, *274*, 128–136. https://doi.org/10.1016/j.bbr.2014.08.005
Ding, J., Ponce-Coria, J., & Delpire, E. (2013). A Trafficking-Deficient Mutant of KCC3 Reveals Dominant-Negative Effects on K–Cl Cotransport Function. *PLoS ONE*, *8*(4), e61112. https://doi.org/10.1371/journal.pone.0061112
Dixon, M. J., Gazzard, J., Chaudhry, S. S., Sampson, N., Schulte, B. A., & Steel, K. P. (1999). Mutation of the Na-K-Cl co-transporter gene Slc12a2 results in deafness in mice. *Human Molecular Genetics*, *8*(8), 1579–1584. https://doi.org/10.1093/hmg/8.8.1579
Durocher, Y. (2002). High-level and high-throughput recombinant protein production by transient transfection of suspension-growing human 293-EBNA1 cells. *Nucleic Acids Research*, *30*(2), 9e – 9. https://doi.org/10.1093/nar/30.2.e9
Dutta, S., & Sengupta, P. (2016, May 1). Men and mice: Relating their ages. *Life Sciences*. Elsevier Inc. https://doi.org/10.1016/j.lfs.2015.10.025
Dyck, P. (1975). Inherited Neuronal Degneration and atrophy affecting peripheral sensory and autonomic neurons. In P. Dyck, P. Thomas, & E. Lambert (Eds.), *Peripheral Neuropathy* (pp. 825–867). Philidelphia: WB Saunders Co.
Eggermann, K., Gess, B., Häusler, M., Weis, J., Hahn, A., & Kurth, I. (2018). Hereditary Neuropathies. *Deutsches Aerzteblatt Online*, *115*(6), 91–97. https://doi.org/10.3238/arztebl.2018.0091
Evans, R. L., Park, K., James Turner, R., Watson, G. E., Nguyen, H. Van, Dennett, M. R., … Melvin, J. E. (2000). Severe impairment of salivation in Na+/K+/2Cl- cotransporter (NKCC1)-deficient mice. *Journal of Biological Chemistry*, *275*(35), 26720–26726. https://doi.org/10.1074/jbc.M003753200
Feeney, D. M., Gonzalez, A., & Law, W. A. (1982). Amphetamine, haloperidol, and experience interact to affect rate of recovery after motor cortex injury. *Science*, *217*(4562), 855–857. https://doi.org/10.1126/science.7100929
Filteau, M.-J. J., Pourcher, E., Bouchard, R. H., Baruch, P., Mathieu, J., Bedard, F., … Vincent, P. (1991). Corpus callosum agenesis and psychosis in Andermann syndrome. *Arch Neurol*, *48*(12), 1275–1280. https://doi.org/10.1001/archneur.1991.00530240079027
Flagella, M., Clarke, L. L., Miller, M. L., Erway, L. C., Giannella, R. A., Andringa, A., … Shull, G. E. (1999). Mice lacking the basolateral Na-K-2Cl cotransporter have impaired epithelial chloride secretion and are profoundly deaf. *Journal of Biological Chemistry*, *274*(38), 26946–26955. https://doi.org/10.1074/jbc.274.38.26946
Flores, B., Schornak, C. C., & Delpire, E. (2019a). A role for KCC3 in maintaining cell

volume of peripheral nerve fibers. *Neurochemistry International*, *123*, 114–124. https://doi.org/10.1016/j.neuint.2018.01.009

Flores, B., Schornak, C., & Delpire, E. (2019b). A role for KCC3 in maintaining cell volume of peripheral nerve fibers. *Neurochemistry International*. https://doi.org/10.1016/j.neuint.2018.01.009

Gagnon, K. B., & Delpire, E. (2013). Physiology of SLC12 transporters: lessons from inherited human genetic mutations and genetically engineered mouse knockouts. *American Journal of Physiology Cell Physiology*, *304*(8), C6930–C714. https://doi.org/10.1152/ajpcell.00350.2012

Gagnon, K. B. E., England, R., & Delpire, E. (2006). Characterization of SPAK and OSR1, Regulatory Kinases of the Na-K-2Cl Cotransporter. *Molecular and Cellular Biology*, *26*(2), 689–698. https://doi.org/10.1128/mcb.26.2.689-698.2006

Gagnon, K, & Delpire, E. (2012). Molecular physiology of SPAK and OSR1: two Ste20-related protein kinases regulating ion transport. *Physiological Reviews*, *92*(4), 1577–1617. https://doi.org/10.1152/physrev.00009.2012

Gagnon, Kenneth. (2012). High-grade Glioma Motility Reduced by Genetic Knockdown of KCC3. *Cellular Physiology and Biochemistry*, *30*, 466–476.

Gagnon, Kenneth B E, England, R., & Delpire, E. (2006). Volume sensitivity of cation-Cl- cotransporters is modulated by the interaction of two kinases: Ste20-related proline-alanine-rich kinase and WNK4. *American Journal of Physiology. Cell Physiology*, *290*(1), C134-42. https://doi.org/10.1152/ajpcell.00037.2005

Gamba, G., Saltzberg, S. N., Lombardi, M., Miyanoshita, A., Lytton, J., Hediger, M. A., … Hebert, S. C. (1993). Primary structure and functional expression of a cDNA encoding the thiazide-sensitive, electroneutral sodium-chloride cotransporter. *Proceedings of the National Academy of Sciences of the United States of America*, *90*(7), 2749–2753. https://doi.org/10.1073/pnas.90.7.2749

Gamba, Gerardo. (2005). Molecular physiology and pathophysiology of electroneutral cation-chloride cotransporters. *Physiological Reviews*, *85*(2), 423–493. https://doi.org/10.1152/physrev.00011.2004

Gamba, Gerardo. (2009, October). The thiazide-sensitive Na+-Cl- cotransporter: Molecular biology, functional properties, and regulation by WNKs. *American Journal of Physiology - Renal Physiology*. https://doi.org/10.1152/ajprenal.00159.2009

Garneau, A. P., Slimani, S., Tremblay, L. E., Fiola, M. J., Marcoux, A. A., & Isenring, P. (2019). K+-Cl- cotransporter 1 (KCC1): A housekeeping membrane protein that plays key supplemental roles in hematopoietic and cancer cells. *Journal of Hematology and Oncology*, *12*(1), 74. https://doi.org/10.1186/s13045-019-0766-x

Geng, Y., Hoke, A., & Delpire, E. (2009). The Ste20 Kinases Ste20-related Proline-Alanine-rich Kinase and Oxidative-stress Response 1 Regulate NKCC1 Function in Sensory Neurons. *Journal of Biological Chemistry*, *284*(21), 14020–14028. https://doi.org/10.1074/jbc.M900142200

Gerelsaikhan, T., & James, R. (2000). Transmembrane Topology of the Secretory Na-K-2Cl Cotransporter NKCC1 Studied by in Vitro Translation*.

https://doi.org/10.1074/jbc.M007751200
Gillen, C. M., Brill, S., Payne, J. A., & Forbush, B. (1996). Molecular cloning and functional expression of the K-Cl cotransporter from rabbit, rat, and human. A new member of the cation-chloride cotransporter family. *The Journal of Biological Chemistry*, *271*(27), 16237–16244. Retrieved from http://www.ncbi.nlm.nih.gov/pubmed/8663127
Gitelman, H. J., Graham, J. B., & Welt, L. G. (1966). A new familial disorder characterized by hypokalemia and hypomagnesemia. *Transactions of the Association of American Physicians*, *79*, 221–235.
Glykys, J., Dzhala, V. I., Kuchibhotla, K. V, Feng, G., Kuner, T., Augustine, G., … Staley, K. (2009). Differences in cortical vs. subcortical GABAergic signaling: a candidate mechanism of electroclinical dissociation of neonatal seizures. *Neuron*, *63*(5), 657–672. https://doi.org/10.1016/j.neuron.2009.08.022
Gonzalez, M. A., Lebrigio, R. F. A., Van Booven, D., Ulloa, R. H., Powell, E., Speziani, F., … Züchner, S. (2013). GEnomes Management Application (GEM.app): a new software tool for large-scale collaborative genome analysis. *Human Mutation*, *34*(6), 842–846. https://doi.org/10.1002/humu.22305
Gordon, R. D. (1986). The Syndrome of Hypertension and Hyperkalemia With Normal Glomerular Filtration Rate: Gordon's Syndrome. *Australian and New Zealand Journal of Medicine*. Aust N Z J Med. https://doi.org/10.1111/j.1445-5994.1986.tb01145.x
Grimm, P. R., Coleman, R., Delpire, E., & Welling, P. A. (2017). Constitutively active SPAK causes hyperkalemia by activating NCC and remodeling distal tubules. *Journal of the American Society of Nephrology*, *28*(9), 2597–2606. https://doi.org/10.1681/ASN.2016090948
Grimm, P. R., Taneja, T. K., Liu, J., Coleman, R., Chen, Y.-Y., Delpire, E., … Welling, P. A. (2012). SPAK Isoforms and OSR1 Regulate Sodium-Chloride Co-transporters in a Nephron-specific Manner. *Journal of Biological Chemistry*, *287*(45), 37673–37690. https://doi.org/10.1074/jbc.M112.402800
Grubb, B. R., Pace, A. J., Lee, E., Koller, B. H., & Boucher, R. C. (2001). Alterations in airway ion transport in NKCC1-deficient mice. *American Journal of Physiology - Cell Physiology*, *281*(2), C615-23. https://doi.org/10.1152/ajpcell.2001.281.2.c615
Hamann, S., Herrera-Perez, J. J., Zeuthen, T., & Alvarez-Leefmans, F. J. (2010). Cotransport of water by the Na + -K + -2Cl − cotransporter NKCC1 in mammalian epithelial cells. *The Journal of Physiology*, *588*(21), 4089–4101. https://doi.org/10.1113/jphysiol.2010.194738
Hampel, P., Römermann, K., MacAulay, N., & Löscher, W. (2018). Azosemide is more potent than bumetanide and various other loop diuretics to inhibit the sodium-potassium-chloride-cotransporter human variants hNKCC1A and hNKCC1B. *Scientific Reports*, *8*(1). https://doi.org/10.1038/s41598-018-27995-w
Hannemann, A., & Flatman, P. W. (2011). Phosphorylation and Transport in the Na-K-2Cl Cotransporters, NKCC1 and NKCC2A, Compared in HEK-293 Cells. *PLoS ONE*, *6*(3), e17992. https://doi.org/10.1371/journal.pone.0017992
Hantke, J., Carty, L., Wagstaff, L. J., Turmaine, M., Wilton, D. K., Quintes, S., … Jessen, K.

R. (2014). c-Jun activation in Schwann cells protects against loss of sensory axons in inherited neuropathy. *Brain*, *137*(11), 2922–2937. https://doi.org/10.1093/brain/awu257
Harris, A. N., Grimm, P. R., Lee, H. W., Delpire, E., Fang, L., Verlander, J. W., … Weiner, I. D. (2018). Mechanism of hyperkalemia-induced metabolic acidosis. *Journal of the American Society of Nephrology*, *29*(5), 1411–1425. https://doi.org/10.1681/ASN.2017111163
Hauser, H., Phillips, M. C., & Stubbs, M. (1972). Ion Permeability of Phospholipid Bilayers. *Nature*, *239*(5371), 342–344. https://doi.org/10.1038/239342a0
Heath, W. (1991). Myelin Sheath Survival following Axonal Degeneration in doubly myelinated nerve fibers. *The Journal of Neuroscience*, *11*(December), 4003–4014.
Hebert, S. C., Mount, D. B., & Gamba, G. (2004). Molecular physiology of cation-coupled Cl Ÿ cotransport : the SLC12 family, 580–593. https://doi.org/10.1007/s00424-003-1066-3
Hewett, D., Samuelsson, L., Polding, J., Enlund, F., Smart, D., Cantone, K., … Purvis, I. (2002). Identification of a psoriasis susceptibility candidate gene by linkage disequilibrium mapping with a localized single nucleotide polymorphism map. *Genomics*, *79*(3), 305–314. https://doi.org/10.1006/geno.2002.6720
Hiki, K., D'Andrea, R. J., Furze, J., Crawford, J., Woollatt, E., Sutherland, G. R., … Gamble, J. R. (1999). Cloning, characterization, and chromosomal location of a novel human K+-Cl- cotransporter. *The Journal of Biological Chemistry*, *274*(15), 10661–10667. Retrieved from http://www.ncbi.nlm.nih.gov/pubmed/10187864
Hinz, L., Torrella Barrufet, J., & Heine, V. M. (2019). KCC2 expression levels are reduced in post mortem brain tissue of Rett syndrome patients. *Acta Neuropathologica Communications*, *7*(1), 196. https://doi.org/10.1186/s40478-019-0852-x
Hoffmann, E., Lambert, I., & Pedersen, S. (2009). Physiology of cell volume regulation in vertebrates. *Physiological Reviews*, *89*(1), 193–277. https://doi.org/10.1152/physrev.00037.2007
Howard, H., Dubé, M. P., Prévost, C., Bouchard, J. P., Mathieu, J., & Rouleau, G. (2002). Fine mapping the candidate region for peripheral neuropathy with or without agenesis of the corpus callosum in the French Canadian population. *European Journal of Human Genetics*, *10*(7), 406–412. https://doi.org/10.1038/sj.ejhg.5200815
Howard, H., Mount, D., Rochefort, D., Byun, N., Dupré, N., Lu, J., … Rouleau, G. (2002). The K-Cl cotransporter KCC3 is mutant in a severe peripheral neuropathy associated with agenesis of the corpus callosum. *Nature Genetics*, *32*(3), 384–392. https://doi.org/10.1038/ng1002
Hübner, C. A., Stein, V., Hermans-Borgmeyer, I., Meyer, T., Ballanyi, K., & Jentsch, T. J. (2001). Disruption of KCC2 reveals an essential role of K-Cl cotransport already in early synaptic inhibition. *Neuron*, *30*(2), 515–524. Retrieved from http://www.ncbi.nlm.nih.gov/pubmed/11395011
Jennings, M., & Al-Rohil, N. (1990). Kinetics of activation and inactivation of swelling-stimulated K+/C1− transport: The volume-sensitive parameter is the rate constant for inactivation. *Journal of General Physiology*, *95*(6), 1021–1040. https://doi.org/10.1085/jgp.95.6.1021

Kahle, K., Flores, B., Bharucha-Goebel, D., Zhang, J., Donkervoort, S., Hegde, M., … Delpire, E. (2016). Peripheral motor neuropathy is associated with defective kinase regulation of the KCC3 cotransporter. *Science Signaling*, *9*(439), ra77. https://doi.org/10.1126/scisignal.aae0546

Kahle, K. T., & Delpire, E. (2016). Kinase-KCC2 coupling: Cl ⁻ rheostasis, disease susceptibility, therapeutic target. *Journal of Neurophysiology*, *115*(1), 8–18. https://doi.org/10.1152/jn.00865.2015

Kahle, K. T., Khanna, A. R., Alper, S. L., Adragna, N. C., Lauf, P. K., Sun, D., & Delpire, E. (2015). K-Cl cotransporters, cell volume homeostasis, and neurological disease. *Trends in Molecular Medicine*, *21*(8), 513–523. https://doi.org/10.1016/j.molmed.2015.05.008

Kahle, K. T., Khanna, A. R., Duan, J., Staley, K. J., Delpire, E., & Poduri, A. (2016). The KCC2 Cotransporter and Human Epilepsy: Getting Excited About Inhibition. *The Neuroscientist*, *22*(6), 555–562. https://doi.org/10.1177/1073858416645087

Kahle, K. T., Rinehart, J., & Lifton, R. P. (2010, December). Phosphoregulation of the Na-K-2Cl and K-Cl cotransporters by the WNK kinases. *Biochimica et Biophysica Acta - Molecular Basis of Disease*. https://doi.org/10.1016/j.bbadis.2010.07.009

Kahle, K. T., Staley, K. J., Nahed, B. V, Gamba, G., Hebert, S. C., Lifton, R. P., & Mount, D. B. (2008). Roles of the cation–chloride cotransporters in neurological disease. *Nature Clinical Practice Neurology*, *4*(9), 490–503. https://doi.org/10.1038/ncpneuro0883

Kahle, K, Deeb, T. Z., Puskarjov, M., Silayeva, L., Liang, B., Kaila, K., & Moss, S. J. (2013). Modulation of neuronal activity by phosphorylation of the K-Cl cotransporter KCC2. *Trends in Neurosciences*. https://doi.org/10.1016/j.tins.2013.08.006

Kahle, K, Merner, N. D., Friedel, P., Silayeva, L., Liang, B., Khanna, A., … Awadalla, P. (2014). Genetically encoded impairment of neuronal KCC2 cotransporter function in human idiopathic generalized epilepsy. *EMBO Reports*, *15*(7), 766–774. https://doi.org/10.15252/EMBR.201438840

Kahle, K, & Staley, K. (2008). The bumetanide-sensitive Na-K-2Cl cotransporter NKCC1 as a potential target of a novel mechanism-based treatment strategy for neonatal seizures. *Neurosurgical Focus*, *25*(3), E22. https://doi.org/10.3171/FOC/2008/25/9/E22

Kahle, K, & Staley, K. J. (2012). *Neonatal Seizures and Neuronal Transmembrane Ion Transport*. (J. Noebels, M. Avoli, & M. Rogawski, Eds.), *Jasper's Basic Mechanisms of the Epilepsies [Internet]* (4th ed.). Bethesda: National Center for Biotechnology Information (US). Retrieved from https://www.ncbi.nlm.nih.gov/books/NBK98206

Kahle, K, Staley, K. J., Nahed, B. V, Gamba, G., Hebert, S. C., Lifton, R. P., & Mount, D. B. (2008). Roles of the cation-chloride cotransporters in neurological disease. *Nature Clinical Practice. Neurology*, *4*(9), 490–503. https://doi.org/10.1038/ncpneuro0883

Kahle, Kristopher, Wilson, F., Leng, Q., Lalioti, M., O'Connell, A., Dong, K., … Lifton, R. P. (2003). WNK4 regulates the balance between renal NaCl reabsorption and K + secretion. *Nature Genetics*, *35*(4), 372–376. https://doi.org/10.1038/ng1271

Kaila, K., Price, T. J., Payne, J. A., Puskarjov, M., & Voipio, J. (2014). Cation-chloride cotransporters in neuronal development, plasticity and disease. *Nature Reviews. Neuroscience*, *15*(10), 637–654. https://doi.org/10.1038/nrn3819

Kaila, K., Rivera, C., Voipio, J., Payne, J. A., Ruusuvuori, E., Lahtinen, H., … Saarma, M. (1999). The K+/Cl- co-transporter KCC2 rendersGABA hyperpolarizing during neuronal maturation. *Nature*, *397*(6716), 251–255. https://doi.org/10.1038/16697

Kandel, E., Schwartz, J. H., & Jessell, T. M. (2000). Perception of Pain. In *Principles of Neural Science* (4th ed., pp. 474–508). New York: McGraw-Hill.

Kaplan, M. R., Plotkin, M. D., Brown, D., Hebert, S. C., & Delpire, E. (1996). Expression of the mouse Na-K-2Cl cotransporter, mBSC2, in the terminal inner medullary collecting duct, the glomerular and extraglomerular mesangium, and the glomerular afferent arteriole. *Journal of Clinical Investigation*, *98*(3), 723–730. https://doi.org/10.1172/JCI118844

Karadsheh, M., Byun, N., Mount, D., & Delpire, E. (2004). Localization of the kcc4 potassium–chloride cotransporter in the nervous system. *Neuroscience*, *123*(2), 381–391. https://doi.org/10.1016/J.NEUROSCIENCE.2003.10.004

Katona, I., & Weis, J. (2018). Diseases of the peripheral nerves. In *Handbook of Clinical Neurology* (Vol. 145, pp. 453–474). Elsevier. https://doi.org/10.1016/B978-0-12-802395-2.00031-6

Kelley, M. R., Cardarelli, R. A., Smalley, J. L., Ollerhead, T. A., Andrew, P. M., Brandon, N. J., … Moss, S. J. (2018). Locally Reducing KCC2 Activity in the Hippocampus is Sufficient to Induce Temporal Lobe Epilepsy. *EBioMedicine*, *32*(2018), 62–71. https://doi.org/10.1016/j.ebiom.2018.05.029

Kiehn, O. (2016). Decoding the organization of spinal circuits that control locomotion. *Nature Reviews Neuroscience*, *17*(4), 224–238. https://doi.org/10.1038/nrn.2016.9

Klein, C. J., Duan, X., & Shy, M. E. (2013). Inherited neuropathies: clinical overview and update. *Muscle & Nerve*, *48*(4), 604–622. https://doi.org/10.1002/mus.23775

Koumangoye, R., Omer, S., & Delpire, E. (2018). Mistargeting of a truncated Na-K-2Cl cotransporter in epithelial cells. *American Journal of Physiology - Cell Physiology*, *315*(2), C258–C276. https://doi.org/10.1152/ajpcell.00130.2018

Kursan, S., McMillen, T. S., Beesetty, P., Dias-Junior, E., Almutairi, M. M., Sajib, A. A., … Di Fulvio, M. (2017). The neuronal K+Cl- co-transporter 2 (Slc12a5) modulates insulin secretion. *Scientific Reports*, *7*(1). https://doi.org/10.1038/s41598-017-01814-0

Kwon, C.-H., Zhou, J., Li, Y., Kim, K. W., Hensley, L. L., Baker, S. J., & Parada, L. F. (2006). Neuron-specific enolase-cre mouse line with cre activity in specific neuronal populations. *Genesis*, *44*(3), 130–135. https://doi.org/10.1002/gene.20197

Laird, J. M. A., García-Nicas, E., Delpire, E. J., & Cervero, F. (2004). Presynaptic inhibition and spinal pain processing in mice: A possible role of the NKCC1 cation-chloride co-transporter in hyperalgesia. *Neuroscience Letters*, *361*(1–3), 200–203. https://doi.org/10.1016/j.neulet.2003.12.015

Larbrisseau, A, Vanasse, M., Brochu, P., & Jasmin, G. (1984). The Andermann syndrome: agenesis of the corpus callosum associated with mental retardation and progressive sensorimotor neuronopathy. *The Canadian Journal of Neurological Sciences. Le Journal Canadien Des Sciences Neurologiques*, *11*(2), 257–261.

Larbrisseau, Albert, Vanasse, M., Brochu, P., & Jasmin, G. (1984). The Andermann

Syndrome: Agenesis of the Corpus Callosum Associated with Mental Retardation and Progressive Sensorimotor Neuronopathy. *Canadian Journal of Neurological Sciences / Journal Canadien Des Sciences Neurologiques*, *11*(2), 257–261. https://doi.org/10.1017/S0317167100045509

Lauf, P., & Adragna, N. (2000). K-Cl cotransport: Properties and molecular mechanism. *Cellular Physiology and Biochemistry*, *10*(5–6), 341–354. https://doi.org/10.1159/000016357

Lauf, P., Bauer, J., Adragna, N., Fujise, H., Zade-Oppen, M., Hai Ryu, K., & Delpire, E. (1992). Erythrocyte K-Cl cotransport: properties and regulation. *American Journal of Physiology Cell Physiology*, *263*(5), C917–C1117. https://doi.org/10.1152/ajpcell.1992.263.5.C917

Lauf, P. K., Bauer, J., Adragna, N., Fujise, H., Zade-Oppen, M., Ryu, K. H., & Delpire, E. (1992). Erythrocyte K-Cl cotransport: Properties and regulation. *American Journal of Physiology - Cell Physiology*. https://doi.org/10.1152/ajpcell.1992.263.5.c917

Lawson, S. N., & Biscoe, T. J. (1979). Development of mouse dorsal root ganglia: an autoradiographic and quantitative study. *Journal of Neurocytology*, *8*, 265–274. https://doi.org/10.1007/BF01236122

Le Rouzic, P., Ivanov, T. R., Stanley, P. J., Baudoin, F. M.-H., Chan, F., Pinteaux, E., … Luckman, S. M. (2006). KCC3 and KCC4 expression in rat adult forebrain. *Brain Research*, *1110*(1), 39–45. https://doi.org/10.1016/j.brainres.2006.06.055

Lenart, B., Kintner, D. B., Shull, G. E., & Sun, D. (2004). Na-K-Cl cotransporter-mediated intracellular Na+ accumulation affects Ca2+ signaling in astrocytes in an In vitro ischemic model. *Journal of Neuroscience*, *24*(43), 9585–9597. https://doi.org/10.1523/JNEUROSCI.2569-04.2004

Li, J. (2014). Genetic factors for nerve susceptibility to injuries - lessons from PMP22 deficiency. *Neural Regeneration Research*, *9*(18), 1661–1664. https://doi.org/10.4103/1673-5374.141800

Liu, M., & Wood, J. N. (2011). The Roles of Sodium Channels in Nociception: Implications for Mechanisms of Neuropathic Pain. *Pain Medicine*, *12*(suppl 3), S93–S99. https://doi.org/10.1111/j.1526-4637.2011.01158.x

Liu, S., Chang, S., Han, B., Xu, L., Zhang, M., Zhao, C., … Guo, J. (2019). Cryo-EM structures of the human cation-chloride cotransporter KCC1. *Science*, *366*(6464), 505–508.

Lu, J., Karadsheh, M., & Delpire, E. (1999). Developmental regulation of the neuronal-specific isoform of K-CL cotransporter KCC2 in postnatal rat brains. *Journal of Neurobiology*, *39*(4), 558–568. https://doi.org/10.1002/(SICI)1097-4695(19990615)39:4<558::AID-NEU9>3.0.CO;2-5

Lucas, O., Hilaire, C., Delpire, E., & Scamps, F. (2012). KCC3-dependent chloride extrusion in adult sensory neurons. *Molecular and Cellular Neuroscience*, *50*(3), 211–220. https://doi.org/10.1016/j.mcn.2012.05.005

Ludwig, A., Li, H., Saarma, M., Kaila, K., & Rivera, C. (2003). Developmental up-regulation of KCC2 in the absence of GABAergic and glutamatergic transmission. *European*

Journal of Neuroscience, *18*(12), 3199–3206. https://doi.org/10.1111/j.1460-9568.2003.03069.x

Luong, T. N., Carlisle, H. J., Southwell, A., & Patterson, P. H. (2011). Assessment of motor balance and coordination in mice using the balance beam. *Journal of Visualized Experiments*, (49). https://doi.org/10.3791/2376

MacAulay, N., Hamann, S., & Zeuthen, T. (2004). Water transport in the brain: Role of cotransporters. *Neuroscience*, *129*(4), 1029–1042. https://doi.org/10.1016/J.NEUROSCIENCE.2004.06.045

Macnamara, E. F., Koehler, A. E., D'Souza, P., Estwick, T., Lee, P., Vezina, G., … Tifft, C. J. (2019). Kilquist syndrome: A novel syndromic hearing loss disorder caused by homozygous deletion of SLC12A2. *Human Mutation*, *40*(5), 532–538. https://doi.org/10.1002/humu.23722

Mallik, A., & Weir, A. I. (2005). Nerve conduction studies: essentials and pitfalls in practice. *Journal of Neurology, Neurosurgery, and Psychiatry*, *76 Suppl 2*(Suppl 2), ii23-31. https://doi.org/10.1136/jnnp.2005.069138

Mastroianni, N., De Fusco, M., Zollo, M., Arrigo, G., Zuffardi, O., Bettinelli, A., … Casari, G. (1996). Molecular cloning, expression pattern, and chromosomal localization of the human Na-Cl thiazide-sensitive cotransporter (SLC12A3). *Genomics*, *35*(3), 486–493. https://doi.org/10.1006/geno.1996.0388

Mathieu, J, Bédard, F., Prévost, C., & Langevin, P. (1990). [Motor and sensory neuropathies with or without agenesis of the corpus callosum: a radiological study of 64 cases]. *The Canadian Journal of Neurological Sciences. Le Journal Canadien Des Sciences Neurologiques*, *17*(2), 103–108.

Mathieu, Jean, Bedard, F., Prevost, C., & Langevin, P. (1990). Neuropathie Sensitivo-Motrice Hereditaire avec ou sans Agenesie du Corps Calleux: Etude Radiologique et Clinique de 64 Cas. *J. Neurol. Sci*, *17*, 103–108. https://doi.org/10.1017/S0317167100030298

Mathieu, V., Chantôme, A., Lefranc, F., Cimmino, A., Miklos, W., Paulitschke, V., … Kiss, R. (2015). Sphaeropsidin A shows promising activity against drug-resistant cancer cells by targeting regulatory volume increase. *Cellular and Molecular Life Sciences*, *72*(19), 3731–3746. https://doi.org/10.1007/s00018-015-1902-6

Medici, T., & Shortland, P. J. (2015). Effects of peripheral nerve injury on parvalbumin expression in adult rat dorsal root ganglion neurons. *BMC Neuroscience*, *16*(1), 93. https://doi.org/10.1186/s12868-015-0232-9

Melloni, R. H., & DeGennaro, L. J. (1994). Temporal onset of synapsin I gene expression coincides with neuronal differentiation during the development of the nervous system. *The Journal of Comparative Neurology*, *342*(3), 449–462. https://doi.org/10.1002/cne.903420311

Morelli, K. H., Seburn, K. L., Schroeder, D. G., Spaulding, E. L., Dionne, L. A., Cox, G. A., & Burgess, R. W. (2017). Severity of Demyelinating and Axonal Neuropathy Mouse Models Is Modified by Genes Affecting Structure and Function of Peripheral Nodes. *Cell Reports*, *18*(13), 3178–3191. https://doi.org/10.1016/j.celrep.2017.03.009

Mori, T., Kikuchi, E., Watanabe, Y., Fujii, S., Ishigami-Yuasa, M., Kagechika, H., … Uchida,

S. (2013). Chemical library screening for WNK signalling inhibitors using fluorescence correlation spectroscopy. *The Biochemical Journal*, *455*(3), 339–345. https://doi.org/10.1042/BJ20130597

Moriguchi, T., Urushiyama, S., Hisamoto, N., Iemura, S., Uchida, S., Natsume, T., … Shibuya, H. (2005). WNK1 Regulates Phosphorylation of Cation-Chloride-coupled Cotransporters via the STE20-related Kinases, SPAK and OSR1. *Journal of Biological Chemistry*, *280*(52), 42685–42693. https://doi.org/10.1074/jbc.M510042200

Mounkes, L. C., Kozlov, S. V., Rottman, J. N., & Stewart, C. L. (2005). Expression of an LMNA-N195K variant of A-type lamins results in cardiac conduction defects and death in mice. *Human Molecular Genetics*, *14*(15), 2167–2180. https://doi.org/10.1093/hmg/ddi221

Mount, D. B., Mercado, A., Song, L., Xu, J., George, A. L., Delpire, E., … Gamba, G. (1999). Cloning and characterization of KCC3 and KCC4, new members of the cation-chloride cotransporter gene family. *Journal of Biological Chemistry*, *274*(23), 16355–16362. https://doi.org/10.1074/jbc.274.23.16355

Muallem, S., Zhang, B., Loessberg, P., & Starr, A. (1992). Simultaneous Recording of Cell Volume Changes and Intracellular pH or Ca2+ Concentration in Single Osteosarcoma Cells UMR-106-01. *Molecular Biology*, *267*(25), 17658–17664.

Ng, P. C., & Henikoff, S. (2003). SIFT: Predicting amino acid changes that affect protein function. *Nucleic Acids Research*, *31*(13), 3812–3814. https://doi.org/10.1093/nar/gkg509

NINDS. (2019). Charcot-Marie-Tooth Disease Fact Sheet | National Institute of Neurological Disorders and Stroke. Retrieved January 30, 2020, from https://www.ninds.nih.gov/Disorders/Patient-Caregiver-Education/Fact-Sheets/Charcot-Marie-Tooth-Disease-Fact-Sheet

Notartomaso, S., Mascio, G., Scarselli, P., Martinello, K., Fucile, S., Gradini, R., … Nicoletti, F. (2017). Expression of the K+/Cl−cotransporter, KCC2, in cerebellar Purkinje cells is regulated by group-I metabotropic glutamate receptors. *Neuropharmacology*, *115*(2017), 51–59. https://doi.org/10.1016/j.neuropharm.2016.07.032

Oates, P. J. (2002). Polyol pathway and diabetic peripheral neuropathy. *International Review of Neurobiology*. Academic Press Inc. https://doi.org/10.1016/s0074-7742(02)50082-9

Owens, D. F., Boyce, L. H., Davis, M. B. E., & Kriegstein, A. R. (1996). Excitatory GABA responses in embryonic and neonatal cortical slices demonstrated by gramicidin perforated-patch recordings and calcium imaging. *Journal of Neuroscience*, *16*(20), 6414–6423. https://doi.org/10.1523/jneurosci.16-20-06414.1996

Owens, D. F., & Kriegstein, A. R. (2002). Is there more to GABA than synaptic inhibition? *Nature Reviews Neuroscience*. Nat Rev Neurosci. https://doi.org/10.1038/nrn919

Ozaki, S., & Snider, W. D. (1997). Initial trajectories of sensory axons toward laminar targets in the developing mouse spinal cord. *The Journal of Comparative Neurology*, *380*(2), 215–229. https://doi.org/10.1002/(SICI)1096-9861(19970407)380:2<215::AID-CNE5>3.0.CO;2-6

Pace, A. J., Lee, E., Athirakul, K., Coffman, T. M., O'Brien, D. A., & Koller, B. H. (2000).

Failure of spermatogenesis in mouse lines deficient in the Na+-K+- 2Cl- cotransporter. *Journal of Clinical Investigation*, *105*(4), 441–450. https://doi.org/10.1172/JCI8553

Parmantier, E., Lynn, B., Lawson, D., Turmaine, M., Namini, S. S., Chakrabarti, L., … Mirsky, R. (1999). Schwann cell-derived Desert hedgehog controls the development of peripheral nerve sheaths. *Neuron*, *23*(4), 713–724. Retrieved from http://www.ncbi.nlm.nih.gov/pubmed/10482238

Payne, J. A., & Forbush, B. (1994). Alternatively spliced isoforms of the putative renal Na-K-Cl cotransporter are differentially distributed within the rabbit kidney. *Proceedings of the National Academy of Sciences of the United States of America*, *91*(10), 4544–4548. https://doi.org/10.1073/pnas.91.10.4544

Payne, J. A., Stevenson, T. J., & Donaldson, L. F. (1996). Molecular characterization of a putative K-Cl cotransporter in rat brain: A neuronal-specific isoform. *Journal of Biological Chemistry*, *271*(27), 16245–16252. https://doi.org/10.1074/jbc.271.27.16245

Payne, J., Stevenson, T., & Donaldson, L. (1996). Molecular characterization of a putative K-Cl cotransporter in rat brain. A neuronal-specific isoform. *The Journal of Biological Chemistry*, *271*(27), 16245–16252. Retrieved from http://www.ncbi.nlm.nih.gov/pubmed/8663311

Payne, J., Xu, J., Haas, M., Lytle, C., Ward, D., & Forbush, B. (1995). Primary Structure, Functional Expression, and Chromosomal Location of the Bumetanide-Sensitive Na-K-Cl Cotransporter in Human Colon. *The Journal of Biological Chemistry*, *270*(30), 17977–17985.

Pearson, M. ., Lu, J., Mount, D. ., & Delpire, E. (2001). Localization of the K+–Cl− cotransporter, KCC3, in the central and peripheral nervous systems: expression in the choroid plexus, large neurons and white matter tracts. *Neuroscience*, *103*(2), 481–491. https://doi.org/10.1016/S0306-4522(00)00567-4

Pellegrino, C., Gubkina, O., Schaefer, M., Becq, H., Ludwig, A., Mukhtarov, M., … Medina, I. (2011). Knocking down of the KCC2 in rat hippocampal neurons increases intracellular chloride concentration and compromises neuronal survival. *The Journal of Physiology*, *589*(10), 2475–2496. https://doi.org/10.1113/jphysiol.2010.203703

Petitjean, H., Pawlowski, S. A., Fraine, S. L., Sharif, B., Hamad, D., Fatima, T., … Sharif-Naeini, R. (2015). Dorsal Horn Parvalbumin Neurons Are Gate-Keepers of Touch-Evoked Pain after Nerve Injury. *Cell Reports*, *13*(6), 1246–1257. Retrieved from http://www.ncbi.nlm.nih.gov/pubmed/26527000

Piechotta, K., Garbarini, N., England, R., & Delpire, E. (2003). Characterization of the interaction of the stress kinase SPAK with the Na+-K+-2Cl- cotransporter in the nervous system: Evidence for a scaffolding role of the kinase. *Journal of Biological Chemistry*, *278*(52), 52848–52856. https://doi.org/10.1074/jbc.M309436200

Piechotta, K., Lu, J., & Delpire, E. (2002). Cation chloride cotransporters interact with the stress-related kinases Ste20-related proline-alanine-rich kinase (SPAK) and oxidative stress response 1 (OSR1). *Journal of Biological Chemistry*, *277*(52), 50812–50819. https://doi.org/10.1074/jbc.M208108200

Plotkin, M. D., Snyder, E. Y., Hebert, S. C., & Delpire, E. (1997). Expression of the Na-K-

2Cl cotransporter is developmentally regulated in postnatal rat brains: A possible mechanism underlying GABA's excitatory role in immature brain. *Journal of Neurobiology*, *33*(6), 781–795. https://doi.org/10.1002/(SICI)1097-4695(19971120)33:6<781::AID-NEU6>3.0.CO;2-5

Purves, D., Augustine, G. J., Fitzpatrick, D., Katz, L. C., LaMantia, A.-S., McNamara, J. O., & Williams, M. S. (2001). The Primary Motor Cortex: Upper Motor Neurons That Initiate Complex Voluntary Movements. In P. D, A. GJ, & E. Fitzpatrick D, et al. (Eds.), *Neuroscience* (2nd ed.). Sunderland: Sinauer Associates. Retrieved from https://www.ncbi.nlm.nih.gov/books/NBK10962/

Puskarjov, M., Seja, P., Heron, S. E., Williams, T. C., Ahmad, F., Iona, X., … Kaila, K. (2014). A variant of KCC2 from patients with febrile seizures impairs neuronal Cl- extrusion and dendritic spine formation. *EMBO Reports*, *15*(6), 723–729. https://doi.org/10.1002/embr.201438749

Quaggin, S. E., Payne, J. A., Forbush, B., & Igarashi, P. (1995). Localization of the renal Na-K-Cl cotransporter gene (Slc12a1) on mouse Chromosome 2. *Mammalian Genome*, *6*(8), 557–558. https://doi.org/10.1007/BF00356178

Quarmyne, M., Risinger, M., Linkugel, A., Frazier, A., & Joiner, C. (2011). Volume regulation and KCl cotransport in reticulocyte populations of sickle and normal red blood cells. *Blood Cells, Molecules, and Diseases*, *47*(2), 95–99. https://doi.org/10.1016/j.bcmd.2011.04.007

Race, J. E., Makhlouf, F. N., Logue, P. J., Wilson, F. H., Dunham, P. B., & Holtzman, E. J. (1999). Molecular cloning and functional characterization of KCC3, a new K-Cl cotransporter. *The American Journal of Physiology*, *277*(6 Pt 1), C1210-9. Retrieved from http://www.ncbi.nlm.nih.gov/pubmed/10600773

Ramchandren, S. (2017). Charcot-Marie-Tooth Disease and Other Genetic Polyneuropathies. *Continuum: Lifelong Learning In Neurology*, *23*(5), 1360–1377. https://doi.org/10.1212/CON.0000000000000529

Reilly, M. (2009). Classification and diagnosis of the inherited neuropathies. *Annals of Indian Academy of Neurology*. https://doi.org/10.4103/0972-2327.53075

Richardson, C., & Alessi, D. (2008). The regulation of salt transport and blood pressure by the WNK-SPAK/OSR1 signalling pathway. *Journal of Cell Science*, *121*(20), 3293–3304. https://doi.org/10.1242/jcs.029223

Richardson, C., Sakamoto, K., De Los Heros, P., Deak, M., Campbell, D. G., Prescott, A. R., & Alessi, D. R. (2011). Regulation of the NKCC2 ion cotransporter by SPAK-OSR1-dependent and -independent pathways. *Journal of Cell Science*, *124*(5), 789–800. https://doi.org/10.1242/jcs.077230

Richardson, J. D., Aanonsen, L., & Hargreaves, K. M. (1998). Antihyperalgesic effects of spinal cannabinoids. *European Journal of Pharmacology*. https://doi.org/10.1016/S0014-2999(97)01621-X

Rinehart, J., Maksimova, Y., Tanis, J., Stone, K., Hodson, C., Zhang, J., … Lifton, R. (2009). Sites of Regulated Phosphorylation that Control K-Cl Cotransporter Activity. *Cell*, *138*(3), 525–536. https://doi.org/10.1016/j.cell.2009.05.031

Rosenstein, J. M. (1993). Developmental expression of neuron-specific enolase immunoreactivity and cytochrome oxidase activity in neocortical transplants. *Experimental Neurology*, *124*(2), 208–218. https://doi.org/10.1006/exnr.1993.1191

Rossor, A. M., Evans, M. R. B., & Reilly, M. M. (2015). A practical approach to the genetic neuropathies. *Practical Neurology*, *15*, 187–198. https://doi.org/10.1136/practneurol-2015-001095

Russell, J. M. (2000). Sodium-potassium-chloride cotransport. *Physiological Reviews*, *80*(1), 211–276. https://doi.org/10.1152/physrev.2000.80.1.211

Rust, M. B., Faulhaber, J., Budack, M. K., Pfeffer, C., Maritzen, T., Didié, M., … Hübner, C. A. (2006). Neurogenic Mechanisms Contribute to Hypertension in Mice With Disruption of the K-Cl Cotransporter KCC3. *Circulation Research*, *98*(4), 549–556. https://doi.org/10.1161/01.RES.0000204449.83861.22

Rust, Marco B., Alper, S. L., Rudhard, Y., Shmukler, B. E., Vicente, R., Brugnara, C., … Hübner, C. A. (2007). Disruption of erythroid K-Cl cotransporters alters erythrocyte volume and partially rescues erythrocyte dehydration in SAD mice. *Journal of Clinical Investigation*, *117*(6), 1708–1717. https://doi.org/10.1172/JCI30630

Salin-Cantegrel, A., Rivière, J.-B., Dupré, N., Charron, F. M., Shekarabi, M., Karéméra, L., … Rouleau, G. A. (2007). Distal truncation of KCC3 in non-French Canadian HMSN/ACC families. *Neurology*, *69*(13), 1350–1355. https://doi.org/10.1212/01.wnl.0000291779.35643.15

Schmitt, R., Ellison, D. H., Farman, N., Rossier, B. C., Reilly, R. F., Reeves, W. B., … Bachmann, S. (1999). Developmental expression of sodium entry pathways in rat nephron. *American Journal of Physiology - Renal Physiology*, *276*(3 45-3). https://doi.org/10.1152/ajprenal.1999.276.3.f367

Schultheis, P. J., Lorenz, J., Meneton, P., Nieman, M. L., Riddle, T. M., Flagella, M., … Shull, G. E. (1998). Phenotype resembling Gitelman's syndrome in mice lacking the apical Na+-Cl- cotransporter of the distal convoluted tubule. *Journal of Biological Chemistry*, *273*(44), 29150–29155. https://doi.org/10.1074/jbc.273.44.29150

Schwarz, J. M., Rödelsperger, C., Schuelke, M., & Seelow, D. (2010). MutationTaster evaluates disease-causing potential of sequence alterations. *Nature Methods*, *7*(8), 575–576. https://doi.org/10.1038/nmeth0810-575

Sedmak, G., Jovanov-Milošević, N., Puskarjov, M., Ulamec, M., Krušlin, B., Kaila, K., & Judaš, M. (2015). Developmental Expression Patterns of KCC2 and Functionally Associated Molecules in the Human Brain. *Cerebral Cortex*, *26*(12), 4574–4589. https://doi.org/10.1093/cercor/bhv218

Shang, C., Lu, Y. M., & Meng, L. R. (2011). KCC1 gene advances cell invasion ability by regulating ERK signaling pathway in endometrial cancer HEC-1B cell line. *International Journal of Gynecological Cancer*, *21*(5), 795–799. https://doi.org/10.1097/IGC.0b013e318216a169

Shekarabi, M., Moldrich, R., Rasheed, S., Salin-Cantegrel, A., Laganière, J., Rochefort, D., … Rouleau, G. (2012). Loss of Neuronal Potassium/Chloride Cotransporter 3 (KCC3) Is Responsible for the Degenerative Phenotype in a Conditional Mouse Model of

Hereditary Motor and Sensory Neuropathy Associated with Agenesis of the Corpus Callosum. *Journal of Neuroscience*, *32*(11), 3865–3876.

Shekarabi, M., Salin-Cantegrel, A., Laganière, J., Gaudet, R., Dion, P., Rouleau, G. A., … Rouleau, G. A. (2011). Cellular expression of the K(+)–(Cl−) cotransporter KCC3 in the central nervous system of mouse. *Brain Research*, *1374*, 15–26. https://doi.org/10.1016/j.brainres.2010.12.010

Shen, R., Chou, C.-Y., Hsu, K.-F., Liu, H.-S., Dunham, P. B., Holtzman, E. J., & Ellory, J. C. (2001). The KCl cotransporter isoform KCC3 can play an important role in cell growth regulation. *Proceedings of the National Academy of Sciences*, *98*(25), 147141–14719. Retrieved from www.pnas.orgcgidoi10.1073pnas.251388798

Shiozaki, A., Takemoto, K., Ichikawa, D., Fujiwara, H., Konishi, H., Kosuga, T., … Otsuji, E. (2014). The K-Cl cotransporter KCC3 as an independent prognostic factor in human esophageal squamous cell carcinoma. *BioMed Research International*, *936401*. https://doi.org/10.1155/2014/936401

Simon, D., Karet, F., Hamdan, J., Di Pietro, A., Sanjad, S., & Lifton, R. (1996). Bartter's syndrome, hypokalaemic alkalosis with hypercalciuria, is caused by mutations in the Na-K-2CI cotransporter NKCC2. *Nature Genetics*, *13*(2), 183–188. https://doi.org/10.1038/ng0696-183

Sleigh, J. N., Weir, G. A., & Schiavo, G. (2016). A simple, step-by-step dissection protocol for the rapid isolation of mouse dorsal root ganglia. *BMC Research Notes*, *9*, 82. https://doi.org/10.1186/s13104-016-1915-8

Stein, W., & Litman, T. (1990). *Channels, Carriers, and Pumps: An Introduction to Membrane Transport*. San Diego: Academic Press.

Stifani, N. (2014). Motor neurons and the generation of spinal motor neuron diversity. *Frontiers in Cellular Neuroscience*, *8*, 293. https://doi.org/10.3389/fncel.2014.00293

Stil, A., Jean-Xavier, C., Liabeuf, S., Brocard, C., Delpire, E., Vinay, L., & Viemari, J.-C. (2011). Contribution of the potassium-chloride co-transporter KCC2 to the modulation of lumbar spinal networks in mice. *European Journal of Neuroscience*, *33*(7), 1212–1222. https://doi.org/10.1111/j.1460-9568.2010.07592.x

Stokes, J. B. ., Lee, I., & Amico, M. D. (1984). Sodium Chloride Absorption by the Urinary Bladder of the Winter Flounder, *74*(1), 7–16.

Su, W., Shmukler, B. E., Chernova, M. N., Stuart-Tilley, A. K., De Franceschi, L., Brugnara, C., … Brugnara, S. L. A. (1999). Mouse K-Cl cotransporter KCC1: cloning, mapping, pathological expression, and functional regulation. *The American Journal of Physiology*, *277*(5), C899–C912. Retrieved from www.physiology.org/journal/ajpcell

Sun, Y.-T., Lin, T.-S., Tzeng, S.-F., Delpire, E., & Shen, M.-R. (2010). Deficiency of electroneutral K+-Cl- cotransporter 3 causes a disruption in impulse propagation along peripheral nerves. *Glia*, *58*(13), 1544–1552. https://doi.org/10.1002/glia.21028

Sun, Y.-T., Tzeng, S.-F., Lin, T.-S., Hsu, K.-S., Delpire, E., & Shen, M.-R. (2016). KCC3 deficiency-induced disruption of paranodal loops and impairment of axonal excitability in the peripheral nervous system. *Neuroscience*, *335*, 91–102. https://doi.org/10.1016/j.neuroscience.2016.08.031

Sung, J. (1987). Tangled Masses of Central Axons (Central Axonomas) in the Brain Stem: Anatomical Evidence for the Regenerative Growth of Human Central Axons. *Journal of Neuropathology & Experimental Neurology*, *46*(2), 200–213.

Sung, K. W., Kirby, M., McDonald, M. P., Lovinger, D. M., & Delpire, E. (2000a). Abnormal GABA(A) receptor-mediated currents in dorsal root ganglion neurons isolated from Na-K-2Cl cotransporter null mice. *Journal of Neuroscience*, *20*(20), 7531–7538. https://doi.org/10.1523/jneurosci.20-20-07531.2000

Sung, K. W., Kirby, M., McDonald, M. P., Lovinger, D. M., & Delpire, E. (2000b). Abnormal GABAA receptor-mediated currents in dorsal root ganglion neurons isolated from Na-K-2Cl cotransporter null mice. *The Journal of Neuroscience : The Official Journal of the Society for Neuroscience*, *20*(20), 7531–7538. https://doi.org/20/20/7531 [pii]

Takahashi, N., Chernavvsky, D., Gomez, R. A., Igarashi, P., Gitelman, H. J., & Smithies, O. (2000). Uncompensated polyuria in a mouse model of Bartter's syndrome. *Proceedings of the National Academy of Sciences of the United States of America*, *97*(10), 5434–5439. https://doi.org/10.1073/pnas.090091297

Tazir, M., Hamadouche, T., Nouioua, S., Mathis, S., & Vallat, J.-M. (2014). Hereditary motor and sensory neuropathies or Charcot-Marie-Tooth diseases: an update. *Journal of the Neurological Sciences*, *347*, 14–22. https://doi.org/10.1016/j.jns.2014.10.013

Thastrup, J. O., Rafiqi, F. H., Vitari, A. C., Pozo-Guisado, E., Deak, M., Mehellou, Y., & Alessi, D. R. (2012). SPAK/OSR1 regulate NKCC1 and WNK activity: analysis of WNK isoform interactions and activation by T-loop trans-autophosphorylation. *Biochemical Journal*, *441*(1), 325–337. https://doi.org/10.1042/BJ20111879

Uyanik, G., Elcioglu, N., Penzien, J., Gross, C., Yilmaz, Y., Olmez, A., … Winkler, J. (2006). Novel truncating and missense mutations of the KCC3 gene associated with Andermann syndrome. *Neurology*, *66*(7), 1044–1048. Retrieved from https://www.ncbi.nlm.nih.gov/pubmed/16606917

van Paassen, B. W., van der Kooi, A. J., van Spaendonck-Zwarts, K. Y., Verhamme, C., Baas, F., & de Visser, M. (2014). PMP22 related neuropathies: Charcot-Marie-Tooth disease type 1A and Hereditary Neuropathy with liability to Pressure Palsies. *Orphanet Journal of Rare Diseases*, *9*(1), 38. https://doi.org/10.1186/1750-1172-9-38

Velázquez, H., & Silva, T. (2003). Cloning and localization of KCC4 in rabbit kidney: Expression in distal convoluted tubule. *American Journal of Physiology - Renal Physiology*, *285*(1), F49–F58. https://doi.org/10.1152/ajprenal.00389.2002

von Horsten, S., Karl, T., & Pabst, R. (2003). Behavioral phenotyping of mice in pharmacological and toxicological research. *Experimental and Toxicologic Pathology*, *55*(1), 69–83.

Vu, T., Payne, J., & Copenhagen, D. R. (2000). Localization and developmental expression patterns of the neuronal K-Cl cotransporter (KCC2) in the rat retina. *Journal of Neuroscience*, *20*(4), 1414–1423. https://doi.org/10.1523/jneurosci.20-04-01414.2000

Watanabe, M., & Fukuda, A. (2015). Development and regulation of chloride homeostasis in the central nervous system. *Frontiers in Cellular Neuroscience*, *9*, 371.

https://doi.org/10.3389/fncel.2015.00371
Watson, J. C., & Dyck, P. J. B. (2015, July 1). Peripheral Neuropathy: A Practical Approach to Diagnosis and Symptom Management. *Mayo Clinic Proceedings*. Elsevier Ltd. https://doi.org/10.1016/j.mayocp.2015.05.004
Wehner, F., Olsen, H., Tinel, H., Kinne-Saffran, E., & Kinne, R. K. (2003). Cell volume regulation: osmolytes, osmolyte transport, and signal transduction. *Reviews of Physiology, Biochemistry and Pharmacology*, *148*, 1–80. https://doi.org/10.1007/s10254-003-0009-x
Wilson, F. H., Disse-Nicodème, S., Choate, K. A., Ishikawa, K., Nelson-Williams, C., Desitter, I., … Lifton, R. P. (2001). Human hypertension caused by mutations in WNK kinases. *Science*, *293*(5532), 1107–1112. https://doi.org/10.1126/science.1062844
Winklewski, P. J., Sabisz, A., Naumczyk, P., Jodzio, K., Szurowska, E., & Szarmach, A. (2018, February 27). Understanding the physiopathology behind axial and radial diffusivity changes-what do we Know? *Frontiers in Neurology*. Frontiers Media S.A. https://doi.org/10.3389/fneur.2018.00092
Woo, N.-S., Lu, J., England, R., McClellan, R., Dufour, S., Mount, D. B., … Delpire, E. (2002). Hyperexcitability and epilepsy associated with disruption of the mouse neuronal-specific K-Cl cotransporter gene. *Hippocampus*, *12*(2), 258–268. https://doi.org/10.1002/hipo.10014
Yang, J., Yan, R., Roy, A., Xu, D., Poisson, J., & Zhang, Y. (2014). The I-TASSER suite: Protein structure and function prediction. *Nature Methods*. Nature Publishing Group. https://doi.org/10.1038/nmeth.3213
Yang, S. Sen, Hsu, Y. J., Chiga, M., Rai, T., Sasaki, S., Uchida, S., & Lin, S. H. (2010). Mechanisms for hypercalciuria in pseudohypoaldosteronism type II-causing WNK4 knock-in mice. *Endocrinology*, *151*(4), 1829–1836. https://doi.org/10.1210/en.2009-0951
Zachařová, G., & Paleček, J. (2009). Parvalbumin and TRPV1 Receptor Expression in Dorsal Root Ganglion Neurons after Acute Peripheral Inflammation. *Physiol. Res*, *58*, 305–309. Retrieved from www.biomed.cas.cz/physiolres
Zagórska, A., Pozo-Guisado, E., Boudeau, J., Vitari, A. C., Rafiqi, F. H., Thastrup, J., … Alessi, D. R. (2007). Regulation of activity and localization of the WNK1 protein kinase by hyperosmotic stress. *Journal of Cell Biology*, *176*(1), 89–100. https://doi.org/10.1083/jcb.200605093
Zeuthen, T. (1994). Cotransport of K+, Cl- and H2O by membrane proteins from choroid plexus epithelium of Necturus maculosus. *The Journal of Physiology*, *478*(2), 203–219. https://doi.org/10.1113/jphysiol.1994.sp020243
Zhang, J.-H., Morita, Y., Hironaka, T., Emson, P. C., & Tohyama, M. (1990). Ontological study of calbindin-D28k-like and parvalbumin-like immunoreactivities in rat spinal cord and dorsal root ganglia. *The Journal of Comparative Neurology*, *302*(4), 715–728. https://doi.org/10.1002/cne.903020404
Zhang, S., Wu, X., Jiang, T., Lu, Y., Ma, L., Liang, M., & Sun, X. (2009). The up-regulation of KCC1 gene expression in cervical cancer cells by IGF-II through the ERK1/2MAPK

and PI3K/AKT pathways and its significance. *European Journal of Gynaecological Oncology*, *30*(1), 29–34. Retrieved from http://www.ncbi.nlm.nih.gov/pubmed/19317253